

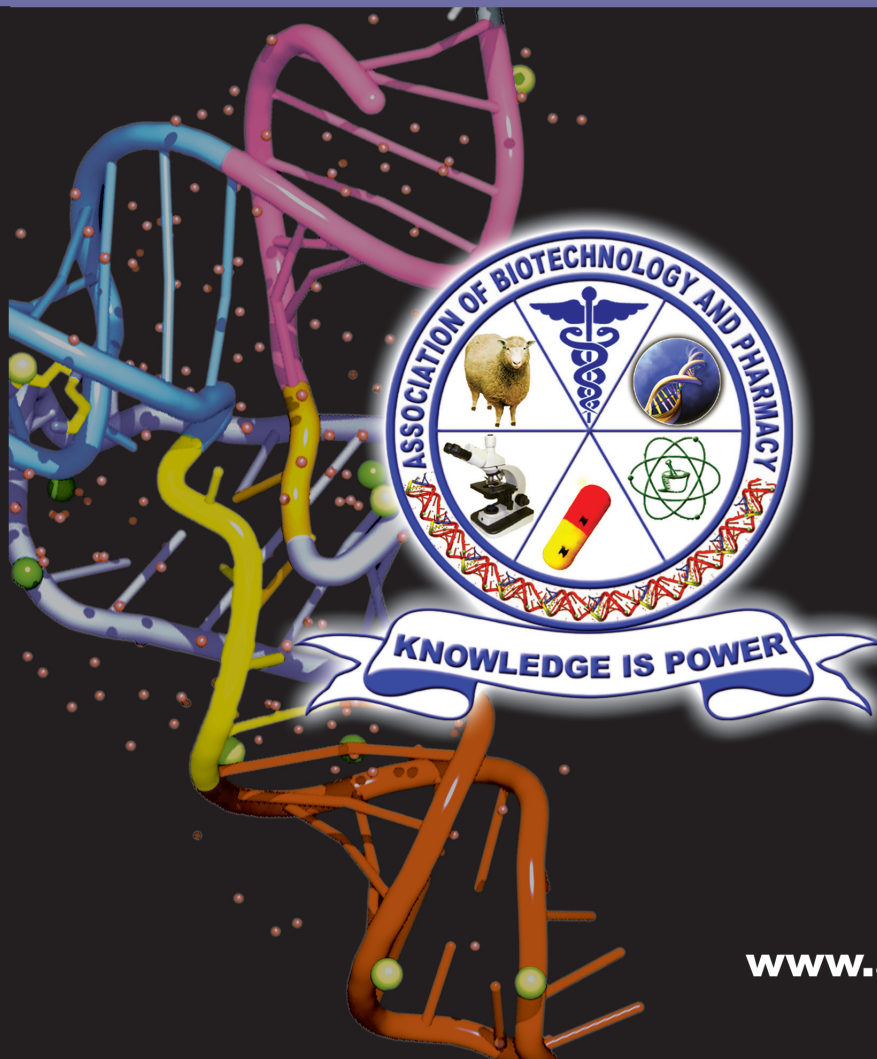
ISSN 0973-8916

Current Trends in Biotechnology and Pharmacy

Volume 10

Issue 3

July 2016



www.abap.co.in

Current Trends in Biotechnology and Pharmacy

ISSN 0973-8916 (Print), 2230-7303 (Online)

Editors

Prof.K.R.S. Sambasiva Rao, India
krssrao@abap.co.in

Prof. Karnam S. Murthy, USA
skarnam@vcu.edu

Editorial Board

Prof. Anil Kumar, India
Prof. P.Appa Rao, India
Prof. Bhaskara R.Jasti, USA
Prof. Chellu S. Chetty, USA
Dr. S.J.S. Flora, India
Prof. H.M. Heise, Germany
Prof. Jian-Jiang Zhong, China
Prof. Kanyaratt Supaibulwatana, Thailand
Prof. Jamila K. Adam, South Africa
Prof. P.Kondaiah, India
Prof. Madhavan P.N. Nair, USA
Prof. Mohammed Alzoghaibi, Saudi Arabia
Prof. Milan Franek, Czech Republic
Prof. Nelson Duran, Brazil
Prof. Mulchand S. Patel, USA
Dr. R.K. Patel, India
Prof. G.Raja Rami Reddy, India
Dr. Ramanjulu Sunkar, USA
Prof. B.J. Rao, India
Prof. Roman R. Ganta, USA
Prof. Sham S. Kakar, USA
Dr. N.Sreenivasulu, Germany
Prof.Sung Soo Kim, Korea
Prof. N. Udupa, India
Dr.P. Ananda Kumar, India
Prof. Aswani Kumar, India
Prof. Carola Severi, Italy
Prof. K.P.R. Chowdary, India
Dr. Govinder S. Flora, USA
Prof. Huangxian Ju, China
Dr. K.S.Jagannatha Rao, Panama
Prof.Juergen Backhaus, Germany
Prof. P.B.Kavi Kishor, India
Prof. M.Krishnan, India
Prof. M.Lakshmi Narasu, India
Prof.Mahendra Rai, India
Prof.T.V.Narayana, India
Dr. Prasada Rao S.Kodavanti, USA
Dr. C.N.Ramchand, India
Prof. P.Reddanna, India
Dr. Samuel J.K. Abraham, Japan
Dr. Shaji T. George, USA
Prof. Sehamuddin Galadari, UAE
Prof. B.Srinivasulu, India
Prof. B. Suresh, India
Prof. Swami Mruthinti, USA
Prof. Urmila Kodavanti, USA

Assistant Editors

Dr.Giridhar Mudduluru, Germany

Dr. Sridhar Kilaru, UK

Prof. Mohamed Ahmed El-Nabarawi, Egypt

Prof. Chitta Suresh Kumar, India

www.abap.co.in

ISSN 0973-8916

Current Trends in Biotechnology and Pharmacy

(An International Scientific Journal)

Volume 10

Issue 3

July 2016



www.abap.co.in

Indexed in Chemical Abstracts, EMBASE, ProQuest, Academic SearchTM, DOAJ, CAB Abstracts, Index Copernicus, Ulrich's Periodicals Directory, Open J-Gate Pharmoinfonet.in Indianjournals.com and Indian Science Abstracts.

Association of Biotechnology and Pharmacy (Regn. No. 28 OF 2007)

The *Association of Biotechnology and Pharmacy (ABAP)* was established for promoting the science of Biotechnology and Pharmacy. The objective of the Association is to advance and disseminate the knowledge and information in the areas of Biotechnology and Pharmacy by organising annual scientific meetings, seminars and symposia.

Members

The persons involved in research, teaching and work can become members of Association by paying membership fees to Association.

The members of the Association are allowed to write the title **MABAP** (Member of the Association of Biotechnology and Pharmacy) with their names.

Fellows

Every year, the Association will award Fellowships to the limited number of members of the Association with a distinguished academic and scientific career to be as Fellows of the Association during annual convention. The fellows can write the title **FABAP** (Fellow of the Association of Biotechnology and Pharmacy) with their names.

Membership details

(Membership and Journal)		India	SAARC	Others
Individuals	– 1 year	Rs. 600	Rs. 1000	\$100
	LifeMember	Rs. 4000	Rs. 6000	\$500
Institutions (Journal only)	– 1 year	Rs. 1500	Rs. 2000	\$200
	Life member	Rs.10000	Rs.12000	\$1200

Individuals can pay in two instalments, however the membership certificate will be issued on payment of full amount. All the members and Fellows will receive a copy of the journal free

Association of Biotechnology and Pharmacy
(Regn. No. 28 OF 2007)
#5-69-64; 6/19, Brodipet
Guntur – 522 002, Andhra Pradesh, India

Current Trends in Biotechnology and Pharmacy

ISSN 0973-8916

Volume 10 (3)	CONTENTS	July 2016
Research Papers		
	Identification of Secreted Proteins during Protease-Activated Receptors 2 Activation in Gastrointestinal Smooth Muscle Cells <i>Sorratod Bosuwan, Sittiruk Roytrakul, Karnam S. Murthy and Wimolpak Sriwai</i>	194-221
	Homology Modeling of Endoxylanase from <i>Trichoderma pseudokoningii</i> <i>Bandikari Ramesh, Seelam Naga Sivudu, Katike Umamahesh and Obulam Vijaya Sarathi Reddy</i>	222-228
	Pharmacokinetic analysis of atorvastatin against experimental hepatotoxicity with special reference to CYP3A4 functioning in rats <i>M. Anudeep Reddy, B. Kala Kumar, G. Boobalan, M. Vijay Kumar, M. Kasi Reddy, C.S.V. Satish Kumar and A. Gopala Reddy</i>	229-236
	Indirect somatic embryogenesis and evaluation of genetic fidelity of <i>in vitro</i> propagated plants of <i>Bunium persicum</i> (Boiss.) Fedtsch by using DNA markers <i>Rajinder Kaur, Neha Sharma, Sadiq Majeed and Yogeeta Thakur</i>	237-247
	Optimization of process parameters for α -amylase production using Artificial Neural Network (ANN) on agricultural wastes <i>Santosh Kumar Mishra, Shashi Kumar, Surendra Kumar, Ravi Kant Singh</i>	248-260
	Isolation and Characterization of Extracellular Lipase Producing Bacterial Isolates From Effluent Waste of Paint Industry <i>Shiney Hangloo, Anuradha Sourirajan, Chand Raina, Asha Chaubey and Kamal Dev</i>	261-273
	Evaluation of Incubation Parameters in a TUNEL assay for Detecting Apoptotic cells in Cumulus Oocyte Complexes and <i>in vitro</i> produced early Embryos of Buffalo <i>Asit Jain, Tripti Jain, G K Sachdeva, Sachinandan De and Tirtha Kumar Datta</i>	274-279
	Effect of Growth Regulators on Regeneration Through Leaf and Stem Derived Callus in <i>Physalis minima</i> Linn. <i>Sandhya H. and Srinath Rao</i>	280-285
	Synthesis of Silver Nanoparticles from Different Plant Leaf Extracts and Its Analysis using UV-Spectroscopy <i>Lavanya Kakarla and Chakravarthy Rama</i>	286-289
	Review Paper Pyrosequencing- A Pioneer Technique of New Epoch <i>Rekha Khandia and Ashok Munjal</i>	290-298
	<i>News Item</i>	i - iii

Information to Authors

The *Current Trends in Biotechnology and Pharmacy* is an official international journal of *Association of Biotechnology and Pharmacy*. It is a peer reviewed quarterly journal dedicated to publish high quality original research articles in biotechnology and pharmacy. The journal will accept contributions from all areas of biotechnology and pharmacy including plant, animal, industrial, microbial, medical, pharmaceutical and analytical biotechnologies, immunology, proteomics, genomics, metabolomics, bioinformatics and different areas in pharmacy such as, pharmaceuticals, pharmacology, pharmaceutical chemistry, pharma analysis and pharmacognosy. In addition to the original research papers, review articles in the above mentioned fields will also be considered.

Call for papers

The Association is inviting original research or review papers and short communications in any of the above mentioned research areas for publication in *Current Trends in Biotechnology and Pharmacy*. The manuscripts should be concise, typed in double space in a general format containing a title page with a short running title and the names and addresses of the authors for correspondence followed by Abstract (350 words), 3 – 5 key words, Introduction, Materials and Methods, Results and Discussion, Conclusion, References, followed by the tables, figures and graphs on separate sheets. For quoting references in the text one has to follow the numbering of references in parentheses and full references with appropriate numbers at the end of the text in the same order. References have to be cited in the format below.

Mahavadi, S., Rao, R.S.S.K. and Murthy, K.S. (2007). Cross-regulation of VAPC2 receptor internalization by m2 receptors via c-Src-mediated phosphorylation of GRK2. *Regulatory Peptides*, 139: 109-114.

Lehninger, A.L., Nelson, D.L. and Cox, M.M. (2004). *Lehninger Principles of Biochemistry*, (4th edition), W.H. Freeman & Co., New York, USA, pp. 73-111.

Authors have to submit the figures, graphs and tables of the related research paper/article in Adobe Photoshop of the latest version for good illumination and alignment.

Authors can submit their papers and articles either to the editor or any of the editorial board members for onward transmission to the editorial office. Members of the editorial board are authorized to accept papers and can recommend for publication after the peer reviewing process. The email address of editorial board members are available in website www.abap.in. For submission of the articles directly, the authors are advised to submit by email to krssrao@abap.co.in or krssrao@yahoo.com.

Authors are solely responsible for the data, presentation and conclusions made in their articles/research papers. It is the responsibility of the advertisers for the statements made in the advertisements. No part of the journal can be reproduced without the permission of the editorial office.

Identification of Secreted Proteins during Protease-Activated Receptor 2 Activation in Gastrointestinal Smooth Muscle Cells

Sorratod Bosuwan¹, Sittiruk Roytrakul², Karnam S. Murthy³ and Wimolpak Sriwai^{4*}

¹Department of Medical Technology, School of Allied Health Sciences, Thammasat University, PathumThani, 12121, Thailand

²Proteomics Research Laboratory, National Center for Genetic Engineering and Biotechnology, PathumThani, 12120, Thailand

³Department of Physiology, VCU Program in Enteric Neuromuscular Sciences, Virginia Commonwealth University, Richmond, Virginia, United States of America

⁴Department of Medical Technology, School of Allied Health Sciences, Thammasat University, PathumThani, 12121, Thailand

*For Correspondence - sriwai@tu.ac.th

Abstract

Protease-activated receptor 2 is a member of G protein-coupled receptor and expressed in a wide variety of cells. PAR2 is involved in several physiological and pathophysiological processes, including growth and development, inflammation, migration, and apoptosis depending on cell types. However, the role of PAR2 in the context of secretory function of inflammatory proteins in smooth muscle cells remains unknown. The aim of the present study was to determine the secretory proteins involved in inflammatory process upon PAR2 activation in smooth muscle cells. Gastric smooth muscle cells were left untreated or treated with PAR2 activating peptide (PAR2-AP) SLIGKV (1 μ M) for up to 48 hours in serum-free medium. Untreated media were used as negative controls. Secretome were collected at 48 hours and subjected to proteomic analysis by LC-MS/MS. A total of 310 peptides were detected and found to correspond to 275 proteins. This approach identified 160 significant changes in protein levels. These proteins were expressed at significantly different levels in treated sample as compared with untreated sample. These proteins could be classified by their functions in inflammation, proliferation and apoptosis, and

response to stress. It resulted in the first LC-MS/MS based secretome profiles of gastrointestinal smooth muscle cells. Such secretory protein may be of pathological significance in the role of PAR2 in regulating the inflammation, proliferation, and apoptotic process and may offer protection of cells against physiological stress.

Keyword: Protease-activated receptor 2, PAR2, Proteomics, LC-MS, Inflammation

Introduction

The proteinase-activated receptors (PARs) belong to the family of G protein-coupled receptors. PARs consist of four members, PAR1, PAR2, PAR3 and PAR4, which can be cleaved by certain serine proteases. These serine proteases derive from leukocyte, coagulation factors, pathogen, and many different sources. The unique mechanism of activation involves irreversible enzymatic cleavage of the N-terminus domains at a specific site and unmasking a tethered ligand that triggers intracellular signaling (1-4). Signaling by activated PARs is terminated by receptor phosphorylation and association with β -arrestins. PARs also can be activated without enzymatic cleavage by synthetic activating peptides (PAR-APs), as short as six amino acids.

PAR-APs correspond to the tethered ligand domain that can directly bind to and activate PARs (5, 6).

PAR2 signaling has been implicated in the development of inflammatory bowel diseases. PAR2 are found on the surface of several cell types (7) including epithelial cell (1), fibroblasts, endothelial cells (8), keratinocytes (9, 10), sensory neurons (11), inflammatory cells (12), and smooth muscle cell (13). The primary function of smooth muscle cells is to alter the stiffness or diameter of hollow organs by contracting and relaxing. It has been reported that gastric smooth muscle cells constitutively express high levels of PAR2 and are able to mediate PAR2-AP-induced contraction (13). Growing evidence has shown that smooth muscle cells secrete highly active signaling proteins, which have a regulatory role in the muscles and other organs via endocrine, autocrine, or paracrine actions (14). It has significant capacity to synthesize and secrete various signaling proteins including cytokines, chemokines, and peptide growth factors (15-17). These active signaling proteins are suggested to mediate the course of several common and highly debilitating chronic diseases, such as atherosclerosis (18,19), asthma (20,21), and inflammatory bowel diseases (22). Despite extensive research on the secretory function of vascular and airway smooth muscle, there is considerably less study regarding gastrointestinal smooth muscle.

Characterization of the sets of proteins secreted from smooth muscle cells and subsequent analysis of their functions are a critical first step in better understanding the regulation of muscle during normal and pathological processes. Here, we sought to identify the secreted proteome induced by PAR2-AP, SLIGKV. This study uses the rabbit gastric smooth muscle cell as a model system and a proteomics approach to analyze the secretome of smooth muscle during PAR2 activation. We identified 172 significant changes in protein levels compared to control and associated with wide

range of biological processes. Among these proteins, inflammatory proteins such as IL-25, IL-17RE, and TLR2 were found to be secreted. This work expands our knowledge of the secretory function and potential roles of PAR2 on smooth muscle cell. Mediators released from smooth muscle may serve as autocrine and paracrine factors that are involved in progression of an inflammatory process.

Materials and Methods

Cell culture : Rabbit gastric smooth muscle cells (a kind gift from Murthy KS., the VCU Program in Enteric Neuromuscular Sciences, Virginia Commonwealth University, Richmond, Virginia, United States of America) were cultured in DMEM containing 200 units/milliliter (U/ml) penicillin, 200 milligrams/milliliter(mg/ml)streptomycin, 100 mg/ml gentamycin, 2.5 mg/ml amphotericin B and 10% fetal bovine serum (DMEM-10)(13). The cultured plate was incubated at 37°C in a CO₂ incubator. DMEM-10 medium was replaced every three days for 2–3 weeks until the cells attained confluence. All experiments were done on cells in the first passage.

PAR2 activation of smooth muscle cells : For PAR2 activation experiment, cells were divided into two groups: control and PAR2-AP (SLIGKV) (Bachem, Torrance, CA) stimulated smooth muscle cells. Smooth muscle cells were washed twice with sterile PBS and then exposed to serum free medium for 18 - 24 h. PAR2-AP was directly diluted in cell culture medium of treatment group to achieve a final concentration of 1 µm. After 48-h treatment the serum free conditioned medium was collected. The resulting supernatant contains secreted proteins. The supernatant were subjected to lyophilization and stored at -80°C until experiment was performed. An experiment was repeated three independent times.

Determination of protein concentration by

Lowry method : The freeze dry media were resuspended in 0.5% sodium dodecyl sulfate and protein concentration was determined by Lowry method (23). Absorbance of the solution was measured at 750 nm using a spectrophotometer.

The protein concentration was calculated using a standard curve of BSA solution.

Prefractionation protein by sodium dodecyl sulfate polyacrylamide gel electrophoresis (SDS-PAGE) : Proteins were separated on SDS-PAGE mini gel with the HoeferMiniVE electrophoresis system (Amersham Biosciences, UK) (8 x 9 x 0.1 cm). The polyacrylamide gel was prepared according to the method as previously described (24). For PAGE, the stacking gel had 5% acrylamide while the separating gel contained 12.5% in Tris-HCl pH 8.3. Fifty micrograms of each protein sample was then mixed with equal volume of 5X concentrated sample buffer (0.125M Tris-HCl pH 6.8, 20% glycerol, 5% SDS, 0.2 M dithiothreitol (DTT), 0.02% bromophenol blue) and heat at 95°C for 10 min before placing on the gel. Low molecular weight protein standard marker (Amersham Biosciences, UK) was used to estimate size of polypeptides. Electrophoresis was performed in SDS electrophoresis buffer (25mM Tris-HCl pH 8.3, 192mM glycine, 0.1% SDS) until the tracking dye reached the bottom of the gel. Performed gels were stained by silver (25).

In-gel digestion : The gel pieces were subjected to in-gel digestion using an in-house method developed by Proteomics Laboratory, Genome Institute, National Center for Genetic Engineering and Biotechnology (BIOTEC), National Science and Technology Development Agency (NSTDA), Thailand. In short, protein bands were cut into 15 segments according to size and transferred to 96-well plate. The gel pieces were dehydrated with 100% acetonitrile (ACN), reduced with 10 millimolars (mM) DTT in 10mM ammonium bicarbonate at room temperature for 1 h and alkylated with 100mM Iodoacetamide (IAA) in 10mM ammonium bicarbonate at room temperature for 1 h in the dark. The gel pieces were dehydrated twice with 100% ACN for 5 min and 10 microliters (μ l) of trypsin solution (10 ng/ μ l trypsin in 50% ACN / 10mM ammonium bicarbonate) was added for in-gel digestion of proteins followed by incubation for 20 min at room

temperature. To keep the gels immersed throughout digestion, 20 μ l of 30% ACN was added and incubation continued for a few hours to over night at 37°C. The digested peptides were extracted from the gel using 30 μ l of 50% ACN in 0.1% formic acid and incubation continued while shaking for 10 min at room temperature. Extracted peptides were collected and transferred into the new tube. The extracted peptides were dried by using a speed-vac concentrator and stored the vial at -80 °C for mass spectrometric analysis.

Identification of protein by liquid chromatography coupled to mass spectrometry (LC/MS-MS) configuration :

Quantitative LC/MS-MS was performed on 1 μ g of protein digest per sample, using a nanoACQUITY UPLC system (Waters Corp., Milford, MA, USA) coupled to a Waters SYNAPT™ HDMS™ system (Waters Corp., Manchester, UK) via a nanoelectrospray ionization source. Briefly, the sample was separated using an analytical reversed phase column (75 μ m x 250 mm, Waters Corp., Milford, MA, USA) packed with 1.7 μ m ethylene bridged hybrid (BEH) C₁₈ stationary phase. The A solvent is HPLC grade water with 0.1% formic acid. The B solvent is acetonitrile with 0.1% formic acid. The sample was initially transferred with a solvent to the trap column with a flow rate of 15 microliters/minute (μ l/min) for 1 min. After which the analytical separation was performed using a 60-min gradient of 2 to 40% acetonitrile with 0.1% formic acid at a flow rate of 350 nl/min followed by a 15 min rinse of 80% acetonitrile. The column temperature was maintained at 35 °C. The analysis of tryptic peptides was performed using a SYNAPT™ HDMS™ mass spectrometer which was operated in the V-mode of analysis with a resolution of at least 10,000 full-width half-maximum, using positive nanoelectrospray ion mode. The time-of-flight analyzer of the mass spectrometer was externally calibrated with a (Glu¹) fibrinopeptide B mixture from m/z 50 to 1600. The collision gas used was argon, maintained at a constant pressure of 2.0×10^{-3}

mbar in the collision cell. The lock mass, (Glu¹) fibrinopeptide B, was delivered from the auxiliary pump of the nanoACQUITY system with a concentration of 100 fmol/μl at 0.5 μl/min to the reference sprayer of the nanolock spray source. The data were post-acquisition lock-mass corrected using the monoisotopic mass of the doubly charged precursor of (Glu¹) fibrinopeptide B, delivered through the reference sprayer, which was sampled every 20 s. Accurate mass precursor and fragment ion LC-MS data were collected with data direct acquisition mode. The MS/MS survey was over range from 50 to 1990. The intact mass spectra were deconvoluted to the zero charge state (Ensemble 1, Iterations 50, auto peak width determination) using MaxEnt 3, a deconvolution software available within MassLynx 4.0.

Proteins quantitation and identification :

DeCyder MS differential analysis software (DeCyderMS, GE Healthcare) was used for identification and quantitation of peptides based on MS signal intensities of individual LC-MS. Quantitation of peptides was performed using the PepDetect module. Peptides were matched across different signal intensity maps between the control and treated samples using the PepMatch module. The relative abundances of peptides were expressed as log₂ intensities. All log₂ intensities of the sample were normalized with the ion intensity distribution of a reference standard, bovine serum albumin (BSA).

The analyzed MS/MS data from DeCyderMS were submitted to database search using the Mascot software version 2.2 (Matrix Science, London, UK). The data was searched against the NCBI database for protein identification. Search parameters were taxonomy (*Oryctolagus cuniculus*); enzyme (trypsin); variable modifications (carbamidomethyl, oxidation of methionine residues); mass values (monoisotopic); protein mass (unrestricted); peptide mass tolerance (1 Da); fragment mass tolerance (±0.4 Da); peptide charge state (1+, 2+ and 3+); max missed cleavages (1) and instrument = ESI-QUAD-TOF. Proteins

considered as identified proteins had at least one peptides with an individual mascot score corresponding to p<0.05.

To assign proteins to gene symbols, protein lists are mapped to corresponding entries in UniProt Knowledgebase (UniProtKB) of all known proteins based on protein names and sequences. Searches were performed against the *Homo sapiens* protein data sets.

Bioinformatic analysis : Normalized quantitative data sets were used for subsequent analyses. A 2-fold cutoff value was set to identify proteins whose expression was significantly increased or decreased. To assign biological functions and processes to the entire data set of over-expressed or highly suppressed proteins, Gene ontologies of identified and quantified proteins were determined with PANTHER software (<http://www.pantherdb.org>) and UniprotKB databases (<http://www.uniprot.org>). Proteins with 2-fold or greater changes in expression upon treatment were used for gene-pathway annotations using Reactome tools (Reactome V57) (<http://www.reactome.org/>) and to create protein-protein interaction networks via STRING database (Ingenuity Systems, version 10.0 (<http://string-db.org/>)). Networks represent a highly interconnected set of proteins derived from the input data set. To predict which pathways are being affected by the changes in protein expression, a Fisher's exact test was applied to the mapping of significantly over-expressed proteins in the data set to each pathway to determine the significance of any over-representation of the proteins to that pathway.

Results

Protein identification and characterization :

To identify secretory proteins upon PAR2 activation in gastric smooth muscle cell, we systematically assessed the supernatant contains secreted proteins or secretome of smooth muscle cell activated with specific peptide, SLIGKV, for 48 hours compared to untreated cells. After LC-MS/MS analysis of the isolated peptides, all MS/MS spectra were

searched against rabbit protein database. MS analysis results are summarized in Table 1. A total of 300 peptides were detected from supernatant across all samples. The analysis of these supernatant samples resulted in the identification of 271 and 256 peptides under untreated and PAR2-induced conditions, respectively. We assigned protein names and sequences to human gene symbols using UniProtKB based on a target reference of human proteins. Total 300 GI numbers obtained from the MS data were converted to UniProtKB accession numbers and found to correspond to 275 genes. From these proteins, 212 proteins were common to both control and treatment sample.

Smooth muscle secretome composition is changed by PAR2-AP treatment :

Functional classification of secreted proteins revealed a change in secretome composition after PAR-2 AP treatment. Protein expression profiles were compared between untreated and PAR2-induced sample. Of the 275 differentially expressed proteins we found that 160 proteins had expression levels that differed by more than 2.0 fold in treatment sample when compared to untreated sample, comprising 61 up-regulated and 99 down-regulated proteins (Figure 2A). We selected the 160 differentially expressed proteins as candidate secreted proteins associated with PAR2 activation. Details of these proteins are presented in Table 1. Those proteins were subjected to K-means clustering having the K-means performs optimally for 6 clusters as determined by Figures of Merit (FOM) method (Figure 2B). Cluster analysis classified samples into a small number of groups based on the similarities of expression. Clearly each of the 6 clusters shows proteins specifically expressed in one of the conditions.

Proteins in cluster 2 were highly expressed at control condition (Figure 2C), whereas proteins in cluster 3 were highly expressed at PAR2 treatment condition (Figure 2D). Proteins in cluster 1 and 6 were highly expressed in both treated and untreated

conditions but the expressions of proteins in cluster 4 and 5 were relatively repressed in both conditions. In cluster 2, results showed several proteins involved in metabolic processes, cellular processes, and biological regulation. Interestingly, proteins related to immune system process, apoptotic process, and response to stimulus were found. Immune-related protein was included complement component C1q receptor (CD93). Apoptotic-related protein was included apoptosis-stimulating of p53 protein 2 (TP53BP2). In addition, the expressions of dual specificity mitogen-activated protein kinase kinase 5 (MAP2K5), leucine-rich repeat-containing protein 16A (LRRRC16A), low-density lipoprotein receptor-related protein 6 (LRP6), collagen alpha-1(VII) chain (COL7A1), and pleckstrin homology domain-containing family G member 4B (PLEKHG4B) were also observed in this cluster. In cluster 3, immune-related proteins (interleukin-25) was identified.

Protein annotation and ontology enrichment analysis :

To investigate the properties of identified proteins, we then performed functional enrichment of secreted proteins using PANTHER. The biological characterization of secreted proteins could be classified according to molecular function, biological process, and cellular component (Figure 1). Gene set enrichment analysis revealed that all the differentially expressed proteins were enriched in 31 Gene Ontology (GO) terms ($p < 0.05$), including 10 molecular functions, 13 biological processes, and 8 cellular components. The gene ontology analysis of our secretome suggested these genes were associated with GO molecular function such as binding (33%), catalytic activity (29%), and receptor activity (10%). The GO biological process results revealed several proteins involved in metabolic processes (24%), cellular processes (22%), and biological regulation (13%). In addition, the GO cellular component results revealed several proteins located in cell part (42%), organelle (23%), and extracellular region (11%), and. Proteins that were not described or unspecified in the

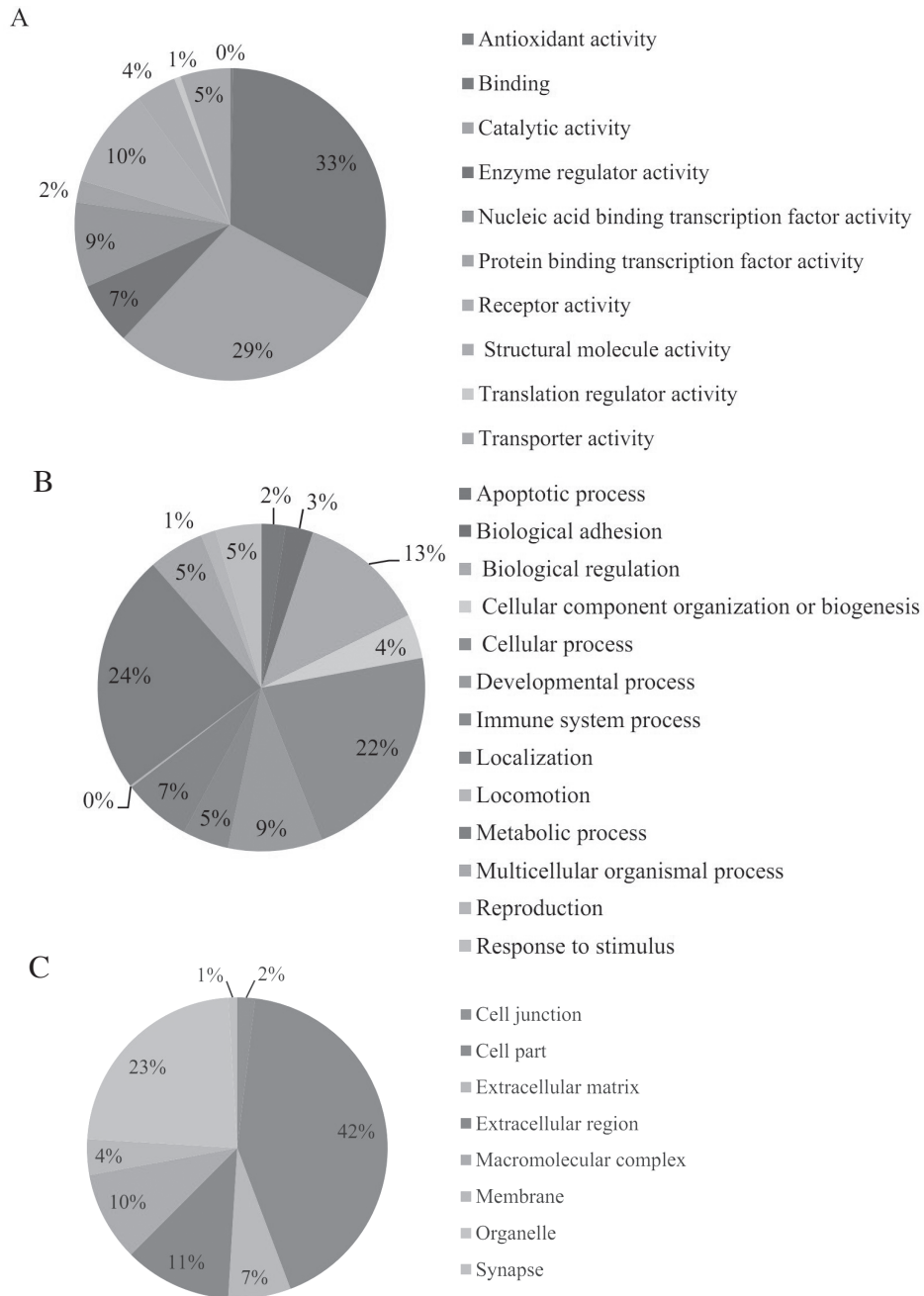
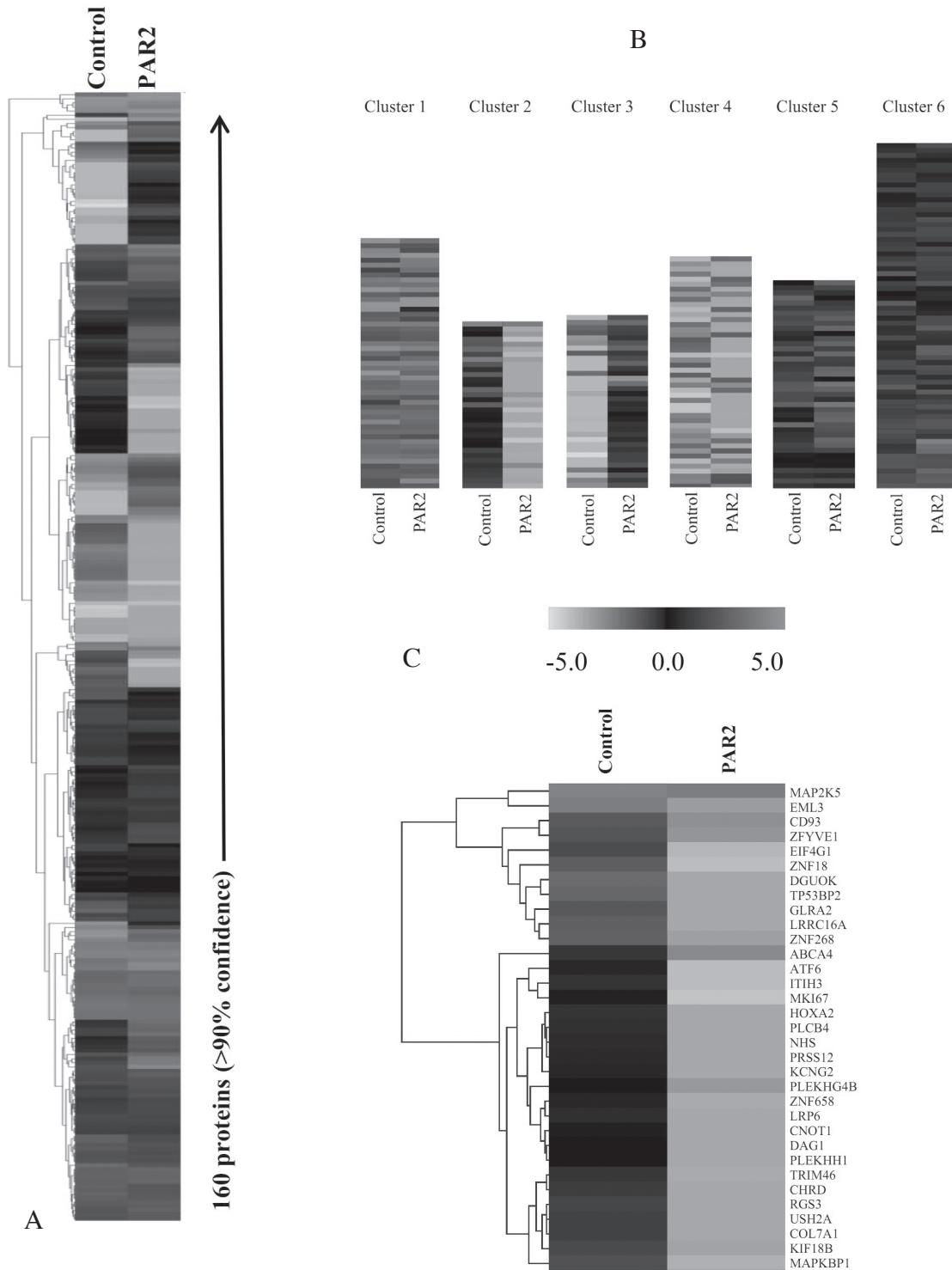


Fig. 1. Analysis of functional distribution of smooth muscle phosphoproteins. Gene ontology characterization of identified phosphoproteins whose expression found to be increased or decreased by 2-fold or greater compared to control, according to (A) GO molecular functions, (B) GO biological processes, and (C) GO cellular component.



Activation in Gastrointestinal Smooth Muscle Cells

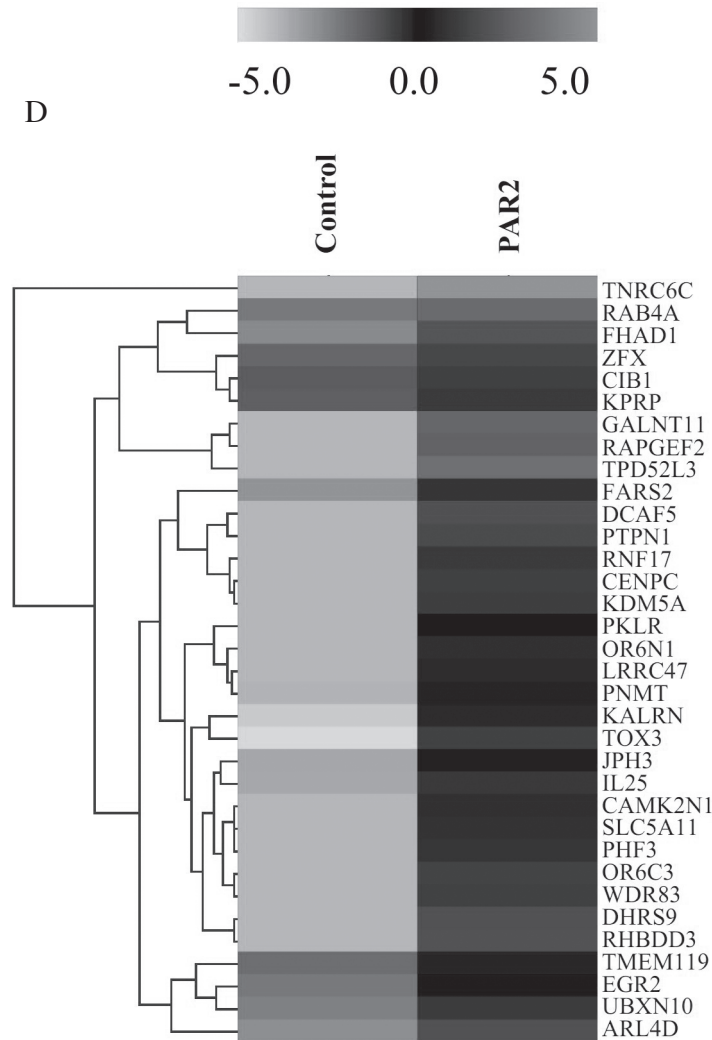


Fig. 2. Heat map of hierarchical clustering analysis of proteins differentially regulated by PAR2. Clustering was done using MeV tools. Analysis was performed based on log₂ intensities of 160 proteins differentially expressed, between the 1 μ M PAR2 treatment and control groups. Rows represent genes and columns represent samples. Color bar indicates log₂-intensity value and corresponding colors (red, black, and green for up-regulated, not changing and down regulated, respectively). The color scale is shown by the bar at the top. Protein genes grouped into 10 clusters on the basis of the similarity of expression (clustering type: K-means clustering, Distance metric: Euclidean distance). The number of the expressed genes and the percentage in each cluster are indicated. (A) Total, (B) protein clusters, (C) cluster 2, and (D) cluster 3.

UniProtKB and GO database were screened out and not further assessed for this report.

Functional classification of secreted proteins revealed a change in secretome composition after treatment. Protein expression profiles were compared between untreated and PAR2-induced sample. Of the 275 differentially expressed proteins we found that 160 proteins had expression levels that differed by more than 2.0 fold in treatment sample when compared to untreated sample, comprising 61 upregulated and 99 downregulated proteins (Table 1). We selected the 160 differentially expressed proteins as candidate secreted proteins associated with PAR2 activation. Details of these proteins are presented in Table 1.

In order to identify significantly enriched pathways and biological processes within the gene sets, pathway and gene ontology were analyzed using 160 differentially expressed proteins via DAVID tools. Functional annotation in DAVID showed that 10 clusters (cluster 1, 2, 3, 4, 5, 6, 8, 9, 13, and 15) were found to be significantly enriched (p -value < 0.05) for 31 GO terms (Table 2). The majority of enriched clusters of pathways and GO biological processes are related to regulation of signal transduction (cluster 1 and 2), developmental process and segmentation (cluster 3 and 4), cytokinesis and cell cycle (cluster 5 and 6), response to biotic stimulus (cluster 8 and 15), programmed cell death (cluster 9), nitrogen compound and nucleic acid metabolic process (cluster 13).

To further interpret the likely roles of differentially expressed proteins involved in PAR2 activation, these proteins were categorized by Reactome cellular pathway. Of the 160 differentially expressed proteins we found that 99 proteins were mapped into 20 pathways as being significantly ($p < 0.05$) overrepresented after PAR2 stimulation. Twenty four biological pathways from the Reactome database relevant for the PAR2 signaling were investigated, and the most significantly enriched functional pathway according to their p -value and FDR values

was interleukin-17 signaling pathway represented in Table 3. The up-regulated protein interleukin-17 receptor E (IL17RE) and interleukin-25 (IL25) (Table 3) was predicted to be involved in this function. The differentially expressed proteins which included in top 20 enriched functional pathways comprised 11 up-regulated and 14 down-regulated proteins upon PAR2 activation.

Discussion

In the present study, we determined the secretory proteins involved in inflammatory process upon PAR2 activation by PAR2-AP in smooth muscle cells using LC-MS/MS based method. Rabbit gastric smooth muscle was used because human tissue was not readily available. It is best known that smooth muscle can change its appearance and its function in response to a wide array of stimuli. This is referred to as the phenotypic plasticity (26). Smooth muscle can lose its contractile apparatus and become a secretory cell in response to the right stimuli. It has been shown that smooth muscle cells secrete highly active signaling proteins (14), indicating the validity of the approach taken. We demonstrate that the PAR2 activation induces robust protein secretion in smooth muscle cells. A total of 310 peptides were detected and found to correspond to 275 proteins. This approach identified 160 proteins with a 2-fold change in treated sample as compared with untreated sample. These proteins could be classified by their functions in inflammation, cytokinesis and cell cycle, regulation of apoptosis, developmental process and response to stress.

Although many of the altered proteins were mainly related to regulation of small G-protein signaling, developmental process, cell cycle and apoptosis, and response to stress, more recent work has focused on the ability of muscle to influence immune function through cytokine and growth factor production. Growing evidence has shown that smooth muscle cells secrete highly active signaling proteins (14). Nonetheless, results are limited at this point to a few cytokines and chemokines such as IL-1 beta (27), IL-8 and IL-6 (20), and monocyte chemotactic protein

Table 1: Identified protein from smooth muscle secretome and relative expression relative abundances of peptides. Protein names which were identified to be significantly upregulated or downregulated by proteomic experiment were shown. Analysis focused on proteins whose expression changed at least ± 2 fold in treated sample compared with control sample. The relative abundances of peptides were expressed as log₂ intensities.

Protein Name	UniProt Accession	Peptide	Control	PAR2	Log ₂ Fold Change
1-phosphatidylinositol 4,5-bisphosphate phosphodiesterase beta-4	Q15147	INGDK	5.47	0	-5.470
2',3'-cyclic-nucleotide 3'-phosphodiesterase	P09543	AAPSDSLPR	2.98	1.08	-1.900
Activating transcription factor 7-interacting protein 1	Q6VMQ6	MEASFGSPSK	9.83	5.03	-4.800
ADP-ribosylation factor-like protein 4D	P49703	EFVQSVPTK	2.14	3.48	1.340
Aldose reductase	P15121	AIADK	6.22	3.16	-3.060
Collagen alpha-1 (V) chain	P20908	VTKFLXR	8	6.76	-1.240
AMP deaminase 2	Q01433	DFYNIR	3.13	0	-3.130
Ankyrin repeat domain-containing protein 39	Q53RE8	DLLAA	5.73	4.37	-1.360
Antigen KI-67	P46013	RQRTVPR	4.91	0.26	-4.650
Apoptosis-stimulating of p53 protein 2	Q13625	ENGVNSPR	7.67	0	-7.670
Atrial natriuretic peptide-converting enzyme	Q9Y5Q5	ASGAR	4.26	8.5	4.240
Beta-1,3-galactosyltransferase 6	Q96L58	HXEVR	6.61	4.05	-2.560
Brain-specific angiogenesis inhibitor 1-associated protein 2-like protein 1	Q9UHR4	AGAFK	0	2.63	2.630
Breast cancer type 2 susceptibility protein	P51587	NASLISTLKK	4.35	3	-1.350
Bridging integrator 3	Q9NQY0	KFGSVFSLNMAVK	9.83	7.9	-1.930
Butyrophilin subfamily 3 member A2	P78410	DHVTR	7.62	6.29	-1.330
Calcium and integrin-binding protein 1	Q99828	GGSGSR	3.63	5.72	2.090
Calcium/calmodulin-dependent protein kinase II inhibitor 1	Q7Z7J9	APPGV	0	4.25	4.250
CAP-Gly domain-containing linker protein 4	Q8N3C7	XGILK	5.03	2.97	-2.060
CCR4-NOT transcription complex subunit 1	A5YKK6	LKVGGVDPK	5.09	0	-5.090
Centlein	Q9NXG0	AAKKK	2.25	0	-2.250
Centriole, cilia and spindle-associated protein	Q6IQ19	GPAEEDTEAR	4.16	2.86	-1.300
Centromere protein C	Q03188	KAKGNMEK	0	5.77	5.770
Centrosomal protein of 290 kDa	O15078	ASGILTSEK	9.66	8.58	-1.080
Chordin	Q9H2X0	AAEGS	4.51	0	-4.510
Chromodomain-helicase-DNA-binding protein 9	Q3L8U1	AGGHK	0	2.35	2.350
Coiled-coil domain-containing protein 168	Q8NDH2	GVLTK	0	2.89	2.890
Collagen alpha-1 (VII) chain	Q02388	GVDGDKGPR	4.35	0	-4.350
Complement component C1q receptor	Q9NPY3	AEAPLAMIR	7.14	1.74	-5.400
Cyclic AMP-dependent transcription factor ATF-6 alpha	P18850	SPVVR	5.28	0.44	-4.840
Prostaglandin G/H synthase 2	P35354	VAKASIDQSR	2.84	0	-2.840

Protein Name	UniProt Accession	Peptide	Control	PAR2	Log ₂ Fold Change
DDB1- and CUL4-associated factor 5	Q96JK2	AGTSHK	0	6.39	6.390
Dehydrogenase/reductase SDR family member 9	Q9BPW9	TFDEK	0	3.47	3.470
Deleted in malignant brain tumors 1 protein	Q9UGM3	YTRIPSR	5.91	4.8	-1.110
Deoxyguanosine kinase, mitochondrial	Q16854	MAAGR	7.91	0	-7.910
Deoxynucleotidyltransferase terminal-interacting protein 1	Q9H147	ATGGK	3.18	1	-2.180
DNA replication licensing factor MCM5	P33992	AGITTTLSNR	6.28	8.31	2.030
DnaJ homolog subfamily B member 2	P25686	AGTQGGARGDAAER	3.36	0.99	-2.370
Dual specificity mitogen-activated protein kinase kinase 5	Q13163	NQQGPP	9.11	2.27	-6.840
Dystroglycan	Q14118	APIIR	4.98	0	-4.980
E3 SUMO-protein ligase EGR2	P11161	NGVAGDGMINIDMTGEK	2.77	4.44	1.670
Echinoderm microtubule-associated protein-like 3	Q32P44	VASGQTAGVDK	8.8	1.33	-7.470
Ecto-NOX disulfide-thiol exchanger 2	Q16206	DMEEAKEK	5.89	4.85	-1.040
Etoposide-induced protein 2.4 homolog	O14681	ATAGH	2.36	0	-2.360
Eukaryotic translation initiation factor 3 subunit B	P55884	DRLSQSK	7.28	4.71	-2.570
FERM, RhoGEF and pleckstrin domain-containing protein 2	O94887	ALTDLPR	10.23	7.41	-2.820
Flap endonuclease GEN homolog 1	Q17RS7	VDTEASK	5.63	6.94	1.310
Forkhead-associated domain-containing protein 1	B1AJZ9	LYLDMSK	2.3	6.57	4.270
Gamma-aminobutyric acid receptor subunit gamma-1	Q8N1C3	GKVLAAAR	5.74	7.72	1.980
Gamma-aminobutyric acid receptor subunit rho-2	P28476	VFPDGHVLYSMR	4.81	6.16	1.350
Glycine receptor subunit alpha-2	P23416	GRTSGYDAR	7.06	0	-7.060
Golgin subfamily A member 2	Q08379	SEETR	5.9	7.48	1.580
Histone H2AX	P16104	APSGGK	6.56	4.1	-2.460
Homeobox protein Hox-A2	O43364	RVEIAALLDLTER	5.56	0	-5.560
Hyccin	Q9BYI3	QGHSK	2.14	0	-2.140
Eukaryotic translation initiation factor 4 gamma 1	Q04637	GGPGGELPR	6.47	0.6	-5.870
Inter-alpha-trypsin inhibitor heavy chain H3	Q06033	AVSQGKTAGLVK	4.7	0.47	-4.230
Interleukin-17 receptor E	Q8NFR9	VASDASGLQR	5.42	7.06	1.640
Interleukin-25	Q9H293	ASEDGPLNSR	1.39	4.05	2.660
Junctophilin-3	Q8WXH2	LGARAEPR	1.41	4.43	3.020
Kalirin	O60229	ETSER	0.49	4.32	3.830
KAT8 regulatory NSL complex subunit 3	Q9P2N6	IPTLIDR	5.81	7.04	1.230
Keratinocyte proline-rich protein	Q5T749	VGGPR	3.53	5.53	2.000
Kinesin-like protein KIF18B	Q86Y91	LQAEVAALR	4.18	1.13	-3.050
Leiomodin-3	Q0VAK6	ISKLDPKK	6.59	4.19	-2.400
F-actin-uncapping protein LRRRC16A	Q5VZK9	EFIFV	7.35	0	-7.350
Leucine-rich repeat-containing protein 42	Q9Y546	TPMAAEPR	4.08	5.19	1.110

Protein Name	UniProt Accession	Peptide	Control	PAR2	Log ₂ Fold Change
Leucine-rich repeat-containing protein 47	Q8N1G4	ADGER	0	5.03	5.030
Leucine-rich repeat-containing protein 7	Q96NW7	ASMTK	2.67	0	-2.670
Limbin	Q86UK5	ATRAAAVDR	3.59	0	-3.590
Low-density lipoprotein receptor-related protein 6	O75581	QAVVK	4.76	0	-4.760
Lysine-specific demethylase 5A	P29375	ATAAK	0	5.66	5.660
Lysine-tRNA ligase	Q15046	ASGGK	1.51	3.03	1.520
Major facilitator superfamily domain-containing protein 4A	Q8N468	EDASSLPR	9.19	6.41	-2.780
Melanoma-associated antigen B1	P43366	AGSSQVSLR	6.57	3.69	-2.880
Metal transporter CNNM2	Q9H8M5	MIVGEEKK	7.21	5.64	-1.570
Methylcytosine dioxygenase TET3	O43151	GDEGR	5.14	2.89	-2.250
Minor histocompatibility antigen H13	Q8TCT9	FFPANFPNR	3.47	0	-3.470
Mitogen-activated protein kinase-binding protein 1	O60336	LFSGVANAR	3.98	0.79	-3.190
MuT5 protein homolog 5	O43196	AAVLSR	3.58	2.43	-1.150
N-acetylglutamate synthase, mitochondrial	Q8N159	GTGGSR	6.48	5.12	-1.360
NACT, LRR and PYD domains-containing protein 9	Q7RTR0	MKGVAL	2.54	0.98	-1.560
NADH dehydrogenase [ubiquinone] 1 alpha subcomplex subunit 6	P56556	EAGGVXGDCLRK	6.15	4.94	-1.210
Nance-Horan syndrome protein	Q6T4R5	DSGDMSVR	5.41	0	-5.410
Neurogenic locus notch homolog protein 3	Q9JUM47	APEGGGGR	5.25	3.38	-1.870
Neurotysin	P56730	SVTKL	5.36	0	-5.360
Olfactory receptor 4F3/4F16/4F29	Q6IEY1	KMKVAMQRLVSK	6.67	8.3	1.630
Olfactory receptor 6C3	Q9NZP0	NQQVKQAFK	0	3.82	3.820
Olfactory receptor 6N1	Q8NGY5	TGILG	0	5.21	5.210
PDZ domain-containing protein 8	Q8NEN9	DTALTR	5.81	2.91	-2.900
PH and SEC7 domain-containing protein 1	A5PKW4	HGSEPR	3.44	4.54	1.100
PHD finger protein 3	Q92576	MMGPLSQASR	0	4.09	4.090
Phenylalanine-tRNA ligase, mitochondrial	Q95363	TIGGDLVEK	2.01	5.35	3.340
Phenylethanolamine N-methyltransferase	P11086	TAVGV	1.11	4.92	3.810
Pleckstrin homology domain-containing family G member 4B	Q96PX9	RADLDGPR	4.94	1.43	-3.510
Pleckstrin homology domain-containing family H member 1	Q9ULM0	APGTPR	4.94	0	-4.940
Plexin-B3	Q9ULL4	QVTLVPR	9.22	7.58	-1.640
Polypeptide N-acetylgalactosaminyltransferase 11	Q8NCW6	MMGSVTVR	0	7.33	7.330
Potassium voltage-gated channel subfamily G member 2	Q9UJ96	LRCCAPVR	5.28	0	-5.280
pre-rRNA processing protein FTSJ3	Q8Y81	GVGRK	1.11	0	-1.110
Probable ATP-dependent RNA helicase DDX60	Q8Y21	IASKK	3.64	0	-3.640
Protein ERGIC-53	P49257	MAGSR	0	2.76	2.760

Protein Name	UniProt Accession	Peptide	Control	PAR2	Log ₂ Fold Change
Protein FAM24A	A6NFZ4	LSSSYDFAR	3.75	2.52	-1.230
Protein FAM60A	Q9NP50	AGPSLKTTLKPKK	6.37	4.33	-2.040
Protein KIBRA	Q8IX03	SMSSLSPR	4.64	2.88	-1.760
Protein salvador homolog 1	Q9H4B6	LSAPSYLAR	6.39	7.79	1.400
Protein SET	Q01105	SAPAAK	2.06	0.34	-1.720
Putative helicase MOV-10	Q9HCE1	MKPGSEISK	2.78	0	-2.780
Pyruvate kinase PKLR	P30613	AALGPK	0	4.6	4.600
RalGTPase-activating protein subunit alpha-1	Q6GYQ0	ATMLTDK	1.57	0	-1.570
Rap guanine nucleotide exchange factor 2	Q9Y4G8	SSFGK	0	7.11	7.110
Ras-related protein Rab-4A	P20338	RDLDAER	2.78	7.5	4.720
Regulator of G-protein signaling 3	P49796	AGGSR	4.27	0	-4.270
Remodeling and spacing factor 1	Q96T23	AAAAAR	4.31	2.92	-1.390
Retinal-specific ATP-binding cassette transporter	P78363	GNGFAGEGKGVA	4.61	1.89	-2.720
Rho guanine nucleotide exchange factor 11	O15085	MIHEGPLTWR	6.08	4.87	-1.210
Rho guanine nucleotide exchange factor 17	Q96PE2	LADVLSPR	8.42	10.73	2.310
Rhomboid domain-containing protein 3	Q9Y3P4	GPGRP	0	3.42	3.420
RING finger protein 17	Q9BXT8	MMNEIQK	0	5.52	5.520
Scavenger receptor cysteine-rich type 1 protein M130	Q86VB7	QLGCGSALK	1.47	0	-1.470
Secreted frizzled-related protein 2	Q96HF1	QGGELVITSVK	2.54	1.36	-1.180
Semaphorin-3F	Q13275	TMTISSK	0.96	3.01	2.050
Serine/threonine-protein kinase VRK2	Q86Y07	DPVAVQTAK	5.42	3.49	-1.930
Serine/threonine-protein phosphatase 2A 65 kDa regulatory subunit A beta isoform	P30154	AAKGPALSAACR	7.34	5.03	-2.310
Serine-protein kinase ATM	Q13315	AADIR	3.66	2.2	-1.460
Smoothelin	P53814	SLSVLSPR	4.8	3.49	-1.310
Sodium/hydrogen exchanger 9B1	Q4ZJ14	ATVQG	5.46	3.03	-2.430
Sodium-dependent serotonin transporter	P31645	GVAGDK	6.21	3.9	-2.310
Sodium/myo-inositol cotransporter 2	Q8WWX8	FGGSR	0	4.16	4.160
Structural maintenance of chromosomes protein 3	Q9UQE7	AATGK	4.11	5.98	1.870
Synemin	O15061	RSPGPGSPDR	4.29	3.01	-1.280

Protein Name	UniProt Accession	Peptide	Control	PAR2	Log ₂ Fold Change
TATA-binding protein-associated factor 172	O14981	DAVETNEK	6.02	3.78	-2.240
Tetratricopeptide repeat protein 28	Q96AY4	DGTSSLPR	7.55	6.29	-1.260
Titin	Q8WZ42	NAVGVSLPR	6.42	5.19	-1.230
Toll-like receptor 2	O60603	AAIKS	2.08	3.18	1.100
TOX high mobility group box family member 3	O15405	AIGEK	0.12	3.85	3.730
Transcription factor 15	Q12870	RAGGAGSVWVVR	3.18	0	-3.180
Transcription factor TFIIIB component B'' homolog	A6H8Y1	EEIGLVEK	1.48	0	-1.480
Transmembrane protease serine 11D	O60235	NNAAK	3.33	0	-3.330
Transmembrane protein 119	Q4V9L6	AGGPR	3.13	4.93	1.800
Trinucleotide repeat-containing gene 6C protein	Q9HCJ0	QQEQKQLLK	0	9.97	9.970
Tripartite motif-containing protein 46	Q7Z4K8	AGAIK	4.6	0.93	-3.670
Tumor protein D55	Q96J77	LGDVKKSATFR	0	7.76	7.760
Tyrosine-protein phosphatase non-receptor type 1	P18031	GVVMLNR	0	6.13	6.130
Ubiquitin-conjugating enzyme E2 G1	P62253	RKVARCVR	0	2.21	2.210
UBX domain-containing protein 10	Q96LJ8	TRPSLPR	2.56	4.01	1.450
Usherin	O75445	GVIEK	4.38	0	-4.380
Vitellogenin outer layer protein 1 homolog	Q7Z5L0	GNAER	3.08	0	-3.080
V-set and immunoglobulin domain-containing protein 10	Q8N0Z9	SLLNLTVADLPR	4.31	5.58	1.270
WD repeat domain-containing protein 83	Q9BRX9	GHAGK	0	3.85	3.850
YTH domain-containing protein 1	Q96MU7	LSSSVRAVRK	5.71	3.61	-2.100
Zinc finger FYVE domain-containing protein 1	Q9HBF4	AVPSR	6.92	1.57	-5.350
Zinc finger protein 18	P17022	GMFGDEEPR	7.29	0.43	-6.860
Zinc finger protein 268	Q14587	SNLTDHQR	4.85	0.92	-3.930
Zinc finger protein 416	Q9BWM5	HCSAKDSLRL	2.1	0.93	-1.170
Zinc finger protein 462	Q96JM2	ARIK	3.86	5.93	2.070
Zinc finger protein 574	Q6ZN55	ATPTK	0	1.25	1.250
Zinc finger protein 658	Q5TYW1	TATPK	7.45	1.24	-6.210
Zinc finger protein 717	Q9BY31	IHTGGKPHGCNK	7.01	8.93	1.920
Zinc finger X-chromosomal protein	P17010	EVGLP	3.31	5.97	2.660

Table 2. Annotation clusters with significantly enriched GO biological processes and pathways in PAR2-AP treated samples. Enrichment analysis was performed for disease (OMIM_DISEASE), functional categories (COG_ONTOLOGY), GO BP (PANTHER_BP_ALL and GOTERM_BP_ALL) and pathway (KEGG and Reactome) using DAVID tools (functional annotation cluster). Genes or terms were ranked based on the p-value. Only significant annotation terms (p-value < 0.05) are shown. FDR: false discovery rate.

Category	Term	p-value	FDR (%)	Genes symbols
Annotation Cluster 1	Enrichment Score: 2.06			
GOTERM_BP_ALL	GO:0051056 Regulation of small GTPase mediated signal transduction	0.001	1.99	O94887, Q6GYQ0, O60229, Q96PE2, Q8WZ42, Q9Y4G8, Q96PX9, O15085, A5PKW4
GOTERM_BP_ALL	GO:0035023 Regulation of Rho protein signal transduction	0.001	2.29	O94887, O60229, Q96PE2, Q8WZ42, Q96PX9, O15085
GOTERM_BP_ALL	GO:0046578 Regulation of Ras protein signal transduction	0.008	12.69	O94887, O60229, Q96PE2, Q8WZ42, Q96PX9, O15085, A5PKW4
Annotation Cluster 2	Enrichment Score: 1.34			
GOTERM_BP_ALL	GO:0035023 Regulation of Rho protein signal transduction	0.001	2.29	O94887, O60229, Q96PE2, Q8WZ42, Q96PX9, O15085
GOTERM_BP_ALL	GO:0046578 Regulation of Ras protein signal transduction	0.008	12.69	O94887, O60229, Q96PE2, Q8WZ42, Q96PX9, O15085, A5PKW4
Annotation Cluster 3	Enrichment Score: 1.27			
GOTERM_BP_ALL	GO:0035282 Segmentation	6.80E-04	1.09	Q13315, Q96HF1, P11161, Q12870, O43364
GOTERM_BP_ALL	GO:0003002 Regionalization	0.006	9.54	Q13315, Q96HF1, O75581, P11161, Q12870, O43364, Q9H2X0
GOTERM_BP_ALL	GO:0007420 Brain development	0.010	15.98	Q13315, O15078, P31645, P51587, P11161, O43364, Q9UM47, Q9H2X0
GOTERM_BP_ALL	GO:0007389 Pattern specification process	0.024	33.09	Q13315, Q96HF1, O75581, P11161, Q12870, O43364, Q9H2X0
GOTERM_BP_ALL	GO:0009952 Anterior/posterior pattern formation	0.029	38.68	Q13315, Q96HF1, O75581, Q12870, O43364
GOTERM_BP_ALL	GO:0001756 Somitogenesis	0.032	41.47	Q13315, Q96HF1, Q12870

Annotation Cluster 4 GOTERM_BP_ALL	Enrichment Score: 1.18 GO:0048856 Anatomical structure development	0.015	21.36	Q96HF1, Q9UGM3, P20908, Q8WZ42, O43364, Q9BPW9, Q13163, Q6T4R5, Q13315, O15078, P53814, Q9UM47, Q14118, A5PKW4, Q02388, O94887, P23416, P31645, P35354, P11161, O75445, Q9Y5Q5, O60229, P09543, O75581, Q12870, P51587, Q9H2X0, Q9NQY0, Q13275, Q9H293, O15085
GOTERM_BP_ALL	GO:007275 Multicellular organismal development	0.028	36.70	Q96HF1, Q9UGM3, P20908, Q8WZ42, Q9BPW9, O43364, Q13163, Q6T4R5, Q13315, O15078, P53814, P29375, Q9UM47, Q14118, A5PKW4, Q02388, O94887, P23416, P31645, P35354, P11161, Q9ULL4, O75445, Q9BXT8, Q9Y5Q5, Q92576, O60229, P09543, O75581, Q12870, P51587, Q9H2X0, Q13275, Q9H293
GOTERM_BP_ALL	GO:0032502 Developmental process	0.038	46.17	Q96HF1, Q9UGM3, P20908, Q8WZ42, Q9BPW9, O43364, Q13163, Q6T4R5, Q13315, O15078, P53814, P29375, Q9UM47, Q14118, A5PKW4, Q02388, O94887, P23416, P31645, P35354, P11161, O75445, Q9ULL4, Q9BXT8, Q9Y5Q5, Q92576, O60229, P09543, O75581, Q12870, P51587, Q9H2X0, Q9NQY0, Q13275, O15085, Q9H293
GOTERM_BP_ALL	GO:0032501 Multicellular organismal process	0.042	49.69	Q9UGM3, Q96HF1, P20908, Q8WZ42, P78363, O43196, O60235, Q9BPW9, O43364, Q8N1C3, Q13163, Q6T4R5, Q9NZP0, Q13315, O15078, P53814, P29375, Q9UM47, Q14118, A5PKW4, P16104, Q02388, O94887, Q6IEY1, P23416, P31645, P35354, P49257, P11161, O75445, Q9ULL4, Q9BXT8, Q9Y5Q5, Q92576, O60229, Q7Z5L0, P09543, Q8NGY5, O75581, Q12870, P51587, P28476, Q9H2X0, Q13275, O15085, Q9H293

Annotation Cluster 5 GOTERM_BP_ALL	Enrichment Score: 1.04 GO:0000910 Cytokinesis	0.046	53.20	P51587, Q9NQY0, O15085
Annotation Cluster 6 GOTERM_BP_ALL	Enrichment Score: 0.94 GO:0007126 Meiosis	0.001	2.19	Q13315, P46013, O43196, P51587, Q9UQE7, P16104
GOTERM_BP_ALL	GO:0051327 M phase of meiotic cell cycle	0.001	2.19	Q13315, P46013, O43196, P51587, Q9UQE7, P16104
GOTERM_BP_ALL	GO:0051321 Meiotic cell cycle	0.002	2.39	Q13315, P46013, O43196, P51587, Q9UQE7, P16104
GOTERM_BP_ALL	GO:0007292 Female gamete generation	0.002	3.37	Q13315, Q7Z5L0, P35354, O43196, P51587
GOTERM_BP_ALL	GO:0006259 DNA metabolic process	0.026	34.58	Q13315, P33992, Q01105, Q99828, Q17RS7, O43196, P51587, Q6VMQ6, Q9UQE7, P16104
GOTERM_BP_ALL	GO:0006281 DNA repair	0.032	40.77	Q13315, Q99828, Q17RS7, O43196, P51587, Q9UQE7, P16104
Annotation Cluster 8 GOTERM_BP_ALL	Enrichment Score: 0.84 GO:0009607 Response to biotic stimulus	0.042	50.10	Q9UGM3, P30613, P35354, O43196, P25686, O60603, P18850, Q9H293
Annotation Cluster 9 GOTERM_BP_ALL	Enrichment Score: 0.78 GO:0006917 Induction of apoptosis	0.018	25.27	Q13315, O60229, Q13625, Q96PE2, O14681, P51587, O60603, O15085
GOTERM_BP_ALL	GO:0012502 Induction of programmed cell death	0.018	25.60	Q13315, O60229, Q13625, Q96PE2, O14681, P51587, O60603, O15085
GOTERM_BP_ALL	GO:0043065 Positive regulation of apoptosis	0.028	36.52	Q13315, O60229, Q13625, Q96PE2, P35354, O14681, P51587, O60603, O15085
GOTERM_BP_ALL	GO:0043068 Positive regulation of programmed cell death	0.029	37.57	Q13315, O60229, Q13625, Q96PE2, P35354, O14681, P51587, O60603, O15085
GOTERM_BP_ALL	GO:0010942 Positive regulation of cell death	0.029	38.28	Q13315, O60229, Q13625, Q96PE2, P35354, O14681, P51587, O60603, O15085
Annotation Cluster 13 GOTERM_BP_ALL	Enrichment Score: 0.69 GO:0006807 Nitrogen compound metabolic process	0.021	29.36	Q96MU7, Q9BY31, O43196, Q96L58, Q9HCE1, O43364, Q6VMQ6, Q9BWM5, Q9BRX9, Q13315, A5YKK6, Q96JM2, Q17RS7, P17022, Q14587, Q01433, P29375, Q9UQE7, Q3L8U1, Q9UM47, P16104, Q8N159, Q06033, Q01105, Q99828, Q5TYW1, Q8IY81, P11086, Q04637, P11161, A6H8Y1, P33992, Q15046, Q92576, Q96T23, Q6ZN55, O95363, P09543, P17010, Q12870, P51587, Q16854, P18850

Activation in Gastrointestinal Smooth Muscle Cells

GOTERM_BP_ALL	GO:0006139 Nucleobase, nucleoside, nucleotide and nucleic acid metabolic process	0.029	37.38	Q96MU7, Q9BY31, O43196, Q9HCE1, O43364, Q6VMQ6, Q9BWM5, Q9BRX9, Q13315, Q96JM2, A5YKK6, Q17RS7, P17022, Q14587, Q01433, P29375, Q9UQE7, Q3L8U1, Q9UM47, P16104, Q01105, Q99828, Q5TYW1, Q8IY81, Q04637, P11161, A6H8Y1, P33992, Q15046, Q92576, Q96T23, Q6ZN55, Q95363, P09543, P17010, Q12870, P51587, Q16854, P18850
GOTERM_BP_ALL	GO:0034641 Cellular nitrogen compound metabolic process	0.034	42.79	Q96MU7, Q9BY31, O43196, Q9HCE1, O43364, Q6VMQ6, Q9BWM5, Q9BRX9, Q13315, Q96JM2, A5YKK6, Q17RS7, P17022, Q14587, Q01433, P29375, Q9UQE7, Q3L8U1, Q9UM47, P16104, Q8N159, Q01105, Q99828, Q5TYW1, Q8IY81, P11086, Q04637, P11161, A6H8Y1, P33992, Q15046, Q92576, Q96T23, Q6ZN55, Q95363, P09543, P17010, Q12870, P51587, Q16854, P18850
GOTERM_BP_ALL	GO:0065007 Biological regulation	0.048	55.04	P20908, P78363, Q6VMQ6, Q9BPW9, Q96PX9, Q15147, Q9NZP0, P49796, A5YKK6, Q6GYQ0, O14981, Q8WXH2, Q9NXG0, Q9UQE7, O94887, Q6IEY1, Q01105, P35354, P49257, Q04637, Q9ULL4, Q9UHR4, Q6ZN55, Q13625, Q8NGY5, P62253, Q12870, P28476, O60603, P49703, Q16206, Q9H4B6, Q96PE2, Q8WZ42, Q9BY31, O14681, Q9Y4G8, O43364, Q9HCE1, Q13163, Q9BWM5, Q13315, Q96JM2, P17022, Q14587, P29375, Q3L8U1, Q9UM47, A5PKW4, Q9UJ96, P16104, P31645, Q5TYW1, P11161, O75445, P55884, P18031, Q9Y5Q5, P33992, A6H8Y1, P20338, O60229, Q96T23, Q9HCJ0, P17010, O75581, P51587, P18850, Q9H2X0, Q13275, Q9NQY0, O15085, Q8NEN9
Annotation Cluster 15 GOTERM_BP_ALL	Enrichment Score: 0.55 GO:0009607 Response to biotic stimulus	0.042	50.10	Q9UGM3, P30613, P35354, O43196, P25686, O60603, P18850, Q9H293

Table 3. Lists of top 20 significantly enriched pathways in PAR2-AP treated samples. Pathway overrepresentation analysis was performed using Reactome tools with functional interactors. Genes or terms were ranked based on the p-value. Only significant annotation terms (p-value < 0.05) are shown. FDR: false discovery rate.

Pathway name	p-value	FDR	Entities found	Interactors found
Interleukin-17 signaling	5.21E-03	0.62	Q8NFR9, Q9H293	
Glycolysis	1.07E-02	0.62	P30613, P30154	
Purine salvage	1.32E-02	0.62	Q01433, Q16854	
Fructose metabolism	2.94E-02	0.62	P15121	Q08379
Deposition of new CENPA-containing nucleosomes at the centromere	3.25E-02	0.62	Q96T23, Q03188, P16104	
Nucleosome assembly	3.25E-02	0.62	Q96T23, Q03188, P16104	
Negative regulation of TCF-dependent signaling by WNT ligand antagonists	3.49E-02	0.62	Q96HF1, O75581	O75581
Inhibition of PKR	3.49E-02	0.62		Q8IY81, Q9HCE1
YAP1- and WWTR1 (TAZ)-stimulated gene expression	3.85E-02	0.62	Q3L8U1	Q13625, Q9Y4G8
Defective POMT2 causes MDDGA2, MDDGB2 and MDDGCG2	3.89E-02	0.62	Q14118	Q14118
Defective POMT1 causes MDDGA1, MDDGB1 and MDDGCG1	3.89E-02	0.62	Q14118	Q14118
Defective POMGNT1 causes MDDGA3, MDDGB3 and MDDGCG3	3.89E-02	0.62	Q14118	Q14118
GABA A (rho) receptor activation	3.89E-02	0.62	P28476	
Fructose biosynthesis	3.89E-02	0.62	P15121	
Resolution of D-loop Structures through Holliday Junction Intermediates	4.10E-02	0.62	Q13315, Q17RS7, P51587	Q08379, P51587
Resolution of D-Loop Structures	4.22E-02	0.62	Q13315, Q17RS7, P51587	Q08379, P51587
The canonical retinoid cycle in rods (twilight vision)	4.40E-02	0.62	P78363, Q9BPW9	
Transport of the SLBP Dependant Mature mRNA	4.63E-02	0.62		Q13625, Q04637, P55884
Ligand-gated ion channel transport	4.72E-02	0.62	P23416, P28476	
Signaling by Hippo	4.82E-02	0.62	Q8IX03, Q9H4B6	Q13625, Q9Y4G8, Q9H4B6

(MCP) (18). These active signaling proteins are suggested to be very important in cell proliferation (28) and the development of non-immune diseases with etiological origins in inflammatory processes such as atherosclerosis (18) as well as that of immune system disorders like asthma (20) and inflammatory bowel diseases (29,30). However, considering the variety of secretory proteins that are available much less is known concerning the proteins that synthesize and secrete from gastrointestinal smooth muscle cells and their significance of these proteins in the context of inflammatory processes, and the present discussion will therefore be restricted to proteins involved in inflammatory responses, growth and cell survival.

PAR2 influences the secretion of inflammatory molecules : Role of PAR2 in the regulation of inflammation is supported by several studies. Inflammatory mediators such as interleukin 1 alpha, tumor necrosis factor alpha and lipopolysaccharide increased the expression of PAR2 in cultured human umbilical vein endothelial cells (31). PAR2 activation also stimulates the release of prostanoids in endothelial cells (32) as well as the release of IL-6, IL-8 and PGE2 in fibroblasts (33). In the gastrointestinal tract, PAR2 has been reported to be constitutively expressed in various cell types such as smooth muscle cells, interstitial cells of Cajal, and enterocytes (1,13, 34). Recent evidence has shown that activation of PAR2 increase impairment of the epithelial barrier, neutrophil infiltration, and pro-inflammatory cytokines secretion (22, 35) which are parameters of inflammation.

In this study, the immune-related proteins of smooth muscle cell in response to PAR2 have been characterized. In our quantitative secretome analysis, the secreted proteins released from smooth muscle cells during PAR2 activation including cytokine (IL-25) and receptors (IL-17RE and TLR2).

IL-25 (also known as IL-17E) can stimulate the production of IL-10 and inhibits production of mucosal IFN-gamma in DSS-induced colitis (36).

IL-25 also promotes type 2 helper T (Th2) cell responses (37). Type 2 responses assist with the resolution of cell-mediated inflammation. Recombinant IL-25 is able to significantly inhibit the production of IL-1 beta, IL-6, and TNF-alpha by peripheral blood mononuclear cells from active Vogt-Koyanagi-Harada syndrome patients (38). Contrary to these findings, it has been shown that IL-17E induces activation of NF-kB and stimulates production of the proinflammatory chemokine IL-8 in renal cell carcinoma cell lines (39).

IL-17RE is a specific receptor for IL-17C (40). Activation of IL-17RE stimulates to production of antibacterial peptides as well as pro-inflammatory molecules such as TNF and IL-1 beta via NF-kB and MAPK signaling pathway (40-43). In contrast to that IL-17 may play a protective role depending on the state of disease. There is evidence shown that IL-17R-deficient mice are more susceptible to alveolar bone loss induced by *P. gingivalis* (23). These protective effects of IL-17 could be attributed to its ability to regulate COX-2 and PGE2 production.

In addition, we showed that TLR2 is present in culture supernatant of smooth muscle cells, its levels is increased after PAR2 activation. In agreement with our results, recent evidence has identified a linkage between PAR2 and TLR2. PAR2 is needed for TLR2 mRNA expression as determined by silencing PAR2 in cultured epithelial cells with subsequent bacterial stimulation (44). TLR over-activation may lead to end organ damage and serious acute and chronic inflammatory conditions. Therefore, TLR responses must be tightly regulated to control disease outcomes. A soluble form of TLR2 (sTLR2) has recently been identified as a regulator of TLR2-mediated inflammatory responses to bacteria. sTLR2 acts as a decoy microbial receptor and disrupts the interaction of TLR2 with its co-receptor, CD14. Therefore, it is capable of blunting immune responses without abrogating microbial recognition (45). The present study shows that TLR2 is identified in culture supernatant of smooth muscle cell and

assumed to be in its soluble form which may participate in regulating the inflammatory response. Taken together, PAR2 may contribute to protective role during inflammation since PAR2-AP stimulates secretion of IL-25, IL-17RE, and TLR2 from smooth muscle cells.

Protein expression profiling of culture supernatant revealed down-regulation of prostaglandin G/H synthase 2 (PTGS2), sCD93, and CD163 during PAR2 activation. PTGS2 (also known as cyclooxygenase-2 or COX-2) converts arachidonate to prostaglandin H₂ (PGH₂) which can then be metabolized to several products with differing biologic activities, including prostacyclin, thromboxane, prostaglandin D₂, prostaglandin E₂, and prostaglandin F_{2a}. Prostanoids exert both pro-inflammatory and anti-inflammatory actions not only by acting as mediators of acute inflammation but also by regulating gene expression in mesenchymal and epithelial cells at inflammatory site. The present study shows that the smooth muscle cells secrete COX-2 either constitutively or after stimulation with PAR2-AP. Cox-2 is an endoplasmic reticulum-resident enzyme and its expression is inducible (46). In agreement with our results, COX-2 is capable of secreting from goblet cells into the intestinal lumen along with mucins. High mucin COX-2 from goblet cells may increase luminal prostaglandin synthesis, alter epithelial permeability, and modulate intestinal immune responses (47). Thus reduced level of COX-2 after stimulation with PAR2-AP may lead to the anti-inflammatory effects.

sCD93 is a receptor for complement C1q, mannose-binding lectin (MBL2), and pulmonary surfactant protein A (SPA) (48-50). The function of sCD93 is involved in removal or destruction of pathogens and immune complexes mediated by monocyte and macrophage phagocytosis (50). A soluble form of CD93 (sCD93) has recently been identified (51). It was demonstrated that sCD93 level is increased during inflammation *in vivo* (52). Serum level of sCD93 is increased in asthmatic patients compared to healthy controls (53). High level of sCD93 in peritoneal lavage

fluid from wild-type mice significantly enhances engulfment of apoptotic cells *in vitro* when compared to inflammatory fluid from sCD93-deficient mice [52]. Consistent with the previous observation that sCD93 induced monocyte adherence and enhanced phagocytosis (54). Thus, reduced level of sCD93 after PAR2 activation may lead to defective clearance of apoptotic cells. To our knowledge, this is the first report to identify the smooth muscle cells as a source of sCD93.

CD163 is a cell surface glycoprotein that is required for clearance and endocytosis of apoptotic cells or hemoglobin/haptoglobin complexes by macrophages (55). Recently soluble form of CD163 (sCD163) has been identified. Soluble CD163 is a normal plasma protein with normal level to be in the range of 0.7–4.69 $\mu\text{g/ml}$ (56). sCD163 actively inhibits phorbol-ester-induced proliferation of lymphocytes (57). Only the soluble form of the CD163 participates in anti-inflammation by inhibition of activated T-lymphocyte, whereas the clearance of hemoglobin uses CD163 in its cell-bound form (58). These observations confirm that sCD163 participates in the anti-inflammatory process, through the reduction of immune response. Thus, reduced level of sCD163 after PAR2 activation may lead to the reduction of anti-inflammatory response.

Taken together, our data support previous studies that PAR2 is capable of regulating inflammation through not only on upregulation of pro-inflammatory mechanisms but also on suppression of the anti-inflammatory response by smooth muscle cells. Activation of PAR2 stimulates the release of cytokine and soluble proteins such as IL-25, IL-17RE and TLR2 which further stimulate the production of pro-inflammatory cytokines and immunoregulating cytokines. In addition, activation of PAR2 attenuates an anti-inflammatory program through suppression of sCD93, sCD163, and COX-2 secretion. Further studies are needed to address how IL-25, IL-17RE, TLR2, COX-2, sCD93, and sCD163 fit into the existing network of the

numerous inflammatory and anti-inflammatory proteins.

PAR2 positive regulation of apoptosis and cell cycle : Apoptosis is a physiological phenomenon. The significance of apoptosis is to remove senescent cells (59) and the over functional cells. Deregulation of apoptosis is associated with the pathogenesis of a number of disorders, such as tumor cell growth. Interestingly, differentially expressed proteins related to apoptotic process were found upon activation of PAR2. In our quantitative secretome analysis, the secreted proteins identified included serine-protein kinase ataxia telangiectasia mutated (ATM), breast cancer type 2 susceptibility protein (BRCA2), and apoptosis-stimulating of p53 protein 2 (ASPP2).

ATM is a serine protein kinase implicated in cell cycle regulation and DNA repair (60). Upon DNA damage, eukaryotic cells activate multiple events such as ATM-Chk2 and/or ATR-Chk1 checkpoint to arrest the cell cycle and initiate DNA repair (61). If damage is beyond repair, ATM kinase employs apoptosis to remove excessively damaged cells and stimulates cytokine secretion to alert neighboring cells. A defect in ATM kinase has severe consequences in repairing certain types of damage to DNA. All ataxia telangiectasia (AT) patients contain mutations in the *ATM* gene. ATM kinase is the DNA repair gene shown to be involved in cancer predisposition. Leukemia and lymphoma is the most frequently malignancy found in 38% of AT homozygotes (62). ATM kinase alterations are present at diagnosis in about 25% of individuals with chronic lymphocytic leukemia. These alterations are associated with a poor prognosis (63). The mutated *ATM* genes predispose to breast cancer development and adverse radiotherapy responses (64). ATM kinase augments cell survival by activating NF-kappaB (65,66). ATM kinase is also able to promote the phosphorylation of cyclin D1 Thr286 (67). Phosphorylation of cyclin D1 promotes the nuclear-to-cytoplasmic redistribution of cyclin D1 during S phase of the cell cycle and inhibits the

process of cell division (68). Therefore, ATM kinase appears essential for regulated cell division. There has thus far, been one report in which activation of PAR2 promoted DNA synthesis, upregulated Cyclin D1 activity, and increased colonic cancer cell proliferation (69). The present study shows that activation of PAR2 promotes ATM kinase secretion by smooth muscle cell. This result implies possible role of PAR2 in the regulation of cell division and may involve in the manipulation of cell survival outcomes after cell stress.

Breast cancer type 2 susceptibility protein (*BRCA2*) is a human tumor suppressor gene and responsible for repairing DNA. *BRCA2* protein has been shown to be able to bind to RAD51, p53, and p21^{WAF-1/CIP1} proteins. It has been shown that *BRCA2*-defective cancer cells are unable to repair the double-strand DNA breaks induced by ionizing radiation (70). Deficiency of either RAD51 or *BRCA2* protein in embryonic mice leads to extreme sensitivity to irradiation, suggesting a role in double-stranded DNA break repair (71). Both p21^{WAF-1/CIP1} and p53 protein are known to cause cell cycle arrest, implicating *BRCA2* in the DNA repair process. *BRCA2* protein is associated with high risks of breast cancer. *BRCA2* is a nuclear protein and is induced in late G1/earlyS phase, before DNA synthesis (72,73). In spite of this *BRCA2* protein has sequence homology and biochemical analogy to the granin family of secreted proteins, suggesting *BRCA2* is a secreted protein (74). Bernard-Gallon *et al.* (75) demonstrated that *BRCA2* proteins are localized in the cytoplasm and cell nuclei of normal mammary tissues, of carcinomas in situ, and of invasive carcinomas as well as in secretions inside the ducts of mammary tissue. However, the breast is an exocrine gland, thus becoming secretory in nature. Surprisingly, we identify *BRCA2* protein from supernatant of primary cultured smooth muscle cell using LC-MS/MS method. Although the primary role of smooth muscle cells is contraction, they exhibit their specialized secretory function. Our finding suggests that

BRCA2 protein is secreted in the secretome of smooth muscle cell and the secretion is decreased in the presence of PAR2-AP. Reduced levels of BRCA2 protein in cells may allow the accumulation of unrepaired DNA damages and can lead to increased mutations. Some of these mutations can cause cells to divide in an uncontrolled way and form a tumor. To our knowledge, this is the first report to identify the smooth muscle cells as a source of BRCA2 protein.

Apoptosis-stimulating of p53 (ASPP) protein 2 (also called ASPP2) is a pro-apoptotic regulator that belongs to a member of ASPP family of p53 interacting proteins. ASPP2 regulates apoptosis and cell growth through interactions with other regulatory molecules including members of the p53 family. ASPP2 induces apoptosis via stimulation the apoptotic function of p53 but not cell cycle arrest (76). Co-expression of ASPP2 with p53 significantly enhanced the transactivation function of p53 on promoters of proapoptotic genes, such as Bax and PIG3 (76). The expression of ASPP2 is frequently suppressed in many cancers (77-79). Here, we identify ASPP2 from supernatant of primary cultured smooth muscle cells. The protein level of ASPP2 is absent in cells stimulated with PAR2-AP but increases in untreated samples. In pathological conditions, the expression of ASPP2 can suppress tumor growth and confer cellular sensitivity to treatments. Lack of costimulators of p53, as in case of PAR2-activation, could also account for the loss of the tumor suppressor function of p53 which may contribute to increase cell survival. Hence, PAR2 may inhibit the apoptotic function of p53 by lower ASPP2 protein level.

Proteases activate PARs by irreversible cleavage, so that the exposed tethered ligand is always available to interact with the cleaved receptor. Thus activation would result in sustained signaling unless there were efficient mechanisms to terminate the signal. Nonetheless, during normal physiological condition, signaling by PAR2 is efficiently

terminated by receptor phosphorylation and association with β -arrestins (80). In addition, the action of protease can be terminated by its removal from the vicinity of the receptor. Altered endothelial or epithelial integrity is thought to expose the underlying smooth muscle cells to proteases that derive from the circulation, inflammatory cells, and from intestinal lumen. Thus proteases are always available for receptor activation. Prolonged activation of PAR2 alters protein secretion patterns in gastrointestinal smooth muscle cells. Here we reported that many of the altered proteins were mainly related to regulation of small G-protein signaling, developmental process, cell cycle, apoptosis, and response to stress. Interference with the normal signaling by prolonged activation of PAR2 can alter the balance among the different pathways responding to that signal, thus generating functional heterogeneity that may affect proliferation, quiescence, survival, apoptosis, or inflammation. Many proteases that activate PARs are produced during inflammation. These proteases derive from inflammatory cells, the coagulation cascade and other sources. Beside expression of PARs themselves are also elevated during inflammation (31). PAR2 agonists activate the NF-kappa B pathway in keratinocytes (81) and endothelial cells (82). NF-kappa B is known to regulate the expression of many genes including immune-mediating genes and inflammatory genes, anti-apoptotic genes, cell proliferation regulation genes, and genes encoding negative regulators of NF-kappa B (83). These observations indicate that NF-kappa B may play a critical role in the pathogenesis of chronic inflammation. Recent evidences have suggested that NF-kappa B is a key regulator of inflammation-induced tumor development (84). NF-kappa B stimulates cell proliferation and activates the expression of growth factor genes, proto-oncogene c-MyC (85), and cyclin D1 (86), suggesting that NF-kappa B contributes to cancer development. PAR2 antagonists can also reduce inflammation, emphasizing the importance of PAR2 in inflammation. Growing evidence suggests that PAR2 play important roles in

pathogenesis of chronic inflammation, such as inflammatory bowel disease (29). In addition, PAR2 may also contribute to tumor formation and metastasis since PAR2-AP stimulates proliferation of colon tumor cell lines (69,87). PAR2 is expressed by a wide range of tumor cells (1, 87, 88). These observations emphasize the roles in chronic inflammation and tumor growth.

Conclusions

In summary, the study successfully identified proteins that are differentially secreted by smooth muscle cells upon activation by PAR2 activating peptide. The results of this study provide the first overview of alterations in the secretome of culture smooth muscle cells upon activation with PAR2-AP. Such secreted proteins may be of pathological significance in the role of PAR2 in regulation the inflammation, proliferation, and apoptotic process. Combining candidate secreted proteins with the actual abundance and function of these proteins provides insights into their biological importance in physiological and pathological states. Secreted proteins derived from smooth muscle cells during pathological states may contribute to chronic inflammation or cancer prevention. However, more studies are required to elucidate the mechanisms by which PAR2 mediate its secretory effects on smooth muscle cell in inflammation or cancer. Additional evaluation of diseased tissues or tumor samples with LC-MS/MS may also help identify cellular proteins biologically important for the development and progression of human disease.

References

1. Bohm, S.K., *et al.*, (1996). Molecular cloning, expression and potential functions of the human proteinase-activated receptor-2. *Biochem J*, 314: 1009-16.
2. Xu, W.F., *et al.*, (1998). Cloning and characterization of human protease-activated receptor 4. *Proc Natl Acad Sci U S A*, 95: 6642-6.
3. Nystedt, S., *et al.*, (1994). Molecular cloning of a potential proteinase activated receptor. *Proc Natl Acad Sci U S A*, 91: 9208-12.
4. Vu, T.K., *et al.*, (1991) Molecular cloning of a functional thrombin receptor reveals a novel proteolytic mechanism of receptor activation. *Cell*. 64: 1057-68.
5. Scarborough, R.M., *et al.*, (1992) Tethered ligand agonist peptides. Structural requirements for thrombin receptor activation reveal mechanism of proteolytic unmasking of agonist function. *J Biol Chem*. 267: 13146-9.
6. Nystedt, S., *et al.*, (1995). The mouse proteinase-activated receptor-2 cDNA and gene. Molecular cloning and functional expression. *J Biol Chem*. 270: 5950-55.
7. Nystedt, S., *et al.*, (1995). Molecular cloning and functional expression of the gene encoding the human proteinase-activated receptor 2. *Eur J Biochem*. 232: 84-9.
8. Molino, M., *et al.*, (1998). Differential expression of functional protease-activated receptor-2 (PAR-2) in human vascular smooth muscle cells. *Arterioscler Thromb Vasc Biol*. 18: 825-32.
9. Kanke, T., *et al.*, (2001). Proteinase-activated receptor-2-mediated activation of stress-activated protein kinases and inhibitory kappa B kinases in NCTC 2544 keratinocytes. *J Biol Chem*. 276: 31657-66.
10. Scott, G., *et al.*, (2004). Proteinase-activated receptor-2 stimulates prostaglandin production in keratinocytes: analysis of prostaglandin receptors on human melanocytes and effects of PGE2 and PGF2alpha on melanocyte dendricity. *J Invest Dermatol*. 122:1214-24.
11. Dai, Y., *et al.*, (2004). Proteinase-activated receptor 2-mediated potentiation of transient receptor potential vanilloid subfamily 1 activity reveals a mechanism for proteinase-induced inflammatory pain. *J Neurosci*. 24:4293-9.
12. Fiorucci, S., *et al.*, (2001). Proteinase-activated receptor 2 is an anti-inflammatory signal for colonic lamina propria

- lymphocytes in a mouse model of colitis. *Proc Natl Acad Sci U S A*, 98: 13936-41.
13. Sriwai, W., et al., (2013). Distinctive G Protein-Dependent Signaling by Protease-Activated Receptor 2 (PAR2) in Smooth Muscle: Feedback Inhibition of RhoA by cAMP-Independent PKA. *PLoS One*, 8: e66743.
 14. Gerthoffer, W.T. and C.A. Singer, (2002). Secretory functions of smooth muscle: cytokines and growth factors. *Mol Interv*, 2: 447-56.
 15. Khan, I., et al., (1995). Interleukin 1 beta induces the expression of interleukin 6 in rat intestinal smooth muscle cells. *Gastroenterology*, 108: 1720-8.
 16. Vrees, M.D., et al., (2002). Abnormal motility in patients with ulcerative colitis: the role of inflammatory cytokines. *Arch Surg*, 137:439-45; discussion 445-6.
 17. Schror, K., et al., (2010). Thrombin receptors in vascular smooth muscle cells - function and regulation by vasodilatory prostaglandins. *Thromb Haemost*, 103: 884-90.
 18. Wang, J.M., et al., (1991). Expression of monocyte chemotactic protein and interleukin-8 by cytokine-activated human vascular smooth muscle cells. *Arterioscler Thromb*, 11: 1166-74.
 19. Demetz, G., et al., (2010). Tissue Factor-Factor VIIa complex induces cytokine expression in coronary artery smooth muscle cells. *Atherosclerosis*, 212: 466-71.
 20. Xia, Y.C., et al., (2013). Secreted factors from human mast cells trigger inflammatory cytokine production by human airway smooth muscle cells. *Int Arch Allergy Immunol*, 160:75-85.
 21. Berger, P., et al., (2003). Tryptase-stimulated human airway smooth muscle cells induce cytokine synthesis and mast cell chemotaxis. *FASEB J*, 17: 2139-41.
 22. Shi, H.L., et al., (2015). Alterations in serotonin, transient receptor potential channels and protease-activated receptors in rats with irritable bowel syndrome attenuated by Shugan decoction. *World J Gastroenterol*, 21:4852-63.
 23. Lowry, O.H., et al., (1951). Protein measurement with the Folin phenol reagent. *J Biol Chem*, 193: 265-75.
 24. Laemmli, U.K., (1970). Cleavage of structural proteins during the assembly of the head of bacteriophage T4. *Nature*, 227: 680-5.
 25. Blum, H., H. Beier, and H.J. Gross, (1987). Improved silver staining of plant proteins, RNA and DNA in polyacrylamide gels. *ELECTROPHORESIS*, 8: 93-99.
 26. Halayko, A.J., et al., (1996). Markers of airway smooth muscle cell phenotype. *Am J Physiol*, 270: L1040-51.
 27. Shingu, M., et al., (1991). Recombinant human IL-1 beta and TNF-alpha stimulate production of IL-1 alpha and IL-1 beta by vascular smooth muscle cells and IL-1 alpha by vascular endothelial cells. *Life Sci*, 49: 241-6.
 28. Norioka, K., et al., (1990). Pretreatment of human vascular smooth muscle cells with interleukin-1 enhances interleukin-6 production and cell proliferation (action of IL-1 on vascular smooth muscle cells). *Autoimmunity*, 7: 41-50.
 29. Sato, K., et al., (2006). Impairment of PAR-2-mediated relaxation system in colonic smooth muscle after intestinal inflammation. *Br J Pharmacol*, 148: 200-7.
 30. Akiho, H., et al., (2011). Cytokine-induced alterations of gastrointestinal motility in gastrointestinal disorders. *World J Gastrointest Pathophysiol*, 2: 72-81.
 31. Nystedt, S., V. Ramakrishnan, and J. Sundelin, (1996). The proteinase-activated

- receptor 2 is induced by inflammatory mediators in human endothelial cells. Comparison with the thrombin receptor. *J Biol Chem*, 271: 14910-5.
32. Syeda, F., et al., (2006). Cyclooxygenase-2 induction and prostacyclin release by protease-activated receptors in endothelial cells require cooperation between mitogen-activated protein kinase and NF-kappaB pathways. *J Biol Chem*, 281: 11792-804.
 33. Asokanathan, N., et al., (2015). Activation of protease-activated receptors (PARs)-1 and -2 promotes alpha-smooth muscle actin expression and release of cytokines from human lung fibroblasts. *Physiol Rep*, 3(2).
 34. Sung, T.S., et al., (2015). Protease-activated receptors modulate excitability of murine colonic smooth muscles by differential effects on interstitial cells. *J Physiol*, 593: 1169-81.
 35. Chin, A.C., et al., (2008). Neutrophil-mediated activation of epithelial protease-activated receptors-1 and -2 regulates barrier function and transepithelial migration. *J Immunol*, 181: 5702-10.
 36. McHenga, S.S., et al., (2010). Differential dose effects of recombinant IL-25 on the development of dextran sulfate sodium-induced colitis. *Inflamm Res*, 59: 879-87.
 37. Tamachi, T., et al., (2006). Interleukin 25 in allergic airway inflammation. *Int Arch Allergy Immunol*, 140: 59-62.
 38. Xu, M., et al., (2014). Inhibition of proinflammatory cytokine by IL-25 in Vogt-Koyanagi-Harada syndrome. *Ocul Immunol Inflamm*, 22: 294-9.
 39. Lee, J., et al., (2001). IL-17E, a novel proinflammatory ligand for the IL-17 receptor homolog IL-17Rh1. *J Biol Chem*, 276: 1660-4.
 40. Song, X., et al., (2011). IL-17RE is the functional receptor for IL-17C and mediates mucosal immunity to infection with intestinal pathogens. *Nat Immunol*, 12: 1151-8.
 41. Li, T.S., et al., (2006). Identification and functional characterization of a novel interleukin 17 receptor: a possible mitogenic activation through ras/mitogen-activated protein kinase signaling pathway. *Cell Signal*, 18: 1287-98.
 42. Al-Samadi, A., et al., (2014). IL-17C and its receptor IL-17RA/IL-17RE identify human oral epithelial cell as an inflammatory cell in recurrent aphthous ulcer. *J Oral Pathol Med*, 43: 117-24.
 43. Ramirez-Carrozzi, V., et al., (2011). IL-17C regulates the innate immune function of epithelial cells in an autocrine manner. *Nat Immunol*, 12: 1159-66.
 44. Nhu, Q.M., et al., (2010). Novel signaling interactions between proteinase-activated receptor 2 and Toll-like receptors in vitro and in vivo. *Mucosal Immunol*, 3: 29-39.
 45. Raby, A.C., et al., (2009). Soluble TLR2 reduces inflammation without compromising bacterial clearance by disrupting TLR2 triggering. *J Immunol*, 183: 506-17.
 46. Smith, W.L., D.L. DeWitt, and R.M. Garavito, (2000). Cyclooxygenases: structural, cellular, and molecular biology. *Annu Rev Biochem*, 69: 145-82.
 47. Luo, C., et al., 2002. Expression of cyclooxygenase-2 in intestinal goblet cells of pre-diabetic NOD mice. *Acta Physiol Scand*, 174: 265-74.
 48. Nepomuceno, R.R., et al., (1997). cDNA cloning and primary structure analysis of C1qR(P), the human C1q/MBL/SPA receptor that mediates enhanced phagocytosis in vitro. *Immunity*, 6: 119-29.

49. McGreal, E. and P. Gasque, (2002). Structure-function studies of the receptors for complement C1q. *Biochem Soc Trans*, 30: 1010-4.
50. Steinberger, P., et al., (2002). Identification of human CD93 as the phagocytic C1q receptor (C1qRp) by expression cloning. *J Leukoc Biol*, 71: 133-40.
51. Bohlson, S.S., et al., (2005). CD93 is rapidly shed from the surface of human myeloid cells and the soluble form is detected in human plasma. *J Immunol*, 175: 1239-47.
52. Greenlee, M.C., S.A. Sullivan, and S.S. Bohlson, (2009). Detection and characterization of soluble CD93 released during inflammation. *Inflamm Res*, 58: 909-19.
53. Sigari, N., et al., (2016). Soluble CD93 as a Novel Biomarker in Asthma Exacerbation. *Allergy Asthma Immunol Res*, 8:461-5.
54. Jeon, J.W., et al., (2010). Soluble CD93 induces differentiation of monocytes and enhances TLR responses. *J Immunol*, 185: 4921-7.
55. Fabrick, B.O., C.D. Dijkstra, and T.K. van den Berg, (2005). The macrophage scavenger receptor CD163. *Immunobiology*, 210: 153-60.
56. Moller, H.J., et al., (2002). Identification of the hemoglobin scavenger receptor/CD163 as a natural soluble protein in plasma. *Blood*, 99: 378-80.
57. Hogger, P. and C. Sorg, 2001. Soluble CD163 inhibits phorbol ester-induced lymphocyte proliferation. *Biochem Biophys Res Commun*, 288: 841-3.
58. Frings, W., J. Dreier, and C. Sorg, (2002). Only the soluble form of the scavenger receptor CD163 acts inhibitory on phorbol ester-activated T-lymphocytes, whereas membrane-bound protein has no effect. *FEBS Lett*, 526: 93-6.
59. Fadeel, B. and S. Orrenius, (2005). Apoptosis: a basic biological phenomenon with wide-ranging implications in human disease. *J Intern Med*, 258:479-517.
60. Chaturvedi, P., et al., (1999). Mammalian Chk2 is a downstream effector of the ATM-dependent DNA damage checkpoint pathway. *Oncogene*, 18: 4047-54.
61. Demonacos, C., et al., (2004). A new effector pathway links ATM kinase with the DNA damage response. *Nat Cell Biol*, 6: 968-76.
62. Morrell, D., C.L. Chase, and M. Swift, (1990). Cancers in 44 families with ataxia-telangiectasia. *Cancer Genet Cytogenet*, 50: 119-23.
63. Guarini, A., et al., (2012). ATM gene alterations in chronic lymphocytic leukemia patients induce a distinct gene expression profile and predict disease progression. *Haematologica*, 97(1): p. 47-55.
64. Angele, S., et al., (2003). ATM haplotypes and cellular response to DNA damage: association with breast cancer risk and clinical radiosensitivity. *Cancer Res*, 63: 8717-25.
65. Panta, G.R., et al., (2004). ATM and the catalytic subunit of DNA-dependent protein kinase activate NF-kappaB through a common MEK/extracellular signal-regulated kinase/p90(rsk) signaling pathway in response to distinct forms of DNA damage. *Mol Cell Biol*, 24: 1823-35.
66. Criswell, T., et al., (2003). Transcription factors activated in mammalian cells after clinically relevant doses of ionizing radiation. *Oncogene*, 22: 5813-27.
67. Hitomi, M., et al., 2008. Phosphorylation of cyclin D1 regulated by ATM or ATR controls cell cycle progression. *Mol Cell Biol*, 28: 5478-93.
68. Gladden, A.B. and J.A. Diehl, (2005). Location, location, location: the role of cyclin D1 nuclear localization in cancer. *J Cell Biochem*, 96: 906-13.

69. Ma, Y., et al., (2013). MicroRNA-34a mediates the autocrine signaling of PAR2-activating proteinase and its role in colonic cancer cell proliferation. *PLoS One*, 8(8): e72383.
70. Abbott, D.W., M.L. Freeman, and J.T. Holt, (1998). Double-strand break repair deficiency and radiation sensitivity in BRCA2 mutant cancer cells. *J Natl Cancer Inst*, 90:978-85.
71. Sharan, S.K., et al., (1997). Embryonic lethality and radiation hypersensitivity mediated by Rad51 in mice lacking Brca2. *Nature*, 386: 804-10.
72. Bertwistle, D., et al., (1997). Nuclear location and cell cycle regulation of the BRCA2 protein. *Cancer Res*, 57): 5485-8.
73. Vaughn, J.P., et al., (1996). Cell cycle control of BRCA2. *Cancer Res*, 56:4590-4.
74. Jensen, R.A., et al., (1996). BRCA1 is secreted and exhibits properties of a granin. *Nat Genet*, 12:303-8.
75. Bernard-Gallon, D., et al., (2000). BRCA2 protein expression in sporadic breast carcinoma with or without allelic loss of BRCA2. *Int J Cancer*, 86: 453-6.
76. Samuels-Lev, Y., et al., (2001). ASPP proteins specifically stimulate the apoptotic function of p53. *Mol Cell*, 8: 781-94.
77. Song, B., et al., (2015). Downregulation of ASPP2 in pancreatic cancer cells contributes to increased resistance to gemcitabine through autophagy activation. *Mol Cancer*, 14: 177.
78. Li, S., et al., (2012). Abnormal expression pattern of the ASPP family of proteins in human non-small cell lung cancer and regulatory functions on apoptosis through p53 by iASPP. *Oncol Rep*, 28:133-40.
79. Mak, V.C., et al., (2013). Downregulation of ASPP2 in choriocarcinoma contributes to increased migratory potential through Src signaling pathway activation. *Carcinogenesis*, 34: 2170-7.
80. Dery, O., et al., (1999). Trafficking of proteinase-activated receptor-2 and beta-arrestin-1 tagged with green fluorescent protein. beta-Arrestin-dependent endocytosis of a proteinase receptor. *J Biol Chem*, 274:18524-35.
81. Buddenkotte, J., et al., (2005). Agonists of proteinase-activated receptor-2 stimulate upregulation of intercellular cell adhesion molecule-1 in primary human keratinocytes via activation of NF-kappa B. *J Invest Dermatol*, 124: 38-45.
82. Shpacovitch, V.M., et al., (2002). Agonists of proteinase-activated receptor 2 induce cytokine release and activation of nuclear transcription factor kappaB in human dermal microvascular endothelial cells. *J Invest Dermatol*, 118: 380-5.
83. Karin, M., et al., (2002). NF-kappaB in cancer: from innocent bystander to major culprit. *Nat Rev Cancer*, 2: 301-10.
84. Lu, H., W. Ouyang, and C. Huang, (2006). Inflammation, a key event in cancer development. *Mol Cancer Res*, 4: 221-33.
85. Duyao, M.P., et al., (1992). Transactivation of the c-myc promoter by human T cell leukemia virus type 1 tax is mediated by NF kappa B. *J Biol Chem*, 267: 16288-91.
86. Takebayashi, T., et al., (2003). NF-kappa B-dependent induction of cyclin D1 by retinoblastoma protein (pRB) family proteins and tumor-derived pRB mutants. *J Biol Chem*, 278: 14897-905.
87. Darmoul, D., et al., (2001). Initiation of human colon cancer cell proliferation by trypsin acting at protease-activated receptor-2. *Br J Cancer*, 85: 772-9.
88. D'Andrea, M.R., et al., (2001). Differential expression of protease-activated receptors-1 and -2 in stromal fibroblasts of normal, benign, and malignant human tissues. *Am J Pathol*, 158: 2031-41.

Homology Modeling of Endoxylanase from *Trichoderma pseudokoningii*

Bandikari Ramesh, Seelam Naga Sivudu, Katike Umamahesh and
Obulam Vijaya Sarathi Reddy*

Department of Biochemistry, Sri Venkateswara University, Tirupati - 517 502, India.

*For Correspondence - ovsreddy@yahoo.com

Abstract

Endoxylanase is involved in the degradation of xylan to xylose. It majorly breaks down the hemicelluloses, which are the major components of the cell wall of the plants. In the present study the 3D modeling of endoxylanase from *Trichoderma pseudokoningii* (B0FXM0) was performed by comparing modeling approach using endo 1-4 β -xylanase from *Trichoderma reesei* (PDB ID: 1XYP) as template in modeler7V.7 program server. The best model was selected based on overall stereo-chemical quality (PROCHECK, proSA, Verified_3D), and also verified with Protein Structure Validation Suit (PSVS). The active sites of endoxylanase were identified in CastP server, which showed that the refined model has highly conserved residues.

Key words: Homology modeling, Modeller, Ramachandran plot, Xylanase.

Introduction

Xylan is structural component of cell wall polysaccharides and it is formed by xylose subunit which is linked together by β -1,4-glycosidic linkages. The complete hydrolysis of xylan requires xylanolytic enzymes which are produced by *Trichoderma* spp. These are free-living fungi, they are highly interactive in plant roots, soil and foliar environments and they commercially act as biological control agents (BCAs) against fungal pathogens (1,2). *Trichoderma* has many industrial applications like production of hydrolytic enzymes such as

xylanases and cellulases (3), and production of ethanol (4). Xylanases are potentially used in wood pulp, fruit juice clarification (5) and saccharification of agricultural residues (6). The ligno-cellulases (xylanases and cellulases) are classified into 9 families (A, B, C, D, E, F, G, H and I) based on the hydrophobic cluster analysis and sequence similarly (7). Based on the classification of xylanases, they come under F or G (8, 9). Xylanase hydrolyses xylan into xylo-oligosaccharides and xylose, similar to that of lysozyme, act by retention of anomeric configuration, with two glutamate residues being involved in the catalytic mechanism (10). The first residue is an acid catalyst that protonating the oxygen of the glycosidic bond, splitting two cellulose or hemi-cellulose subunits and forming an oxocarbenium intermediate. The second residue acts as a nucleophilic attack, which binds with the oxocarbenium intermediate and promotes the formation of an OH-form a water molecule, which converts the intermediate into a free xylobiose subunit (10).

The homology modeling of enzymes can often provide invaluable information. The X-ray diffraction is commonly used strategy to study the substrates binding sites of enzymes (11). In absence of crystallographic structures, a variety of advanced homology methods have been developed, which can provide reliable models of proteins that shares 30% or more sequence identity with a known structure (12), for understanding a structure and function. The

objective of our study was to understand, how the three dimensional (3D) model of endoxylanase is generated based on the crystal structure of the template by using the MODELLER 7v.7, validation of model workflow followed in this work given in Fig. 1. These studies are helpful for the further experimental investigations.

Materials and Methods

Sequence retrieval alignment and homology modeling

The 3D model of xylanase was built by homology modeling based on high-resolution crystal structure of homologous proteins. The complete amino acid sequence of the target protein (Endoxylanase) from *Trichoderma pseudokoningii* (B0FXM0) was retrieved from uniprot sequence database in FASTA format (<http://www.uniprot.org/>). The NCBI Basic Local Alignment Search Tool (BLAST) (13,14), for the sequence similarities was used for searching the crystal structure of the closest homologs available in the Brookhaven Protein Data Bank (PDB). Based on maximum identity with high score and lower e-value, xylanase from *Trichoderma reesei* (PDB code: 1XYP) with a resolution of 1.5Å was used as template. Query cover was 84% over the length of 192 residues. The 1XYP was used as a template to build the model by pair-wise alignment using Clustal-W software.

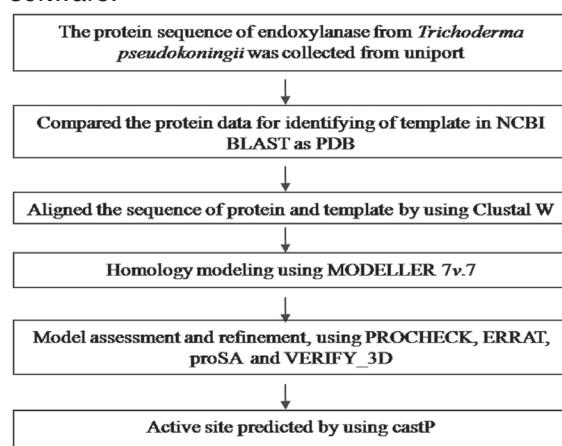


Fig1. Flow chart for complete homology modeling and active site prediction of endoxylanases.

Three dimensional structure generation and validation

The academic version of MODELLER 7v.7 (<http://www.salilab.org/modeller>) was used for 3D structure generation based on the information obtained from sequence alignment (15). Based on homology modeling method, the assumption that the structure of unknown protein will be similar to the known structure of some reference protein out of the five models generated by MODELLER (16,17).

Validation of 3D structure : The validation of structure of model was performed by inspection of the ψ and ϕ distributions of the Ramchandran plot obtained from PROCHECK (18) analysis, the environment profile was inspected by using ERRAT graph (structure evaluation server) (17) and the compatibility of model with sequence were measured by VERIFY_3D (19). The stereochemical quality of protein structure with best G-score was measured by using protein structure validation suite (PSVS) programme server (16). A high verify 3D profile score indicates the high quality of model.

Active site identification : Xylanase (B0FXM0) active site was identified by using CastP server (20,21). This program predicts automatically locating and measuring protein cavities, based on precise computational geometry methods. CastP identifies and measures pockets and pocket mouth opening, as well as cavities. The program specifies the atoms lining pockets, pocket openings and buried cavities. This program server measured the volume and area of pockets and cavities, and the area and circumference of mouth opening.

Results and Discussion

Homology modeling of xylanase

Homology modeling is a clear relation of homology between the sequences of target protein and at least one known structure is found. This approach gives reasonable results based on assumption that tertiary structures of two proteins will be similar if, their sequences are related (23). Template protein sequence was

collected by search in Basic Local Alignment Search Tool (BLAST) as a Brookhaven Protein Data Bank (PDB). The template showed 84% query coverage with $2e-134$ e-value, the template shown maximum sequence alignment against protein. The protein and template were pair-wise aligned by Clustal-W (Omega 1.2.1) server. Alignment of protein sequences were shown in Fig. 2.

Structurally conserved regions (SCRs) for the model and the template were determined by superimposition of the two structures and

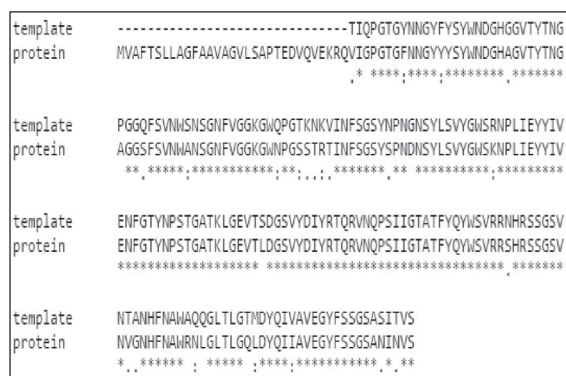


Fig 2. Sequence alignment between protein (B0FXM0) and template (1XYP) in Clustal-W.

multiple sequence alignment. 1XYP used as a reference structure for modeling domain. Coordinates from the reference protein (B0FXM0) to the SCRs, structurally variable regions (SVRs), N-termini and C-termini were assigned to the target sequence based on the satisfaction of spatial restraints. In the MODELLER software 20 templates were generated, among these least energy template was selected. All side chains of the model protein were set by rotamers. It was observed that generated protein has a maximum similarity with template protein, due to the both proteins were showed maximum sequence similarity. In the case of homology modeling and design 3D structure of B0FXM0 protein with template protein, it was shown that they structurally

resemble with each other (24). The final stable structure of the B0FXM0 protein obtained from the help of SPDBV, it is evident that homology to template protein, which is shown in Fig. 3. The secondary structure of protein domain elements were α -helices from 182 A to 191 A residues and β -sheets of residues were 36A-40A, 43A-49A, 74A-81A, 198A-209A, 102A-111A, 115A-123A, 162A-171A, 143A-155A, 133A-140A, 55A-59A, 64A-69A, 212A-219A, 89A-99A, 178A-181A.

Validation of xylanase domain : The overall stereo-chemical quality of model was assessed by Procheck. The Ramachandran plot showed 91.2% residues in most favorable region, 7.7% in allowed region (Table-1), and 1.1% in additional and disallowed region. The results revealed that majority amino acids are in ψ and ϕ distribution consist with right handed α -helix and reliable to be good quality model (Fig. 4). The G-factor indicates the quality of covalent and bond angle distance, were -0.33° for dihydral, for covalent -0.16° and overall -0.06° . The overall main chain and side chain parameter, as evaluated by PROCHECK, are all very favorable. The Ramchandran plot characteristic and G-factor confirm the quality of predicted model, and overall quality factor of 70.681 in ERRAT graph (Fig. 5) indicates acceptable protein environment, as scores of >50 are acceptable for a reasonable model.

In order to investigate the interaction energy of each residue with the remainder of the protein is negative, a second test was done to apply energy criteria using prosall energy plot. The prosa analysis of the model showed maximum residues to have negative interaction energy and some residues with positive energy interaction as shown in Fig. 6.

A final test is the packing of each residue as assessed by verify 3D program that represents the profile obtained with respect to the residues. The compatibility score above zero in the verify-3D graph corresponds to acceptability side chain environment (Fig. 7). In verify-3D protein score for each residue in 21 residue sliding window

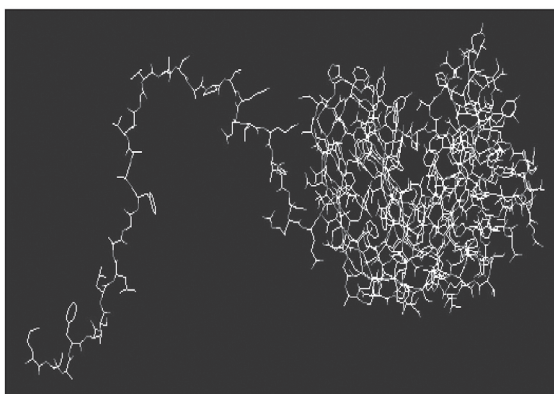


Fig 3. Final refined structure of xylanase obtained from SPDBV.

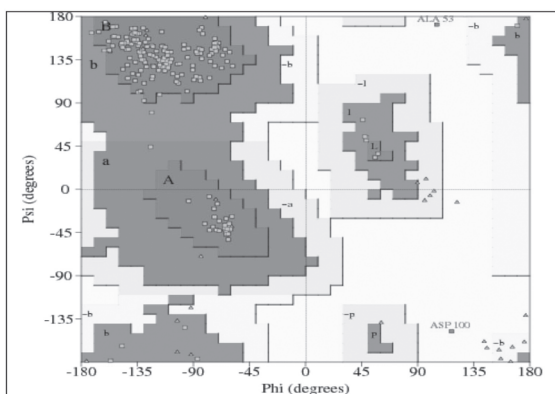


Fig 4. Ramachandran plot of xylanase (B0FXM0) homology model by PROCHECK server.

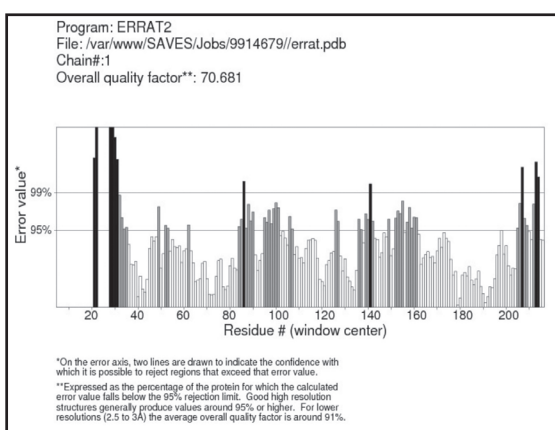


Fig 5. The 3D profile of xylanases model verified by ERRAT server.

Table 1. % of residues falling in the core region of Ramachandran's plot

% of residue in most favored regions	91.2
% of residues in the additionally allowed regions	7.7
% of residues in the generously allowed regions	0.0
% of residues in disallowed regions	1.1
% of non-glycine and non-proline residues	100

helps to further validating the model (0.74) and score found to be near to the template.

The quality of model was also assessed by comparing the predicted structures to the experimentally showed structures superimposition and atoms RMSD assessment. After the refinement process, predicted the possible RMSD (root mean square deviation) deviation for covalent bonds and covalent angles relative to the standard dictionary of xylanase (B0FXM0) were 0.019 Å and 2.1° respectively.

Active site identification of xylanase domain

The possible binding sites of B0FXM0 were searched based on the structural comparison of template with CastP server. The sequence and structures of B0FXM0 and 1XYP are well conserved due to their similar biological function. It shown that secondary structures are highly conserved and the residues, SER 46, TRP 48, ASN74, VAL 76, ASN 101, TYR 103, SER 105, TYR 107, TRP 109, GLU 116, TYR 118, TYR 126, PRO 128, SER 129, THR 130, GLY 131, ALA 132, THR 150, ARG 152, GLN 155, PRO 156, SER 157, ILE 158, PHE 164, GLN 166, TRP 168, TYR 201, ILE 203, ALA 205, GLU 207 and TYR 209 were in Ball like structures in Fig. 8.

Conclusion

The 3D model of xylanase from *Trichoderma pseudokoeningi* was constructed in order to accomplish its molecular modeling and study the active sites of enzyme. The model was validating and it was reliable. In future this work explores docking studies of xylanases *in silico*

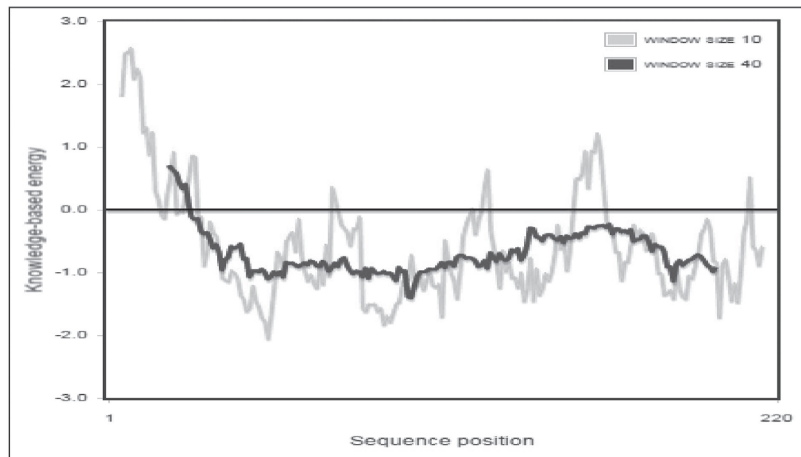


Fig 6. PROSA energy plot calculated for the B0FXM0 homology model.

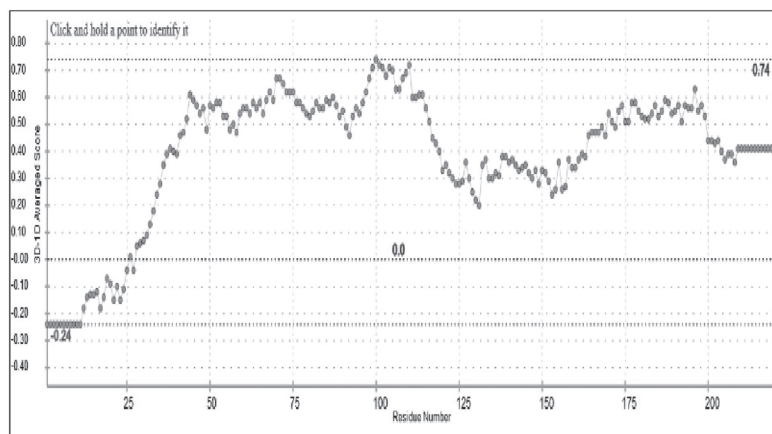


Fig 7. The 3D profiles verified results of B0FXM0 homology model by verify_3D server.

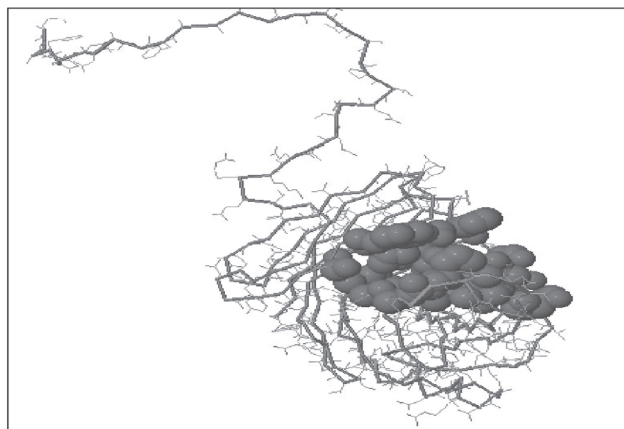


Fig 8. Active site of xylanase model (Ball like structures indicates the active site regions).

and helps to propose the mechanism of enzymes.

Acknowledgement

We are thankful to Dr. S.C. Basappa, former Deputy Director and Scientist, Central Food Technological Research Institute (CFTRI), Mysore, for his encouragement and critical comments on the manuscript.

References

1. Kubicek, C.P., Mach R.L., Peterbauer, C.K. and Lorito, M. (2001). *Trichoderma*: from gene to biocontrol. Journal of Plant Pathology. 83: 11–23.
2. Harman, G.E, Howell, C.R, Viterbo, A, Chet, I. and Lorito, M. (2004). *Trichoderma* species -opportunistic, avirulent plant symbionts. Natures Review Microbiology. 2: 43–56.
3. Archana, M. and Mishra N.C. (2013). Bio-ethanol production from mixed wastes using *Trichoderma viride*. Indian Research Journal of Genetics and Biotechnology. 5: 111-116.
4. Awolu, O.O. and Ibileke, I.O. (2011). Bio-ethanol production from brewer's spent grain, bread wastes and corn fiber. African Journal of Food Science. 5:148-155.
5. Ramesh, B., Sreedharamurthy M., Ramamohan P. and Reddy, O.V.S. (2015). Supplementation of fruit processing waste for endoxylanase production by *Trichoderma koenigii* isolate and its optimization using central composite design: Application of produced endoxylanase in mango juice clarification. Journal of Microbiology Biotechnology Food Science. 5:162-166.
6. Ramesh, B., Vijayakumar, P. and Reddy, O.V.S. (2014). Enhanced production of xylanase by solid state fermentation using *Trichoderma koenigii* isolate: effect of pretreated agro-residues. 3Biotech. 4:655-664.
7. Gilkes, N.R., Henrissat, B., Kilburn, D.G. and Mille, R.C. (1991). Warren, Domains in microbial α -1,4-glycanases: sequence conservation, function, and enzyme families. Microbiology Reviews. 55:303-315.
8. Henrissat, B. (1991). A classification of glycosyl hydrolases based on amino acid sequence similarities. Biochemical Journal. 280:309-316.
9. Henrissat, B and Bairoch, A. (1993). New families in the classification of glycosyl hydrolases based on amino acid sequence similarities. Biochemical Journal. 293:781-788.
10. Beguin, P. and Aubert, J.P. (1994). The biological degradation of cellulose. FEMS Microbiology Reviews. 13:25-58.
11. Sasin, J.M and Bujnicki, J.M (2004). COLORADO3D, a web server for the visual analysis of protein structures. Nucleic Acids Research. 32:586–589.
12. Burley, S.K (2000). An overview of structural genomics. Nature Structural. Biology. 932-934.
13. Altschul, S.F., Gish, W., Miller, W., Myers, E.W. and Lipman, D.J. (1990). A basic local alignment search tool. Journal of Molecular Biology. 215: 403-410.
14. Altschul, S.F., Madden, T.L., Schaffer, A.A., Zhang, J., Zhang, Z., Miller, W. and Lipman, D. J. (1997). Gapped BLAST and PSI-BLAST: a new generation of protein database search programs. Nucleic Acids Research. 50: 3389-3402.
15. Eswar, N., Marti-Renom, M.A., Webb, B., Madhusudhan, M.S., Eramian, D., Shen, M., Pieper, U. and Sali, A. (2006). Comparative protein structure modeling with MODELLER: Current protocols in bioinformatics. John Wiley and Sons, Inc., Supplement 15: 5.6.1-5.6.30.

16. Bowie, J.U., Luthy, R. and Eisenberg, D. (1991). A method to identify protein sequences that fold into a known three-dimensional structure. *Science*. 253: 164-169.
17. Sippl M.J. (1993). Recognition of errors in three-dimensional structures of proteins. *Proteins*. 17: 355-362.
18. Laskowski, R.A., MacArthur, M.W., Moss, D.S. and Thornton, J.M. (1993). PROCHECK: A program to check the stereo-chemical quality of protein structures. *Journal of Applied Crystallography*, 26: 283-291.
19. Brunger, A. (1992). X-PLOR, Version 3.1: A system for X-Ray crystallography and NMR. Yale University, New Haven, CT.
20. Luthy, R., Bowie, J.U. and Eisenberg, D. (1992). Assessment of protein models with three dimensional profiles. *Nature*. 356:83-85.
21. Carpena, X., Loprasert, S., Mongkolsuk, S., Switala, J., Loewen, P.C. and Fita, I. (2003). Catalase-peroxidase KatG of *Burkholderia pseudomallei* at 1.7 Å resolution. *Journal of Molecular Biology*. 327: 475–489.
22. Lovell, S.C, Davis, I.B, Arendall III, W.B, de Bakker, P.I.W, Word, J.M, Prisant, M.G, Richardson, J.S. and Richardson, D.C. (2002). Structure validation by calpha geometry: phi, psi and Cbeta deviation. *Proteins: Structure, Function and Genetics*. 50: 437-450.
23. Kroemer, R.T., Doughty, S.W., Robinson, A.J. and Richards, W.G. (1996). *Protein Engineering*. 6: 493–498.
24. Kotha, P., Rayalu Daddam, J., Sai Gopal Divi, V.R., Dakinedi, S.R. and Dowlathabad, M. (2015). Modeling simulation phylogenetics of leukemia FMS tyrosine kinase 3 (FLT3). *Online Journal of Vet Research*. 16 (1): 8-17.

Pharmacokinetic analysis of atorvastatin against experimental hepatotoxicity with special reference to CYP3A4 functioning in rats

M. Anudeep Reddy, B. Kala Kumar, G. Boobalan*, M. Vijay Kumar, M. Kasi Reddy, C.S.V. Satish Kumar and A. Gopala Reddy

Department of Veterinary Pharmacology and Toxicology, College of Veterinary Science, Rajendranagar, Hyderabad – 500 030, India.

*For Correspondence - bhupalvets@gmail.com

Abstract

Aim: To assess the functional status of CYP3A4 substrate in experimental induced hepatotoxicity treated with N-acetyl L-cysteine and Green tea extract for a period of 14 days in rats.

Materials and methods: Twenty four *Wistar* rats were divided into four groups of 6 rats each and induced hepatotoxicity with acetaminophen (500 mg/Kg *po* once daily for 3 days) in 3 groups. Group 1: Normal control, Group 2, 3 and 4 was administered distilled water (5 ml/kg *po*), N-acetyl L-cysteine (NAC; 300 mg/Kg *po* once daily) and Green tea extract (GTE; 100 mg/Kg *po* once daily), respectively subsequently for 11 days from the last dose of acetaminophen. Atorvastatin (10 mg/kg *po*) was administered on 15th day (24 h after conclusion of treatment schedule) in all the groups. The PK studies were conducted in order to evaluate the CYP3A4 activity using the specific substrate atorvastatin in all the groups.

Results: C_{max} , $t_{1/2}$, AUC_{0-t} and MRT of groups 2 and 4 were significantly ($p < 0.05$) increased, while the total body clearance was significantly ($p < 0.05$) decreased compared to normal control after single dose administration of atorvastatin. The kinetic profile of NAC-treated group 3 was comparable to group 1.

Conclusion: All the pharmacokinetic parameters of atorvastatin revealed similar values when hepatotoxic control was compared to Green tea extract treated group, while N-acetyl L-cysteine

treated group revealed significant alterations in the kinetic profile that support the functional status of CYP3A4 and hence suggesting hepatoprotective potential of NAC.

Key words: Acetaminophen, Atorvastatin, CYP3A4, Green Tea, N-Acetyl L-cysteine

Introduction

The pathogenesis of drug-induced hepatotoxicity accounts for the withdrawal of considerable amount of drugs from the market. In present scenario, drug induced hepatic injury is the common cause of acute and chronic liver diseases (1).

Acetaminophen (N-acetyl-p-aminophenol/APAP), via cytochrome P450 enzyme system (CYP3A4) bioactivated to a reactive metabolite, N-acetyl-para benzoquinone imine (NAPQI) in liver. NAPQI covalently react with proteins and nucleic acids deplete GSH and potentially cause fatal centrilobular hepatic necrosis producing dose-dependent hepatotoxicity (2). The most reliable and commonly employed hepatotoxicity model to test the hepatoprotective potential of drugs is the one induced by acetaminophen (3).

Statins are primarily metabolized by CYP3A4 and co-administration of statins with drugs that inhibit CYP3A4 isoenzyme potentially increase the risk for adverse effects as the metabolism of statins gets slowed down (4).

N-acetyl-L-cysteine (NAC) is a sulfur based

amino acid acts against oxidative stress and prevents damage to cells (5). NAC, the acetylated precursor of the amino acid L-cysteine and reduced glutathione scavenge free radicals, stimulates glutathione synthesis, enhance glutathione-S-transferase activity, and promotes liver detoxification by inhibiting xenobiotic biotransformation (6).

Green tea (*Camellia sinensis*) is rich in polyphenolic compounds that have several therapeutic and antioxidant properties (7). Administration of green tea in streptozotocin-induced diabetic rats protected liver damage due to its antioxidant property (8).

The aim of our investigation was to investigate the metabolic function of CYP3A4 under the influence of Acetaminophen-induced hepatic damage and the hepatic regeneration induced by the drugs in study (NAC and GTE) by assessing the pharmacokinetics of the specific substrate atorvastatin in rats.

Materials and methods

Acetaminophen (Himedia, India), Green Tea extract (Lipton, India) and N-acetyl L-cysteine (SRL, India) were administered in distilled water.

Animals : Male *Wistar albino* rats weighing around 200-250 g were procured from Sanzyme Pvt. Ltd., Hyderabad, India. Institutional Animal Ethics Committee has approved the experimental protocol (Approval No. I/10/14 Dated 27.11.2014). Hepatotoxicity was induced in rats with oral administration of acetaminophen for 3 consecutive days (9).

Experimental design : The study was carried out on 24 rats that were randomly divided into four groups comprising of 6 rats in each group for single dose kinetics of atorvastatin following pre-treatment with the test and standard drugs.

Group 1: Normal control.

Group 2: Acetaminophen (500 mg/Kg *po* once daily for 3 days) and distilled water (5 ml/kg *po*) were administered subsequently for 11 days from the last dose of acetaminophen.

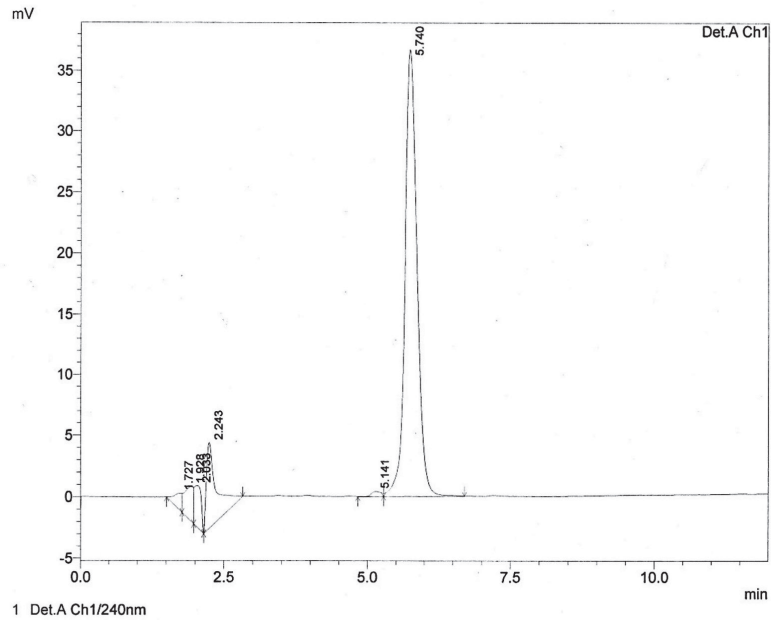
Group 3: Acetaminophen (as in group 2) and N-acetyl L-cysteine (300 mg/Kg *po* once daily) were administered subsequently for 11 days from the last dose of acetaminophen.

Group 4: Acetaminophen (as in group 2) and Green tea extract (100 mg/Kg *po* once daily) were administered subsequently for 11 days from the last dose of acetaminophen.

On the day 15 (24 h after conclusion of treatment schedule), atorvastatin was administered orally @ 10 mg/kg body weight in all the groups.

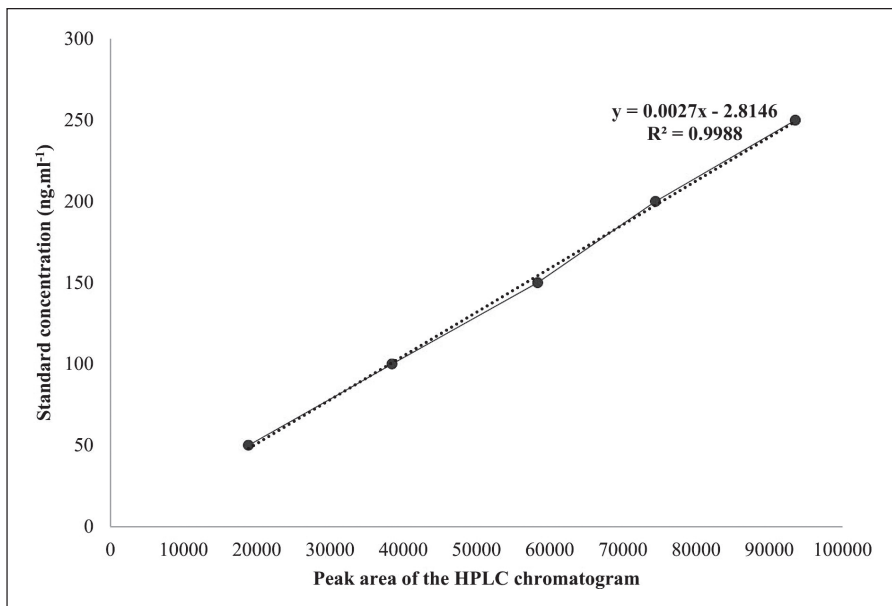
Blood collection for PK studies : Blood (approximately 500 μ l) was collected from retro orbital plexus at 0.25, 0.5, 1, 3, 6, 12 and 24 h post-administration of atorvastatin in the heparinized vials and the plasma was separated and stored at -20°C till further analysis.

HPLC assay of atorvastatin in rat plasma : To the plasma samples (200 μ l), equal volume of phosphate buffer (pH 7.0) was added and mixed well and then atorvastatin was extracted by liquid-liquid extraction technique by using methanol (1:4 ratio). The clear organic phase was separated, filtered through 0.45 μ m syringe filter (Millipore; Millex-HN) and evaporated to dryness at 45°C. The filtrate was reconstituted in 40 μ l methanol and 20 μ l of filtrate was injected manually into HPLC system (Shimadzu – LC20AT) with dual wavelength UV detector (SPD-20A). The chromatographic column was C₁₈ (Phenomenax®, USA; pore diameter 100 \pm 10Å, 250 \times 4.60 mm) coated with 0.5 μ silica gel. The Mobile phase used was an isocratic solution of 0.1 mM ammonium acetate: acetonitrile (50:50), which was filtered through 0.2 μ m nylon filter paper (Pall Corporation, India). The flow rate of mobile phase was maintained @ 1 ml/min. The peak was detected at 240 nm at 6.5min after injection (Fig. 1). Peak areas of the standard plasma samples were plotted against respective known concentrations of plasma atorvastatin to obtain a linear regression line (Fig. 2).



x axis = min, y axis = mV

Fig. 1. Chromatogram of atorvastatin standard in plasma



x axis = Peak area of the HPLC chromatogram, y axis = Standard concentration (ng.ml⁻¹)

Fig. 2. Calibration curve of atorvastatin

Pharmacokinetic analysis of atorvastatin against

Pharmacokinetic analysis : The plasma concentration-time profile of atorvastatin obtained for four groups in the present study were utilized for calculating pharmacokinetic parameters in rats with a linear interactive programme for personal computer software (PK solver 2.0 developed by Zhang *et al.*, 2010 (10)).

Statistical analysis : All data were expressed as mean + SE. Difference in pharmacokinetic data between groups were analyzed using unpaired 't' test with Welch's correction using 'Instat' software. The level of significance was $p < 0.05$.

Results

A mean peak plasma concentration (C_{max}) of 134.32 ± 0.91 ng ml⁻¹ was achieved at 3h and gradually declined to 4.61 ± 0.21 ng ml⁻¹ at 24 h in group 1. Non-compartmental analysis of plasma drug concentrations yielded the mean values for area under plasma drug concentration curve (AUC_{0-t}), time to peak plasma concentration (t_{max}), elimination rate constant (λ), mean elimination half-life ($t_{1/2\lambda}$), mean residence time (MRT), volume of distribution at steady state (V_{dss}) and total body clearance (CL_{λ}) were 1195.59 ± 5.84 ng.h.ml⁻¹, 3h, 0.15 ± 0.00 h⁻¹, 4.41 ± 0.07 h, 6.91 ± 0.07 h, 0.05 ± 0.00 L/kg and 0.008 ± 0.00 L.kg⁻¹.h⁻¹, respectively in group 1 (Table 1 and 2).

The maximum plasma concentration (C_{max}) was significantly ($p < 0.05$) increased in group 2 (154.82 ± 1.73 ng.ml⁻¹) when compared to group 1 (134.32 ± 0.91 ng.ml⁻¹). Similarly, the AUC_{0-t} , $AUC_{0-\infty}$, $AUMC_{0-t}$ and $AUMC_{0-\infty}$ values of groups 2 and 4 were significantly ($p < 0.05$) increased when compared to group 1. The half-life and MRT were significantly ($p < 0.05$) increased in groups 2 (6.23 ± 0.09 h and 9.96 ± 0.77 h) and group 4 (5.79 ± 0.12 h and 8.64 ± 0.17 h), respectively. The total body clearance was significantly ($p < 0.05$) decreased in group 2 (0.005 ± 0.00 L.kg⁻¹.h⁻¹) and group 4 (0.006 ± 0.01 L.kg⁻¹.h⁻¹) when compared to group 1 (0.008 ± 0.00 L.kg⁻¹.h⁻¹). The pharmacokinetic profile of group 3 was significantly ($p < 0.05$) comparable to group 1 (Table 1 and 2; Fig. 3, 4 and 5).

Discussion

In this study we assessed the functional status of CYP3A4 enzyme in experimental induced hepatotoxicity by estimating the plasma concentration and pharmacokinetic parameters of CYP3A4 substrate atorvastatin in normal rats, hepatotoxic control rats and in treated groups.

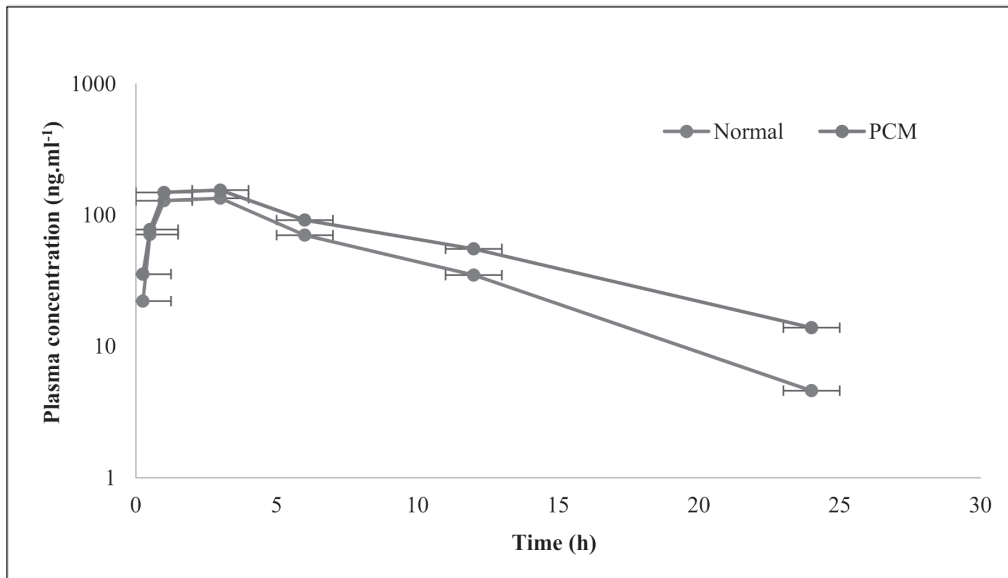
N – acetyl-para-benzoquinoneimine (NAPQI), a toxic metabolite of Acetaminophen, binds with cell macromolecules like proteins and lipids, and causes generation of ROS in liver and kidney, which may be responsible for toxic effects (11). The maximum plasma concentration (C_{max}) and AUC_{0-t} of atorvastatin was significantly increased in PCM induced hepatotoxic control rats, which may be due to the altered metabolism of atorvastatin in the liver owing to the functional disturbance of CYP3A4. The plasma concentration of atorvastatin may either increase or decrease after administration of CYP3A4 inhibitors (12) or inducers, respectively (13).

Acetaminophen induced hepatotoxicity results in inability of body to metabolize atorvastatin, which might have resulted in increased $t_{1/2\lambda}$ and MRT of atorvastatin in the PCM group. Atorvastatin is also a substrate of the intestinal P-glycoprotein efflux transporter, which pumps the drug back into the intestinal lumen during drug absorption (14) and hence reduces the clearance of the drug.

C_{max} and AUC_{0-t} of atorvastatin was significantly decreased in NAC treated group may be due to restoration of liver to normal when compared to that of PCM toxic group. Atorvastatin, when administered in its active acid form, undergoes extensive first pass metabolism mainly by CYP3A4 in the liver (15). Restoration of liver to normal might have favoured the drug metabolism by CYP3A4, which resulted in decreased C_{max} in NAC treated group.

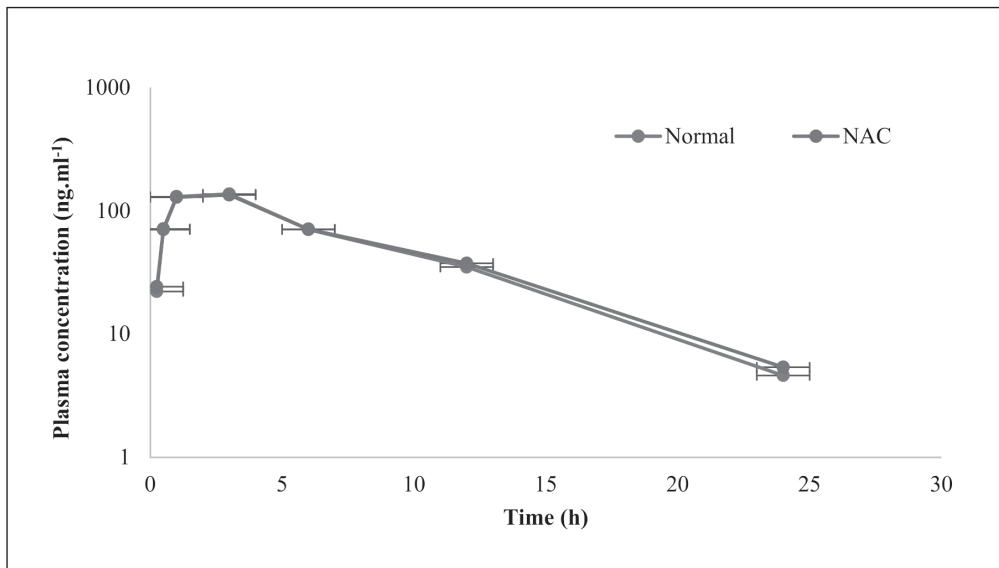
C_{max} , $t_{1/2\lambda}$ and MRT of atorvastatin in GTE group was significantly increased when compared to normal control group and was comparable with that of PCM treated group. Catechins and flavonoids present in green tea

Fig. 3. Plasma atorvastatin concentrations (ng.ml⁻¹) in acetaminophen treated group in comparison with control after single oral administration of atorvastatin (10 mg/kg)



x axis = Time (h), y axis = Plasma concentration (ng.ml⁻¹)

Fig. 4. Plasma atorvastatin concentrations (ng.ml⁻¹) in N-acetyl-L-cysteine (NAC) treated group in comparison with control after single oral administration of atorvastatin (10 mg/kg)



x axis = Time (h), y axis = Plasma concentration (ng.ml⁻¹)

Table 1. Plasma concentrations (ng.ml⁻¹) of atorvastatin after single oral administration of atorvastatin (10 mg/kg) in different groups of rats

Time (h)	Group 1 Normal control	Group 2 PCM control	Group 3 PCM+NAC	Group 4 PCM+GTE
0.25	22.14±0.71	35.5±1.38	27.21±0.71	29.76±0.30
0.5	71.21±1.19	77.56±0.76	72.83±1.11	76.69±0.99
1	128.57±1.79	148.59±1.59	131.68±1.07	136.37±3.72
3	134.32±0.91	154.82±1.73	136.96±0.84	141.09±2.94
6	70.35±1.09	91.61±0.98	82.85±1.52	87.24±1.15
12	34.95±0.65	55.32±0.55	42.05±0.78	48.26±0.88
24	4.61±0.21	13.91±0.55	8.68±0.9	10.88±0.49

*Values are Mean ± SE (n=6)

Table 2. Plasma pharmacokinetic parameters of atorvastatin in different groups of rats after single oral administration of atorvastatin (10 mg/kg)

Parameter	Group 1 Normal control	Group 2 PCM control	Group 3 PCM+NAC	Group 4 PCM+GTE
β (h ⁻¹)	0.15±0.00	0.11±0.00***	0.14±0.00	0.11±0.00***
t _{1/2β} (h)	4.41±0.07	6.23±0.09***	4.62±0.08	5.79±0.12***
AUC _{0-t} (ng.h.mL ⁻¹)	1195.59±5.84	1604.4±13.23***	1214.69±14.28	1451.7±18.35***
AUC _{0-∞} (ng.h.mL ⁻¹)	1225.05±5.64	1794.92±45.87***	1250.76±13.03	1543±20.47***
AUMC _{0-t} (ng.h ² .mL ⁻¹)	7578.31±81.33	11644.24±191.88***	9090.66±357.96**	10380.71±178.26***
AUMC _{0-∞} (ng.h ² .mL ⁻¹)	8473.31±114.84	17988.84±1902.19***	8928.58±95.83	13338.66±366.43*
MRT (h)	6.91±0.07	9.96±0.77***	7.13±0.04	8.64±0.17*
V _{dss} (L.kg ⁻¹)	0.05±0.00	0.05±0.00	0.05±0.00	0.05±0.00
Cl _a (L.kg ⁻¹ .h ⁻¹)	0.008±0.00	0.005±0.00***	0.007±0.00	0.006±0.01***
C _{max} (ng.mL ⁻¹)	134.32±0.91	154.82±1.73***	136.38±0.27	141.09±2.94
t _{max} (h)	3	3	3	3

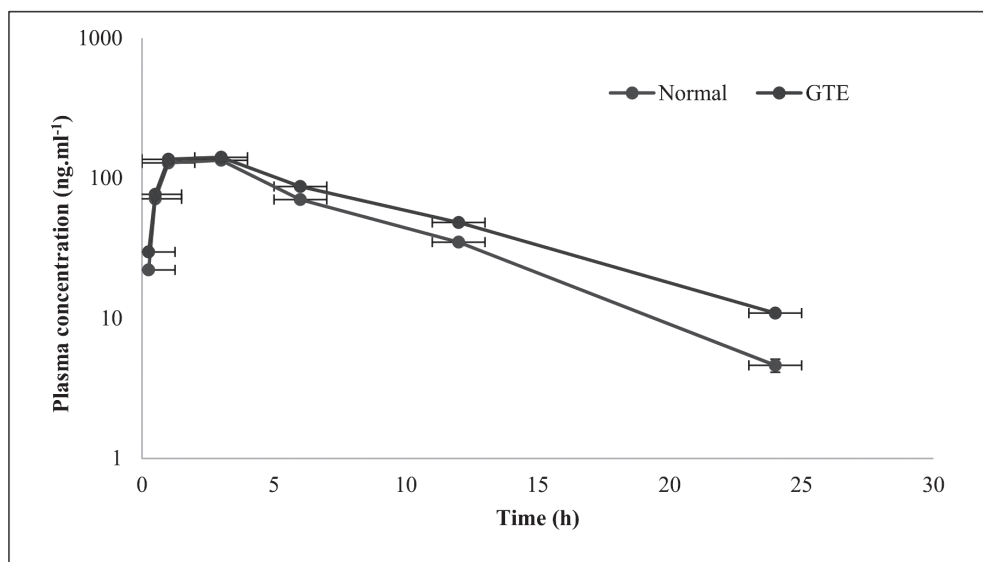
Values are Mean ± SE (n=6); p< 0.05(*), p< 0.01(**), p< 0.001 (***) in comparison to Group 1 (unpaired 't' test with Welch's correction using 'Instat' software)

reduce oxidative stress by effectively scavenge reactive oxygen species and by enhancing the body's antioxidant defences (16). But, the hepatoprotective potential of GTE is comparatively lower when compared to NAC treated group. Among both the drugs in study, the NAC-treated group 3 revealed better metabolic profile of CYP3A4 as compared to Green tea extract-treated group 4.

Conclusion

The present study concluded that pharmacokinetics of atorvastatin metabolism was altered in PCM treated toxic group, which was reflected in increase in C_{max}, AUC_{0-t}, AUMC_{0-t}, AUC_{0-∞} and AUMC_{0-∞} that eventually resulted in prolonged t_{1/2β}, MRT and decrease in total body clearance. Green tea extract could not revive the metabolic functioning of CYP3A4 in comparison to N-acetyl L-cysteine.

Fig. 5. Plasma atorvastatin concentrations (ng.ml⁻¹) in Green tea extract (GTE) treated group in comparison with control after single oral administration of atorvastatin (10 mg/kg)



x axis = Time (h), y axis = Plasma concentration (ng.ml⁻¹)

Acknowledgments

The authors are thankful to the Associate Dean, College of Veterinary Science, Rajendranagar, Hyderabad for providing the necessary financial and infrastructure facilities for this study.

Competing Interests

Authors declare that they have no competing interests.

References

1. Kaplowitz, N. (2004). Drug-induced liver injury. *Clinical Infectious Diseases*, 38 (Suppl 2): 44-48.
2. Zhang, L., Gavin, T., Geohagen, B.C., Liu, Q., Downey, K.J. and LoPachin, R.M. (2013). Protective properties of 2-acetylcyclopentanone in a mouse model of acetaminophen hepatotoxicity. *Journal of Pharmacology and Experimental Therapeutics*, 346(2): 259-269.
3. Olaleye, M.T, Amobonye, A.E., Komolafe, K., Akinmoladun, A.C. (2014). Protective effects of *Parinari curatellifolia* flavonoids against acetaminophen-induced hepatic necrosis in rats. *Saudi Journal of Biological Sciences*, 21(5): 486-492.
4. Rowan, C.G. (2010). Clinical importance of the drug interaction between statins and CYP3A4 inhibitors. Publicly accessible Penn Dissertations. Paper 283.
5. Oh, S.-I., Park, J.-K. and Park, S.-K. (2015). Lifespan extension and increased resistance to environmental stressors by N-Acetyl-L-Cysteine in *Caenorhabditis elegans*. *Clinics*, 70(5): 380-386.
6. Ghezzi, P. (2011). Role of glutathione in immunity and inflammation in the lung. *International Journal of General Medicine*, 4: 105-113.

7. Gonbad, R.A., Afzan, A., Karimi, E., Sinniah, U.R. and Swamy, M.K. (2015). Phytoconstituents and antioxidant properties among commercial tea (*Camellia sinensis* L.) clones of Iran. *Electronic Journal of Biotechnology*, 18: 433–438.
8. Abolfathi, A.A., Mohajeri, D., Rezaie, A. and Nazeri, M. (2012). Protective effects of green tea extract against hepatic tissue injury in streptozotocin-induced diabetic rats. *Evidence-Based Complementary and Alternative Medicine*, 2012: 740671, 10 pages. Doi:10.1155/2012/740671.
9. Sreedevi, C.D., Latha, P.G., Ancy, P., Suja, S.R., Shyamal. S., Shine, V.J., Sini, S., Anuja, G.I. and Rajasekharan, S. (2009). Hepatoprotective studies on *Sida acuta* Burn. f. *Journal of Ethnopharmacology*, 124: 171–175.
10. Zhang, Y., Huo, M., Zhou, J. and Xie, S. (2010). PK solver: An add in program for pharmacokinetic and pharmacodynamics data analysis in Microsoft excel. *Computer methods and program in Biomedicine*, 99: 306-314.
11. Attia, S.M. (2010). Deleterious effects of reactive metabolites. *Oxidative Medicine and Cellular Longevity*, 3(4): 238–253.
12. Borders-Hemphill, V. (2009). Concurrent use of statins and amiodarone. *The Consultant Pharmacist*, 24: 372–379.
13. Lam, S., Partovi, N., Ting, L.S. and Ensom, M.H. (2008). Corticosteroid interactions with cyclosporine, tacrolimus, myco-phenolate, and sirolimus: fact or fiction? *Annals of Pharmacotherapy*, 42:1037–1047.
14. König, J., Müller, F. and Fromm, M.F. (2013). Transporters and drug-drug interactions: important determinants of drug disposition and effects. *Pharmacological Reviews* 65(3): 944-966.
15. Chong, P.H., Seeger, J.D. and Franklin, C. (2011). Clinically relevant differences between the statins: implications for therapeutic selection. *American Journal of Medicine*, 111: 390–400.
16. Higdon, J.V. and Frei, B. (2003). Tea catechins and polyphenols: health effects, metabolism and antioxidant functions. *Critical reviews in food science and nutrition*, 43: 89-143.

Indirect somatic embryogenesis and evaluation of genetic fidelity of *in vitro* propagated plants of *Bunium persicum* (Boiss.) Fedtsch by using DNA markers

Rajinder Kaur, Neha Sharma^{1*}, Sadiq Majeed and Yogeta Thakur^{2,3}

Department of Biotechnology, Dr. Y.S.Parmar University of Horticulture and Forestry, Nauni,
Solan (H.P.) 173230

¹Department of Plant Breeding and Genetics, Punjab Agricultural University, Ludhiana, Punjab, India.

²Central Coordinating Unit, Horticulture Mission for Himachal Pradesh at CPRI Shimla.

³Central Potato Research Institute, Shimla

*For Correspondence - nehahbc@gmail.com

Abstract

A reproducible and efficient protocol was developed for inducing indirect somatic embryogenesis using callus originated from different explants of *Bunium persicum* viz. both immature and mature zygotic embryos, fruit pedicel and cotyledons excised from *in vitro* germinated seedlings. Calli derived from different explants was inoculated on Murashige and Skoog (MS) basal medium of half and full strength supplemented with various concentrations of thiadiazuron, indole butyric acid and with activated charcoal. Callus derived from fruit pedicel gave best response for somatic embryogenesis on MS basal full strength + 0.1% activated charcoal. Half strength MS basal + 1.00 mg/l TDZ + 0.05 mg/l IBA giving as much as 84.33 per cent of somatic embryogenesis and 25.78 was the average number of somatic embryos per callus clump of 200 mg. Maximum of 70.61% somatic embryos showed germination when transferred to half strength MS basal medium. Histological observations revealed that somatic embryos displayed a standard development pattern, from globular to finally cotyledonary stage embryos intervened by heart shaped and torpedo shaped embryos. Molecular characterization of somatic embryo-derived plants was carried out by employing Random Amplified Polymorphic DNA (RAPD) and Inter Simple sequence Repeat (ISSR) primers. DNA extracted from shoots of 15 *Bunium persicum* plantlets regenerated from

somatic embryos and mother plant gave monomorphic banding pattern upon amplification, which indicates that somatic embryogenesis is a suitable technique of micropropagation.

Keywords: Micropropagation, medicinal plant, regeneration, growth regulators, somatic embryogenesis

Introduction

Bunium persicum commonly known in India as 'kalazeera', belonging to the family Apiaceae, is an endangered perennial glabrous herb which is a native of Europe and Western Asia. It has found a prominent place in indigenous system of medicine as it is regarded as a stimulant and has been found to be useful in curing diarrhoea (1), dyspepsia, fever, stomach-ache and obstinate hiccup. Seeds are antihelminthic and insect repellants.

Bunium persicum, the ripe fruits of which form the 'kala zeera' of commerce, is one of the over-exploited, economically important plants. At present, seed is collected from natural populations. Overzealous collection of seed from these populations for commercial purposes has already affected the size and structure of populations. In order to circumvent such problems, the domestication and standardization of agro-practices appear to be necessary for its large scale cultivation.

The species in nature propagates through seed. The seed takes 4-6 months for germination and crop can be harvested after 3 years of sowing. On maturity, it yields 5-10 g mature fruits/plant. Such a long life cycle is a serious impediment in commercial cultivation of this species. This problem can be remedied by applying *in vitro* procedures for rapid mass propagation of *Bunium persicum* (2). Also it was observed that there is paucity of plants of *B. persicum* due to over exploitation of this important medicinal plant species.

Plant tissue culture plays an important role in production and conservation of endangered medicinal plants. Somatic embryogenesis is one of the tissue culture approaches which can be applied for *in vitro* multiplication and conservation. Somatic embryogenesis is a very good approach for *in vitro* propagation of plants, since the plants are single – cell origin, so low frequency of chimeras and the production of a high number of regenerants (3). It is useful in the production of artificial seeds subsequently for *in vitro* conservation of endangered medicinal plants and has been achieved in various medicinal plants. Though, there are a couple of reports on somatic embryogenesis in *B. persicum* and that too with limited success (4, 5) however this study describes the attempt of inducing somatic embryos in different explants. Since tissue culture variations have been observed in numerous crops, so it is very important to study genetic uniformity of somatic embryo-derived plants. Therefore keeping in mind the above introduction the present work was planned.

Materials and Methods

Seeds of Kalazeera were procured from its natural habitat viz., Jammu and Kashmir, i.e., Himalayan mountains of India. Seeds were thoroughly washed and transferred to laminar air flow cabinet for further aseptic sterilization procedures. Seeds were surface sterilized in 0.1% (w/v) mercuric chloride (HgCl₂) for 5 mins and further treated with 0.2% bavistin fungicide; carbendazim.

After this, each single seed was aseptically cultured in (160mm x 25mm) glass tube (Reviera, Mumbai, India) containing Murashige and Skoog (MS) (6) medium supplemented with 100 ppm GA₃ and 3% sucrose. The growing cultures were maintained under 16/8 hour light/dark photoperiod with photoflux intensity 50i mole m⁻²s⁻¹ maintained by cool white fluorescent light.

Calli was induced in different explants on MS basal supplemented with different combinations of (0.50 – 2.00 mg/l) Kinetin (Kn) and (1.00 – 4.00 mg/l) 2,4-dichlorophenoxyacetic acid (2,4-D). However, the calli derived from fruit pedicel were inoculated on half and full strength MS basal medium with different combinations of (0.25- 1.00 mg/l) thiadiazuron (TDZ), (0.05- 0.20 mg/l) indole-3-butyric acid (IBA) and activated charcoal alone. Each experiment consisted of five replicates and was repeated thrice. The observations on induction of somatic embryos from callus were recorded after four weeks of culture and percentage of explants forming somatic embryos was recorded.

The somatic embryos can be identified on the basis of their morphology at different stages of growth and development. After maturation, the germination of somatic embryos was initially attempted on MS basal medium and cultures were incubated under 16 hour photoperiod and 8 hour dark period at 25 ± 2°C and observations were recorded after four weeks of culturing. The term maturation used in this study denoted the development of globular and heart shaped somatic embryos into distinct cotyledonary embryos. Mature embryos were again and again transferred at an interval of four weeks to the same medium under similar culture conditions. Plantlets with well developed root system were transferred to pots containing an autoclaved mixture of soil : sand : FYM (1:1:1) mixture.

Histological Characterization

To study different developmental stages of somatic embryos histological studies were carried out. Embryonic calli and putative somatic embryos originated of different developmental

stages were fixed for four weeks in a formaldehyde: acetic acid: alcohol (FAA) (5: 5: 9) solution and stored at 4°C. The specimens were cut into thin sections and the sections were mounted on to slide and allowed to dry for atleast 10-15 mins before staining. Sections were stained with acetocarmine, safranin, fast green and histological observations were made using Olympus stereo microscope, USA.

Molecular Characterization of Somatic Embryo-Derived Plants:

Genomic DNA from the mother plant and 15 somatic embryo-raised plants were isolated by CTAB (Cetyltrimethyl ammonium Bromide) method according to Doyle and Doyle (7). Five RAPD primers (5383-017, 5383-018, 5383-019, 5383-020 and 5383-021 from Sigma-Aldrich, Bangalore, India) (Table 1) and five ISSR primers (IISRS-3-A, IISRS-3-B, IISRS-3-C, IISRS-3-D and IISRS-3-E from Bioserve, Beltsville, USA) were used to amplify the DNA using protocol of Williams et al. (8) with a few modifications. Reaction conditions and optimum concentrations of various components viz., primer, template DNA, MgCl₂, dNTPs and Taq DNA polymerase for 20 µl reaction mixture were standardized. 20 µl of mixture for RAPD/ISSR-PCR analysis was prepared as follows: 10X PCR buffer (1X), MgCl₂ (25 mM), dNTPs (2.5 mM), Primer (10 pmole/µl), Taq DNA Polymerase (1 U), 60 ng DNA and sterile distilled water to make the final volume 20 µl. All the chemicals procured from Bangalore Genei, India.

The reagents were mixed thoroughly in a 2.0 ml eppendorf tube and vortexed for few seconds. This mixture was equally (17 µl) distributed to each 0.2 ml thin walled PCR reaction tube and then 3.0 µl of DNA was separately added to each tube. The tubes were placed in a thermo cycler (Applied Biosystems Thermal Cycler, California, USA) for cyclic amplification.

The thermal profile for amplification by RAPD was programmed as follows: Initial denaturation at 95°C for 3 mins, 35 cycles each of denaturation at 94°C for 1min, annealing at

36 °C for 1 min, extension at 72° C for 2 mins and final extension at 72°C for 10 mins. The thermal profile for amplification by ISSR was programmed as follows: Initial denaturation at 95°C for 5 mins, 40 cycles each of denaturation at 94°C for 1min, Annealing varied with primer sequence for 1 min, extension at 72° C for 2 mins and final extension at 72°C for 5 mins.

The amplified DNA was mixed thoroughly with 6X loading dye and then electrophoresed in 2.0 per cent agarose gel in 1X TAE buffer. The gel was run at constant voltage at the rate of 5V/cm under submerged conditions for about 3 hour. Ethidium Bromide at rate of 0.5µg/ml was incorporated in the gel. DNA profiles were visualized on a UV transilluminator and photographed by using Gel Documentation System (Syngene, USA).

Analysis of RAPD and ISSR data : Banding pattern generated by using different RAPD and ISSR primers were recorded for monomorphism/polymorphism. Bands which were consistently reproduced across amplifications were considered for the analysis. Faint bands on agarose gels were not taken into consideration. The scoring of bands was done on the basis of their presence ('1') or absence ('0') in the gel.

Results and Discussion

Embryogenic potential is largely a function of explant type, its stage of development and interaction with growth regulators in the medium. Choice of appropriate explant is therefore, critical for embryogenesis. Responsive tissues are generally found in zygotic embryos, cotyledons, cells with embryo sac and tissues associated with the inflorescence (9).

In the present investigation callus initiation was observed within one week of culturing from the cut ends of almost all the explants. Whole surface of explant was covered with callus after the end of fourth week of culturing. The best explant for embryogenic callus induction was fruit pedicel as it gave 100 per cent callus induction when cultured on MS basal medium supplemented with 2.00 mg/l Kn + 4.00 mg/l 2,4-

D, whereas mature zygotic embryos were the least responding even on the best responding medium. MS basal + 0.50 mg/l Kn + 2.00 mg/l 2,4-D was observed to be the least responding medium for callus induction. Callus developed from fruit pedicel, when transferred to different concentrations and combinations of growth regulators (Table 2) for somatic embryo induction it was observed that the number of somatic embryos per callus clump of 200mg was recorded maximum after about four weeks. This was followed by formation of globular stage embryos on the callus after 3-4 weeks in culture.

Further maturation of somatic embryos from globular stage into heart shaped structures and finally to cotyledonary stage structures took place after four weeks and transferred to medium of same composition. When these embryos were transferred to MS basal medium, a maximum of 70.61% somatic embryos showed germination (Table 3). Wakhlu et al. (5) used pericarp of *Bunium persicum* for induction of somatic embryos. Whereas Nair and Gupta (10) attempted somatic embryogenesis in *Piper nigrum*, Chee (11) in *Taxus brevifolia* and Jager and Staden (12) in *Encephalaratos cycadifolis* and all they had used tissues of germinating seeds for induction, maturation and germination of somatic embryos.

Along with the type of explants somatic embryogenesis is strongly dependent upon the presence of growth regulators. The maximum somatic embryo induction was observed on half strength MS basal supplemented with 1.00 mg/l TDZ and 0.05 mg/l IBA (Table 3). These results were found similar to results obtained by Wakhlu et al. (5) in *Bunium*, Halperin (13); Jones (14) in *Daucus carota* and Williams and Collin (15) in *Apium graveolens*. Earlier work done by Wakhlu et al. (5) reported that the number of mature embryos per callus piece on the basal medium was as high as 21 as compared to 10 on medium with growth regulators. Murthy et al. (16) reported TDZ (0.5 μ m) was the best treatment for induction of high frequency somatic embryos in geranium cotyledonary cultures. It has been

shown that TDZ can substitute for both the auxin and cytokinin requirement for inducing somatic embryogenesis in geranium and tobacco tissue cultures (17, 18) and it also induces somatic embryogenesis in peanut explants or seedling cultures which otherwise respond primarily to an auxin for somatic embryo differentiation (18, 19).

Earlier workers have reported that the presence of auxin (20-23), auxin and cytokinin (24-26) and coconut water (20, 27-28) is essential for the induction of somatic embryogenesis. Moreover, when auxins as well as cytokinins are used for embryo induction the ratio of two growth regulators is critical. Generally, a high auxin to cytokinin ratio is necessary for somatic embryogenesis (29-30). The photoperiod was another important factor for somatic embryo induction and further differentiation. Somatic embryo induction was carried out by maintaining the cultures at 25°C for four weeks under a 16 hour photoperiod. Earlier work done by Wakhlu et al. (5) also reported the maintenance of cultures of *Bunium persicum* at 25°C under a 16 h photoperiod for somatic embryo induction.

Histological observations were subsequently carried out to determine the growth stages of somatic embryos. Histological sections indicated that they were true somatic embryos as both shoot and root meristems were present in individual structure. To the best of our knowledge no such study has been carried out earlier in this important medicinal plant species.

After somatic embryogenesis, next requirement is to study stability among somatic embryos raised plants and mother plant. PCR-based molecular markers have emerged as simple, fast, reliable and labor-effective tools for testing the genetic fidelity of *in vitro* raised plantlets. Molecular markers show stability among individuals at the DNA level, which is not influenced by the environment. They are highly informative about genetic uniformity among individuals, populations and cultivars. For the initial screening 10 RAPD 10-mer primers used, only 5 primers produced

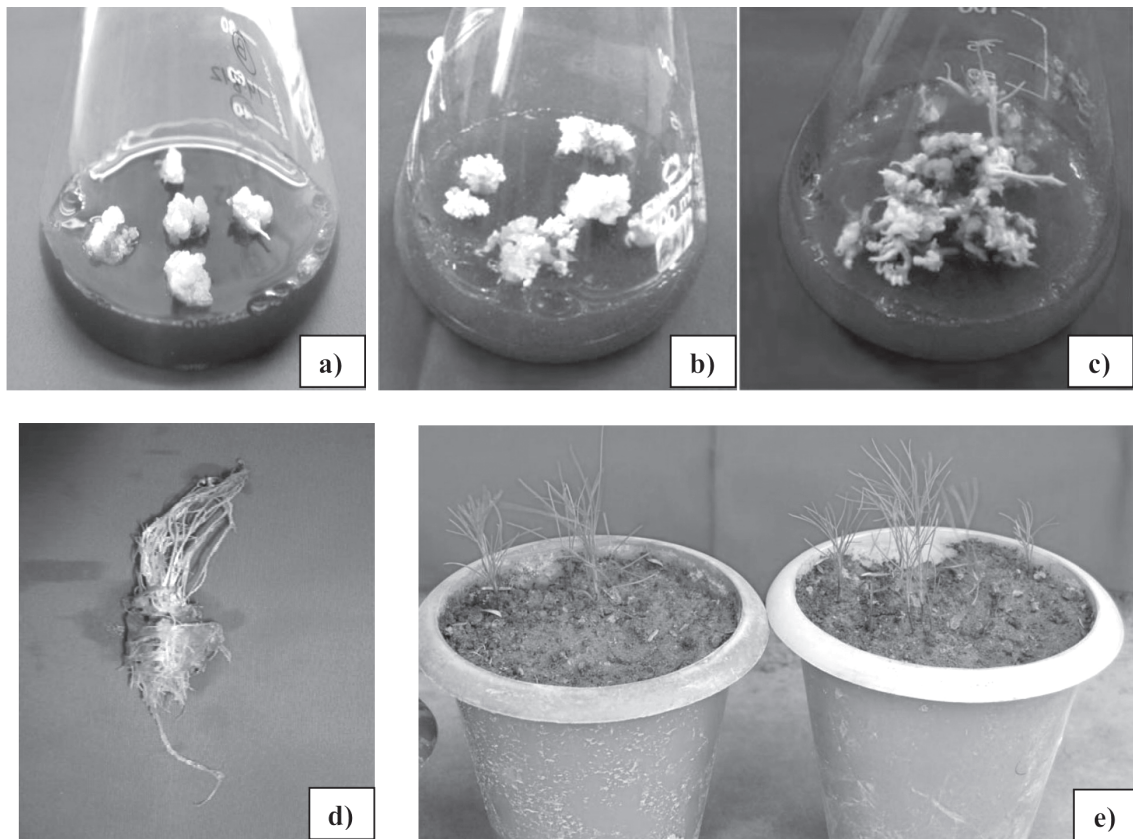


Fig.1. Initiation and regeneration of somatic embryos a) Callus on MS basal + 0.1% Activated charcoal b) Initiation of somatic embryos after four weeks of culturing c) Multiplication of somatic embryos and germination from somatic embryos d) Complete plantlet of *Bunium persicum* e) Hardened plants of *Bunium persicum* after four weeks of hardening

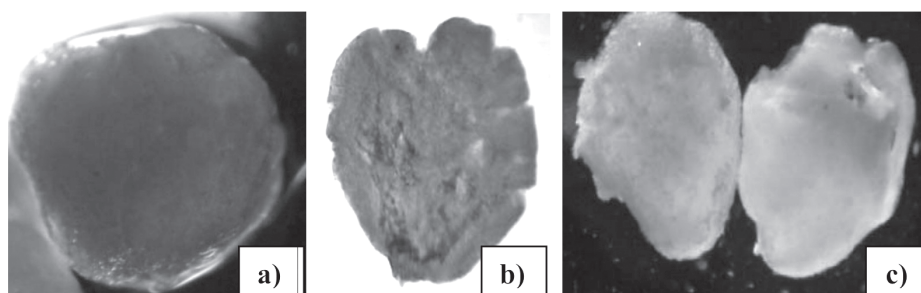


Fig. 2. Different growth stages of somatic embryos a) Globular shape b) Heart shape c) torpedo and cotyledonary shape

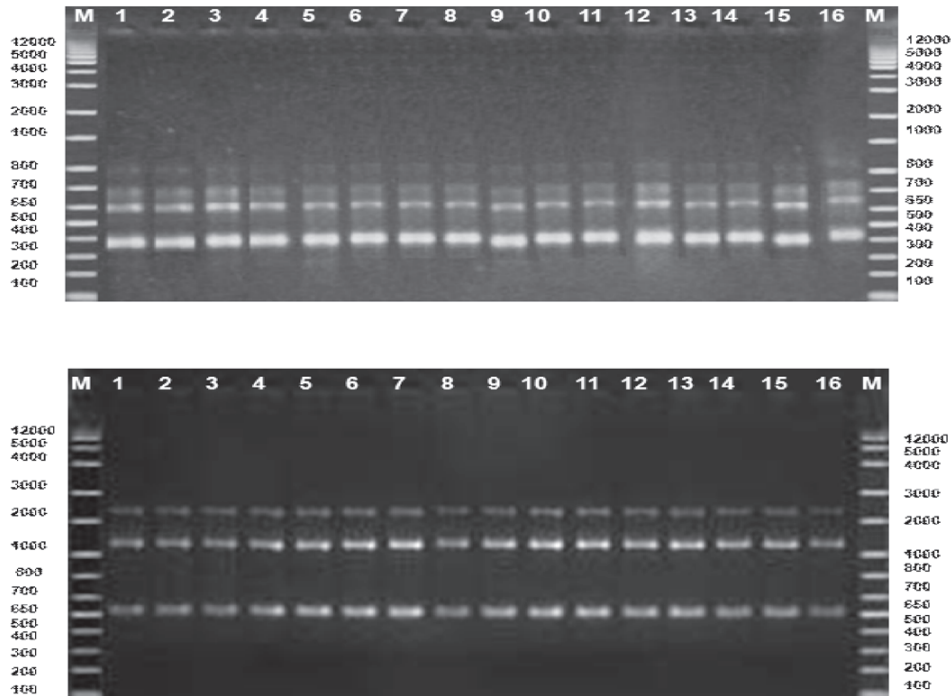


Fig. 3. A: RAPD (5383-018; 5'- TGG GCG TCA A -3') and B: ISSR (IISRS-3-D; 5'- TCT CTC TCT CTC TCT CG -3') banding pattern in both micropropagated plants and field grown plant (Lane 1, mother plant; Lane 2-16 micropropagated plants; M-Known weight molecular marker)

Table 1. List of primers used for fidelity study

S.No.	Primer Name	Primer Type	Primer Sequence	No. of Bases
1.	5383-017	RAPD	5'- GGC ATG ACC T -3'	10
2.	5383-018	RAPD	5'- TGG GCG TCA A -3'	10
3.	5383-019	RAPD	5'- CCA GCA GCT T -3'	10
4.	5383-020	RAPD	5'- GAC TGC ACA C -3'	10
5.	5383-021	RAPD	5'- ACG CAG GCA C -3'	10
6.	IISRS-3-A	ISSR	5'- CTC TCT CTC TCT CTC TT -3'	17
7.	IISRS-3-B	ISSR	5'- CAC ACA CAC ACA CAC AT -3'	17
8.	IISRS-3-C	ISSR	5'- TCT CTC TCT CTC TCT CA -3'	17
9.	IISRS-3-D	ISSR	5'- TCT CTC TCT CTC TCT CG -3'	17
10.	IISRS-3-E	ISSR	5'- ACA CAC ACA CAC ACA CG -3'	17

Table 2. Medium composition for induction of somatic embryo in callus derived from fruit pedicel of *Bunium persicum*.

Treatments (Medium code)	MS strength	Plant Growth Regulators (mg/l)		Activated Charcoal
		TDZ	IBA	
ST-1	Full	-	-	0.1%
ST-2	Full	-	-	0.3%
ST-3	Full	0.25	0.05	-
ST-4	Full	0.50	0.05	-
ST-5	Full	0.75	0.05	-
ST-6	Full	1.00	0.05	-
ST-7	Full	0.25	0.10	-
ST-8	Full	0.50	0.10	-
ST-9	Full	0.75	0.10	-
ST-10	Full	1.00	0.10	-
ST-11	Full	0.25	0.20	-
ST-12	Full	0.50	0.20	-
ST-13	Full	0.75	0.20	-
ST-14	Full	1.00	0.20	-
ST-15	Full	0.25	-	0.1%
ST-16	Full	-	0.05	0.1%
ST-17	Full	0.25	-	0.3%
ST-18	Full	-	0.05	0.3%
ST-19	Half	-	-	0.1%
ST-20	Half	-	-	0.3%
ST-21	Half	0.25	0.05	-
ST-22	Half	0.50	0.05	-
ST-23	Half	0.75	0.05	-
ST-24	Half	1.00	0.05	-
ST-25	Half	0.25	0.10	-
ST-26	Half	0.50	0.10	-
ST-27	Half	0.75	0.10	-
ST-28	Half	1.00	0.10	-
ST-29	Half	0.25	0.20	-
ST-30	Half	0.50	0.20	-
ST-31	Half	0.75	0.20	-
ST-32	Half	1.00	0.20	-
ST-33	Half	0.25	-	0.1%
ST-34	Half	-	0.05	0.1%
ST-35	Half	0.25	-	0.3%
ST-36	Half	-	0.05	0.3%

Table 3. Effect of different concentrations of plant growth regulators on somatic embryo induction in callus derived from fruit pedicel of *Bunium persicum* after four weeks of culturing.

Treatments (Medium code)	MS strength	Plant Growth Regulators (mg/l)		Activated Charcoal	Somatic embryo induction %	Number of somatic embryos per callus clump (200mg)	Germination percent after transfer to MS basal medium
		TDZ	IBA				
ST-1	Full	-	-	0.1%	21.20	4.10	64.65
ST-2	Full	-	-	0.3%	54.98	5.48	52.20
ST-3	Full	0.25	0.05	-	42.50	10.26	62.33
ST-4	Full	0.50	0.05	-	38.25	8.58	59.24
ST-5	Full	0.75	0.05	-	34.33	7.54	57.27
ST-6	Full	1.00	0.05	-	76.87	25.26	69.82
ST-7	Full	0.25	0.10	-	72.67	17.18	67.67
ST-8	Full	0.50	0.10	-	70.36	14.15	67.26
ST-9	Full	0.75	0.10	-	63.03	10.65	61.21
ST-10	Full	1.00	0.10	-	59.31	8.61	57.58
ST-11	Full	0.25	0.20	-	57.32	6.54	53.28
ST-12	Full	0.50	0.20	-	54.98	5.48	52.20
ST-13	Full	0.75	0.20	-	42.59	8.26	42.33
ST-14	Full	1.00	0.20	-	28.25	5.54	59.41
ST-15	Full	0.25	-	0.1%	34.79	9.54	48.27
ST-16	Full	-	0.05	0.1%	72.84	21.26	49.82
ST-17	Full	0.25	-	0.3%	42.98	6.98	67.30
ST-18	Full	-	0.05	0.3%	38.05	7.98	25.80
ST-19	Half	-	-	0.1%	13.66	6.60	70.61
ST-20	Half	-	-	0.3%	31.20	6.10	54.25
ST-21	Half	0.25	0.05	-	64.98	5.48	62.80
ST-22	Half	0.50	0.05	-	23.50	10.26	62.33
ST-23	Half	0.75	0.05	-	38.75	8.58	59.24
ST-24	Half	1.00	0.05	-	84.33	7.54	57.27
ST-25	Half	0.25	0.10	-	56.87	25.78	69.82
ST-26	Half	0.50	0.10	-	42.67	7.18	64.49
ST-27	Half	0.75	0.10	-	70.36	24.15	62.37
ST-28	Half	1.00	0.10	-	63.03	10.65	61.21
ST-29	Half	0.25	0.20	-	59.31	8.61	57.58
ST-30	Half	0.50	0.20	-	57.32	6.54	53.28
ST-31	Half	0.75	0.20	-	44.28	6.48	62.98
ST-32	Half	1.00	0.20	-	42.39	9.26	52.33
ST-33	Half	0.25	-	0.1%	38.25	7.54	49.41
ST-34	Half	-	0.05	0.1%	34.59	13.54	58.27
ST-35	Half	0.25	-	0.3%	72.84	31.26	39.62
ST-36	Half	-	0.05	0.3%	78.67	23.07	

reproducible and scorable bands. These 5 selected RAPD primers were then used for further analysis and gave rise to a total of 16 scorable bands ranging from 300 to 800 bp (Fig. 3A). The number of bands for each primer varied from 2 to 4 with an average of 3.2 bands per primer. The highest number of bands obtained was 4 in case of primer 5383-018 (5'-TGG GCG TCA A -3') and 5383-019 (5'-CCA GCA GCT T -3') and the lowest number of bands, i.e. 2, was obtained in the case of primer 5383-017 (5'-GGC ATG ACC T -3'). RAPD mediated DNA fingerprinting has been extensively used for the detection of polymorphism among the micropropagated medicinal plants.

In ISSR analysis, out of the 5 markers screened, primers generated 14 scorable bands ranging from 650 to 2500 bp in size. The number of bands for each primer varied from 2-3, with an average of 2.8 bands per ISSR primer (Fig. 3B). Lowest number of bands, i.e. 2, was obtained in the case of primer IISRS-3-E (5'-ACA CAC ACA CAC ACA CG -3'). Monomorphic banding pattern was obtained (Fig. 3) with all primers tested which suggested uniformity of somatic embryogenesis derived plants and their trueness-to-type to the mother plant. Both marker analyses revealed no variation among regenerants and mother plant which supports the findings of Cai et al. (31) and He et al. (32) in other medicinal plant species. No polymorphism was observed revealing the genetic stability of *in vitro* regenerated plants. The results of this study clearly indicated that micropropagated plants were genetically identical to that of the mother plant and no variation was induced during clonal propagation.

CONCLUSION

The present study of somatic embryogenesis has been established for rapid *in vitro* multiplication of *Bunium persicum*. The complete procedure from induction of somatic embryos to plantlet recovery completed within 70 days. Such a novel protocol can emphasize

the great potential of biotechnological approaches such as *in vitro* selection, production of synthetic seed and development of genetic transformation studies in this medicinally important plant species. This protocol's main application is to help minimize the pressure on wild populations and conservation of the valuable medicinal plant.

Conflict of interest: All the authors declare that they have no conflict of interest.

Acknowledgements

The authors would like to thank Mini Mission I (Himachal Pradesh) Indian Council of Agricultural Research, New Delhi for the project entitled "Micropropagation and *in vitro* conservation of *Bunium persicum* – an endangered medicinal plant".

References

1. Baser, K. H. C., Ozek, T., Abduganiv, B. E., Abdullaer, U. A. and Aripov, K. N. 1997. Composition of the essential oil of *Bunium persicum* (Boiss.) B. Fedtsch. from Tajikistan. Journal of Essential Oil Research, 9: 597-598.
2. Grewal, S. and Rani, M. (1999). Repetitive somatic embryogenesis in aggregated liquid culture of *Bunium persicum* (Boiss Fedtsch). Indian Journal of Experimental Biology, 37: 70-74.
3. Ammirato, P.V. (1983). Embryogenesis. In: Evans, D.A., Sharp, W.R., Ammirato, P.V. and Yamada, Y. (eds.) Handbook of Plant Cell Culture. Vol. I, Techniques for propagation and breeding. Plenum, New York, pp. 82-123.
4. Grewal, S. (1996). Induction of somatic embryogenesis and organogenesis in *Bunium persicum* (Boiss), callus culture. Indian Journal of Experimental Biology, 34: 356-358.
5. Wakhlu, A.K., Nagari, S. and Barva, K.S. (1990). Somatic embryogenesis and plant regeneration from callus cultures of *Bunium*

- persicum* Boiss. Plant Cell Reports, 9: 137-138.
6. Murashige, T. and Skoog, F. (1962). A revised medium for rapid growth and bioassays with tobacco tissue cultures. *Physiologia Plantarum*, 15: 473-479.
 7. Doyle, J.J. and Doyle, J.J. (1987). A rapid DNA isolation procedure from small quantities of fresh leaf tissues. *Phytochemical Bulletin*, 19: 11-15.
 8. Williams, J.G.K., Kubelik, A.R., Livak, K.J., Rafalski, J.A. and Tingey, S.V. (1990). DNA polymorphisms amplified by arbitrary primers are useful as genetic markers. *Nucleic Acids Research*, 18: 6531-6535.
 9. Litz, R.E. and Grey, D.J. (1992). Organogenesis and somatic embryogenesis. In: Hammerschlag, F.A. and Litz, R.E. (eds.) *Biotechnology of perennial crops*, Wallingford: Cab International, UK, pp. 3-34.
 10. Nair, R.R. and Gupta, S.D. (2003). Somatic embryogenesis and plant regeneration in black Pepper (*Piper nigrum* L.) I. Direct somatic embryogenesis from embryos. *Journal of Horticultural Science and Biotechnology*, 18: 416-421.
 11. Chee, P.P. (1996). Plant regeneration from somatic embryos of *Taxus brevifolia*. *Plant Cell Reports*, 16: 184-187.
 12. Jager, A.K., Staden, J.V. (1996). Somatic embryogenesis in *Encephalartos brevifolia*. *Plant Cell Reports*, 15: 437-440
 13. Halperin, W. (1966). Alternative morphogenetic events in cell suspensions. *American Journal of Botany*, 53: 443-453
 14. Jones, L.M. (1974). Factors influencing embryogenesis in carrot cultures (*Daucus carota* L.). *Annals of Botany*, 38: 1077-1088.
 15. Williams, L. and Collin, H.A. (1976). Embryogenesis and plantlet formation in tissue cultures of celery. *Annals of Botany*, 40: 325-332.
 16. Murthy, B.N.S., Singh, R.P. and Saxena, P.K. (1996). Induction of high frequency somatic embryogenesis in geranium (*Pelargonium X Hortorum Bailey cv Ringo Rose*) cotyledonary cultures. *Plant Cell Reports*, 15: 423-426.
 17. Visser, C., Qureshi, J.A., Gill, R. and Saxena, P.K. (1992). Morphoregulatory role of thidiazuron. *Plant Physiology*, 99: 1704-1707.
 18. Gill, R. and Saxena, P.K. (1992). Direct somatic embryogenesis and plant regeneration from seedling explants of peanut (*Arachis hypogea*); promotive role of thidiazuron. *Canadian Journal of Botany*, 70: 1186-1192.
 19. Saxena, P.K., Malik, K.A. and Gill, R. (1992). Induction by thidiazuron of somatic embryogenesis in intact seedlings of peanut. *Planta*, 187: 421-424.
 20. Halperin, W. and Wetherell, D.F. (1964). Adventive embryony in tissue cultures of wild carrot, *Daucus carota*. *American Journal of Botany*, 51: 274-283.
 21. Kato, M. and Takeuchi, M. (1963). Morphogenesis *in vitro* starting from single cells of carrot root. *Plant Cell Physiology*, 4: 243-245.
 22. Cruz, G.S., Canhota, J.M. and Abreu, M.A.V. (1990). Somatic embryogenesis and plantlet regeneration from zygotic embryos of *Feijoa sellowiana*. *Plant Science*, 66: 263-270.
 23. Xiao, J.N., Muassssng, X.L., Wu, Y.J., Li, X.J., Zhou, M.D. and Engelmann, F. (2004). Direct embryogenesis induced from cotyledons of mango immature zygotic embryos. *In Vitro Cellular and Developmental Biology-Plant*, 40: 196-199.

24. Mitra, G.C. and Chaturvedi, H.C. (1972). Embryoids and complete plants from unpollinated ovaries and from ovules of *in vitro* grown emasculated flower buds of citrus spp. Bulletin of Torrey Botanical Club, 99: 184-189.
25. Kochba, J., Spiegel, R.P. and Safran, H. (1972). Adventive plants from ovules and nucelli in citrus. Planta. 106: 237-245.
26. Kumari, N., Jaiswal, U. and Jaiswal, V.S. (1998). Induction of somatic embryogenesis plantlet regeneration from leaf callus of *Terminalia arjuna* Bedd. Current Science, 75: 1052-1055.
27. Steward, F.C., Maper, M.O., Kert, A.E. and Holsten, R.D. (1964). Growth and development of cultured plant cells. Science, 143: 20-27.
28. Quesada, R.P., Romero, C.S., Munoz, A.D. and Pliego, A.F. (2004). Factors affecting maturation of avocado somatic embryos. Scientia Horticulturae, 102: 61-73.
29. Vieitez, F.J., Ballester, A. and Vieitez, A.M. (1992). Somatic embryogenesis and plant regeneration from cell suspension cultures of *Fagus sylvatica* L. Plant Cell Reports, 11: 609-613.
30. Cuenca, B., San, J.M.C., Martinez, M.T., Ballester, A. and Vieitez, A.M. (1999) Somatic embryogenesis from stem and leaf explants of *Quercus robur* L. Plant Cell Reports, 18: 538-543.
31. Cai, Y., Liu, Y., Liu, Z., Zhang, F., Xiang, F and Xia, G. (2009). High-frequency embryogenesis and regeneration of plants with high content of gentiopicroside from the Chinese medicinal plant *Gentiana straminea* Maxim. In Vitro Cellular Developmental Biology-Plant, 45: 730–739.
32. He, T., Yang, L. and Zhao, Z. (2011). Embryogenesis of *Gentiana straminea* and assessment of genetic stability of regenerated plants using inter simple sequence repeat (ISSR) marker. African Journal of Biotechnology, 10: 7604-7610.

Optimization of process parameters for α -amylase production using Artificial Neural Network (ANN) on agricultural wastes

Santosh Kumar Mishra^a, Shashi Kumar^b, Surendra Kumar^c, Ravi Kant Singh^{d*}

^aDepartment of Biotechnology, IMS Engineering College, Ghaziabad, UP, India

^{b,c}Chemical Engineering Department, Indian Institute of Technology Roorkee, Roorkee 247667, Uttarakhand, India

^dDepartment of Biotechnology, Noida Institute of Engineering & Technology, Gr. Noida, UP, India

*For Correspondence – rksingh.iitr@hotmail.com

Abstract

Studies of α -amylase production using different solid substrates of wheat bran (WB), rice bran (RB) and mustard oil cake (MOC) were carried out using solid state fermentation (SSF) by *Gliomastix indicus*. All the substrate supported microbial growth and enzyme production by this microbial culture. However MOC was found best suited solid substrate for maximum production of α -amylase. MOC was further used as a solid substrate for the study of individual and combined effect of moisture content, incubation temperature, pH, incubation time, salt concentration, and choice of nitrogen source on the production of α -amylase. The Artificial Neural Network (ANN) based model was developed to optimize the process parameters and to correlate the effects of different parameters on α -amylase production. The maximum activity of α -amylase was observed 1785.71U/g with MOC as solid substrate in optimized conditions. Partial purification of crude enzyme sample was carried out using ammonium sulfate precipitation followed by size exclusion chromatography (SEC). The appearance of a single band in SDS-PAGE has shown the presence of α -amylase enzyme having molecular weight ~56kDa. The specific activity of purified enzyme has been observed 6.11U/mg.

Keywords: *Gliomastix indicus*, Solid State Fermentation, Artificial Neural Network, Process Optimization, SDS-PAGE, Molecular Weight.

Introduction

The production of fungal α -amylase has been investigated by various researchers through submerged fermentation and solid state fermentation (1,2,3) and it has been reported that solid state fermentation (SSF) is the most preferred process in developing countries in comparison to submerged fermentation due to advantages and availability of different agricultural wastes (4). The hyphae mode of fungal growth and their good tolerance to less water activity (a_w) and osmotic pressure conditions make fungi as efficient and competitive in natural micro flora for bioconversion of solid substrate (5). However content of synthetic medium are very expensive and uneconomical, so they need to be replaced with more economically available agricultural and industrial byproducts since they are considered as good solid substrate for SSF to produce industrially important enzymes (6).

The production of microbial enzymes in SSF is affected by a variety of physical and chemical factors i.e. composition of nutrients, incubation temperature, pH of medium, particle size of the solid substrate, moisture level of the substrate (7,8) etc . Screening of a number of agro-industrial residues for microbial growth and product formation was optimized by researchers (9). Mustard oil cake (MOC) is an agricultural byproduct obtained after oil extraction. The chemical composition of MOC varies with change

in the oil extraction methods. These oil cakes are fairly rich in protein and carbohydrate & traditionally used as feed ingredients for farm animals and aquaculture feeds (10). Different microorganisms have been reported for amylase production using variable agricultural byproducts (11) but no information is available for the production of α -amylase from *Gliomastix indicus* by using MOC as solid substrate (12).

The optimization of process parameters (moisture content, incubation temperature, pH of medium, incubation time, salt concentration, and nitrogen sources) are considered under the statistical analysis for a cost effective α -amylase production process. Several approaches have been used for the optimization of α -amylase production process by varying one factor at a time method. ANN can be used as alternative method to the polynomial regression based modeling tool, which provides the modeling of complex non linear relationships. In ANN a network is a collection of nodes and their connections. A node represents a computational unit which receives input and processes it to get an output. The connections between nodes determine the flow of information. The concept of artificial neural network is inspired from physiology of biological neurons. It basically has three main tasks: multiplication, addition, and activation. The inputs (signal) received are multiplied with their corresponding weights (strength of signal) and then computed by a mathematical function for the activation of neuron. Another function determines the output of the artificial neuron. The artificial neural network combines these artificial neurons for information processing. The method of information processing by a neuron in ANN is shown in figure-1. The ANN modes are potentially more accurate by considering the maximum experimental data (13,14). The application of ANN approaches are not been reported for modeling and optimization of α -amylase production using *G. indicus* on solid state fermentation system. The ANN tools PYTHIA-the neural network designer was used to optimize all process parameters that affect the amylase

production. The aim of the present study was to investigate the α -amylase production under SSF conditions by *G. indicus* using MOC as solid substrate. The process parameters have been optimized for different parametric condition to achieve maximum production of α -amylase.

Materials and Methods

Microorganism: The microorganism *Gliomastix indicus* (MTCC 3869) was procured from the Institute of Microbial Technology (IMTECH) Chandigarh India. *G. indicus* comprises the properties of filamentous fungi and rapidly grows on all common mycological media such as malt extract, potato dextrose agar etc. This fungal strain was maintained on the potato dextrose agar (PDA) medium which contains; potatoes 200g/l, dextrose 20g/l and agar 15g/l. The pH of the medium was adjusted to 6 by using 1N NaOH. The organism was maintained by the serial transfer on the PDA medium after every fortnight and incubated at 28°C (12,15).

Inoculum preparation: Inoculum was prepared by transferring 5ml suspension culture, into 250ml conical flask containing 95ml of sterile inoculum medium. The composition of the inoculum medium was (g/l): Glucose (20g/l), NH_4NO_3 (3g/l), $\text{MgSO}_4 \cdot 7\text{H}_2\text{O}$ (0.5g/l), KCl (0.5g/l), K_2HPO_4 (1g/l), $\text{FeSO}_4 \cdot 7\text{H}_2\text{O}$ (0.01g/l), with a pH of solution 6.0. The flasks were incubated on a rotary shaker at 200rpm at 30°C for 48 hrs (16).

Optimization of fermentation process: Various factors that affect the secretion of α -amylase enzyme i.e. initial moisture content, incubation temperature, pH of medium, incubation time, salt

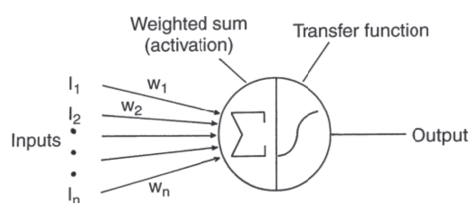


Fig. 1: Information processing by a single neuron in Artificial Neural Network (ANN)

concentration and supplementary nitrogen source were studied. The batch experiments were conducted in 250 ml Erlenmeyer flask containing 5gm of solid substrate with 1ml of salt solution. The sodium chloride (4.5% NaCl) was used as salt solution for further studies. The distilled water was added to processed solid substrate to maintain desired moisture content and sterilized and further after cooling inoculated with 1ml of inoculums and incubated at 30°C for 96 hrs.

Effect of various substrates: The solid substrate like wheat bran (WB), rice bran (RB) and mustard oil cake (MOC) were procured from the local market and were used to observe as potential solid substrate for the production of α -amylase. MOC has been found excellent solid substrate for amylase production using *G. indicus*.

Effect of initial moisture content: To investigate the influence of the initial moisture content (before autoclaving) of the substrate, the fermentation media was supplemented with variable moisture content (40, 60, 70, 80, 90, 100, 120 w/v %) of mustard oil cake (MOC). Desired moisture level was maintained by using distilled water. The optimum moisture level observed in this experiment was further fixed for subsequent experiment.

Effect of incubation temperature: The solid state fermentation was carried out at various incubation temperatures i.e. 20, 25, 30, 35, 40 °C to study their effect on enzyme production, keeping all other conditions at their optimum levels.

Effect of initial pH: While optimizing the initial pH of solution, the pH was varied from 4.0 to 9.0 with 1N HCl or 1N NaOH. The fermentation was carried out at 30°C to study their effects on enzyme production. The other process parameters were 10 % inoculum level, 80 % moisture content and the fermentation process was carried out for 96 hrs at 30°C. The optimum pH of solid substrate achieved by this step was fixed for subsequent experiments.

Effect of incubation time: Different incubation times (48, 72, 96, 120, 144 hrs) were employed to study their effects on α -amylase production. The solid state fermentation was carried out at 30°C keeping all the conditions at their optimum levels. The optimum incubation time achieved by this step was fixed for subsequent experiments.

Effect of concentration of salt solution: Various concentrations of NaCl as salt solution (2.5, 3.5, 4.5, 5.5, and 6.5 %) were employed to study their effects on enzyme production. The fermentation process was carried out at 30°C having other experimental conditions at their optimum levels. The optimum concentration of salt solution (NaCl) to solid substrate achieved by this step was fixed for subsequent experiments.

Effect of supplementary carbon and nitrogen sources: Mustard oil cake (MOC) was supplemented with different carbon (glucose, soluble starch, sucrose, maltose) and nitrogen sources (like peptone, NH₄Cl, NH₄NO₃, Urea, Ammonium phosphate) at different level to study their effects of amylase production. The SSF process was carried out at 30°C keeping all other conditions at their optimum levels.

Enzyme assay: The crude enzyme from the fermented material was extracted by simple contact method. Initially the fermented substrate was mixed thoroughly with distilled water containing 0.1% Tween-80, to total extract volume amounts of 100 ml. Contents were mixed thoroughly by shaking in a rotary shaker at 150 rpm for 1 hr at room temperature. At the end of the extraction, the suspension was centrifuged at 7000 rpm for 15 minutes and the clear supernatant was used as crude enzyme. α -amylase activity was determined by the method of Okolo et al., 2005 (17). The reaction mixture consisted of 1ml of soluble starch, 0.5 ml of 0.1M acetate buffer having pH 5.0 and 0.25 ml of crude enzyme extract. After the 15 minute of the incubation time at 35°C the liberated reducing sugar were estimated by the DNSA method (18). The color developed was read at 540 nm using

Systronics UV-visible spectrophotometer. Glucose was used as the standard. One unit (IU) of α -amylase is defined as the amount of enzyme releasing $1\mu\text{mol}$ of glucose equivalent per minute under the assay condition.

Protein purification and electrophoresis: The crude amylase solution or the cell-free culture medium was fractionated into 0-40, 40-70 and 70-90% ammonium sulfate saturation. These fractions were suspended in a minimum volume of 0.1M acetate buffer at pH 5 and dialysed for 24 h. Single-step purification was carried out by loading cell-free supernatant containing amylase in 1M ammonium sulfate directly onto a phenyl sepharose 6FF column equilibrated with 0.1M acetate buffer at pH 5 containing 1M ammonium sulfate. The fractions were eluted in the same buffer using a decreasing gradient of ammonium sulfate (1-0 M) at a flow of 0.7 ml m^{-1} . The fractions were collected and further analyzed. The crude and dialyzed samples, partially purified precipitate and purified amylase were stored at 4C for further characterization. Standard protein marker was used for the molecular weight determination of protein content using Laemmli method (19).

ANN based Process optimization for α -amylase production: ANN has been used to solve large number of problems in different fields. Most of them are layered feed-forward ANN, with back propagation learning algorithms (14). In layered feed-forward ANNs the artificial neurons are organized in layers, which are input, hidden and output layers. In the present study, three layered ANN was used with four neurons at input layer one for each input parameter, four neurons at single hidden layer and one neuron at output layer as shown in figure-2. The input layer neurons receive inputs, and send the output to the output layer neuron where the final output was calculated using Fermi function. The back propagation algorithm uses supervised mode of learning, in which the algorithm is provided with a set of inputs and outputs which we want the network to compute, and then the error is calculated. In this study 25 set of experimental

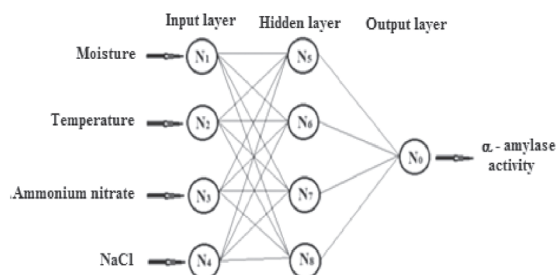


Fig. 2: Three layered artificial neural network for α -amylase activity optimization system

data each with four different process parameters at different level were used for the training purpose as given in table-2 and 3 set of experimental data were used for further validation or testing of model. The process of adjustment of weights in ANN is called *learning* or *training*. During the training phase the signals are first sent in forward direction, and then the errors are propagated backwards to minimize it. The minimization of the error between actual and expected output is the main technique used in the back propagation algorithm. The training begins with random weights, and the goal is to adjust them so that the error will be minimal (20,21,22).

Result and Discussion

The solid state fermentation (SSF) process was observed to be less sensitive than submerged fermentation in terms of chance of contamination (23,24,25). The selection of suitable solid substrate for solid state fermentation process is a critical factor. In lieu of this, the screening of various agriculture byproducts is studied to achieve optimum enzyme activity. In the present studies, three solid substrates (Wheat bran, Mustard oil cake, Rice bran) were used for the studies of microbial growth and enzyme production on *G. indicus*. All the substrates supported microbial growth and enzyme production by this microbial culture, while mustard oil cake (MOC) was found best solid substrate for maximum production of α -amylase as shown in figure-3. During the initial experiments the activity of amylase was found

to be 1161U/g when MOC was used as solid substrate. However if wheat bran and rice bran were used as solid substrate the amylase activity was found comparatively less by using *G. indicus* as microbial strain. Similar type of observation was found in study which has shown that nature of solid substrate affects the production of α -amylase and its activity (26).

Effect of various process parameters over enzyme production: The moisture contents in the solid substrate are also a critical factor in fermentation process and it is already established by several researchers. Maximum enzyme activity was found at 90 to 100% of initial moisture content. However if the moisture level is increased there is a sharp fall in the enzyme activity. This happens because at high moisture content, the porosity of the solid substrate reduced, that limit the oxygen transfer in the fermentation process (27) and further at low moisture content the solubility of nutrients of solid substrate also reduced and reduced the degree of swelling in solid substrate (27,28). This indicates that initial moisture content play a significant role in the solid state fermentation (figure-4). Similar types of studies were performed by various researchers to observe the effect of moisture content on different solid substrate in SSF (29,30,31).

The metabolic activities of the microorganisms are very sensitive with pH of medium. The production of α -amylase on *G. indicus* was found to be affected by changing the pH level and the maximum α -amylase production (1135 U/g) was obtained at pH of nutrients 6 (Figure-5). However if the pH has been increased a sharp decline in the amylase production was reported. However when *Penicillium brevicompactum* was used as fungal strain for α -amylase production the optimal production was reported at pH 5 with similar trend (32,33) A similar trend also has been observed in amylase production when *Bacillus* species was used. The enzyme was optimally produced in the broth at pH 7, although significant production was also evident at pH 8–9 (34).

The maximum enzyme production was found at 96 hours of incubation time (figure-6). Similar type of results was reported for α amylase production by *P. chrysogenum* cultivated in liquid media containing maltose (2%) give optimum production when incubated 6–8 days, at 30°C (32).

The optimum incubation temperature for amylase production was found to be 30°C as shown in figure-7. Most of the fungal species gives maximum production of amylase when incubation temperature was 30°C with suitable moisture content (3,35, 36).

The effect of concentration NaCl as salt solution on enzyme activity was studied and the maximum enzyme activity (1756.63 U/g) was obtained at 4.5% (w/v) NaCl concentration shown in figure-8. It was very important parameter that has to be controlled for optimum production of enzyme which varies from organism to organism. A Box–Behnken design was also employed by researchers to optimize the media composition, which showed that an incubation temperature of 30°C, an initial moisture of 70% and an inoculum rate of 1×10^7 spores/g dry substrate were the optimum conditions to produce α -amylase with *A. oryzae* (37).

The studies on supplementation of inorganic and organic nitrogen sources such as ammonium nitrate, peptone, ammonium chloride, urea and ammonium phosphate at various concentrations were carried out to the mustard oil cake for α -amylase production. All of these sources indicated different trend on enzyme production. Among all of these nitrogen sources, ammonium nitrate gave highest enzyme activity (1527.84 U/g) at 0.1% (w/v) as shown in figure-9. This suggests that ammonium nitrate is the best supplementary nitrogen source.

The supplementary carbon sources such as glucose, sucrose, fructose and starch at 1% (w/v) concentration were added to the MOC for α -amylase production. All of these sources indicated different trend on enzyme production. Among all of these supplementary carbon

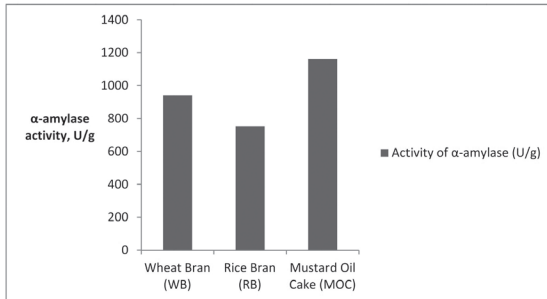


Fig. 3: Effect of different solid substrate on α -amylase production.

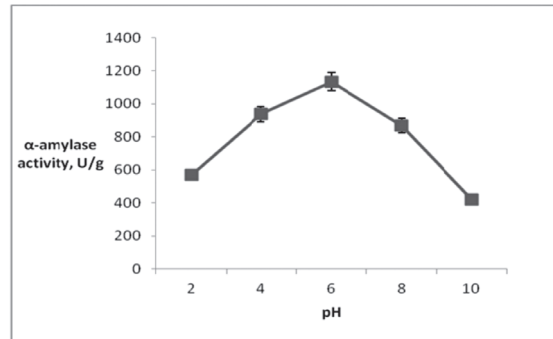


Fig. 5: Effect of pH of medium on α -amylase production.

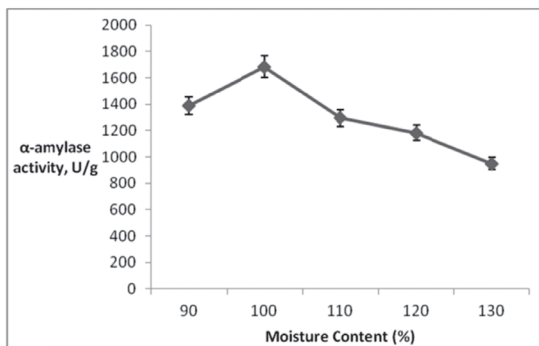


Fig. 4: Effect of moisture content on α -amylase production.

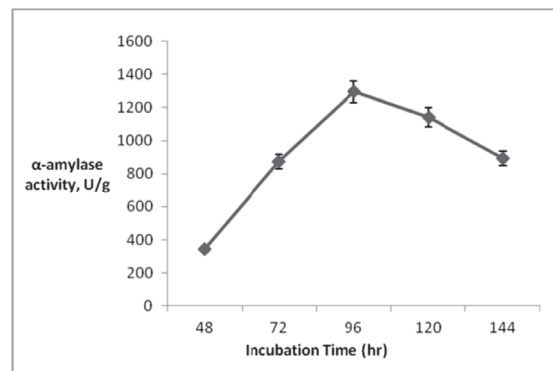


Fig. 6: Effect of incubation time on α -amylase production.

sources, the presence of starch promoted the growth of microorganism and shown higher enzyme activity of 1605 U/g as compare to other carbon sources used. The effect of different supplementary carbon sources on enzyme production is shown in figure-10.

In view of above results, the optimal production of α -amylase was achieved at 100% initial moisture content, 30°C incubation temperature, 96 h incubation time, 4.5% (w/v) concentration of NaCl as additional salt content, 1% (w/v) and 0.1% (w/v) concentration of ammonium nitrate as supplementary nitrogen source with solid state fermentation process on mustard oil cake (MOC) by using *Gliomastix indicus*.

Purification and molecular weight determination of α -amylase:

70-90% saturation of ammonium sulfate has given the maximum precipitated enzyme. The saturated protein has been dialysed for 24 hours and further purified by gel filtration chromatography using a Phenyl sepharose column. 55.4% recovery of the purified amylase protein with a specific activity of 6.11U/mg was achieved by gel filtration. The presence of a single band in SDS-PAGE of the purified enzyme has shown the presence of α -amylase enzyme, with a molecular weight ~56 kDa as shown in figure-11.

Process parameters optimization using ANN:

Three layered ANN architecture having four neurons at input layer, four neurons at hidden

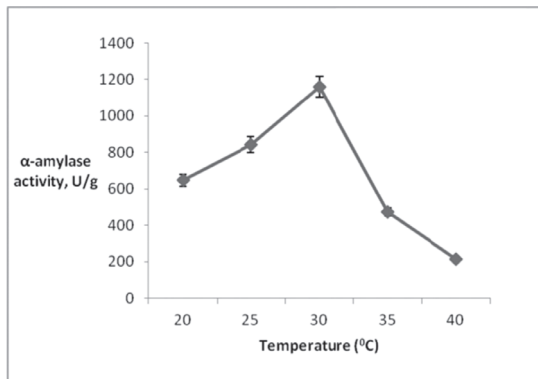


Fig. 7: Effect of incubation temperature on α -amylase production

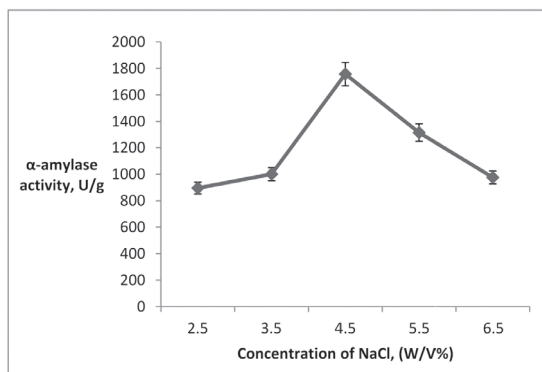


Fig. 8: Effect of NaCl concentration on α -amylase production

layer and one neuron at output layer as shown in figure-2 was used for the process optimization. Three levels of each process parameters (Low, Medium and High) were selected for the optimization purpose as shown in table-1. The overall optimization experiments were designed by selecting the combination of these three levels of each process parameters. The actual design of experiment for training the ANN model is given in table-2. The learning phase of ANN algorithm generates various weights for each node connections. These weights are used to calculate the final prediction value at output level. The weights of different node connections between input and hidden layer neuron connections and the weights of hidden and output layer neuron connections generated after learning phase using

Optimization of process parameters for α -amylase production

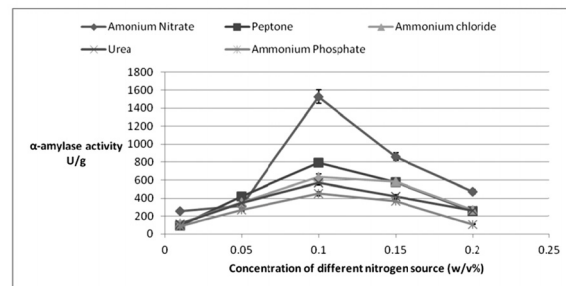


Fig. 9: Effect of different Nitrogen sources with variable concentration on α -amylase production

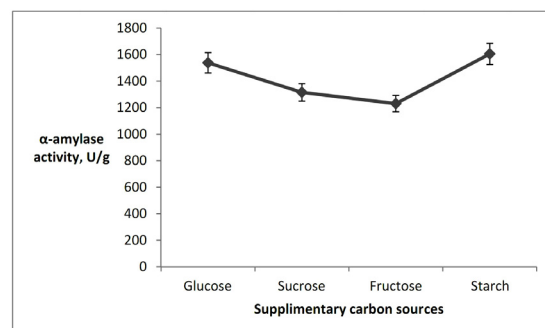


Fig. 10: Effect of supplementary carbon sources on α -amylase production by *G. indicus*

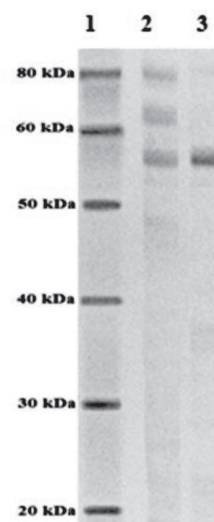


Fig. 11: SDS-PAGE of the purified amylase from *G. indicus* where protein marker is in Lane1, crude enzyme extract in Lane2 and isolated enzyme after chromatography by Phenyl sepharose column at Lane3.

Table 1: The levels of variable selected for the process optimization experiment

Moisture Content (%) X_1	Temperature ($^{\circ}$ C) X_2	NH_4NO_3 (w/v %) X_3	NaCl (w/v %) X_4
40 (L)	20 (L)	0.05 (L)	2.5 (L)
80 (M)	30 (M)	0.10 (M)	4.5 (M)
120 (H)	40 (H)	0.15 (H)	6.5 (H)

Table 2: The actual design of experiment for training data set

Experiment No.	Moisture Content (%) X_1	Temperature ($^{\circ}$ C) X_2	NH_4NO_3 (w/v%) X_3	NaCl (w/v%) X_4
1	M	M	M	M
2	M	M	H	M
3	M	H	M	M
4	M	L	M	M
5	L	M	M	M
6	M	M	M	L
7	H	H	L	L
8	L	L	L	H
9	L	H	L	H
10	L	L	H	H
11	H	M	M	M
12	L	H	H	H
13	M	M	M	H
14	L	H	M	M
15	L	L	L	L
16	H	L	H	L
17	H	H	H	H
18	H	L	M	H
19	M	M	L	M
20	H	H	H	L
21	L	H	H	L
22	H	L	L	L
23	H	L	H	H
24	H	H	L	H
25	L	L	M	L

Table 3: Weights of Input and Hidden Layer neuron connections

Neuron numbers	N5	N6	N7	N8
N1	1.30818	-0.6501	-1.1602	0.4477
N2	2.15291	-0.5038	-0.6445	-0.3763
N3	-2.4248	1.19244	0.05047	1.1231
N4	0.98102	2.55916	0.41366	0.89806

Table 4: Weights of Hidden and Output Layer neuron connections

Neuron numbers	N0
N5	0.50464
N6	-1.4931
N7	-1.5723
N8	1.72489

training data set is given in table-3 and table-4 respectively.

During ANN based optimization process, maximum experimental α -amylase activity (1785.71 IU/g) was considered as 100% and rest of the α -amylase activities under different conditions were normalized accordingly in relation with maximum activity. During the learning phase, ANN model try to mimic the

actual experimental condition by generating the prediction result approximately equal to the experimental result as shown in table-5.

The graphical correlation between experimental and predicted values of α -amylase activities during the training phase are plotted using line graph as shown in figure 12.

Both the lines in the graph are overlapping with each other. It indicates the correctness of the model which means that the predicted values are almost same as the actual experimental data. Further the model was tested against other three set of the process parameters to validate the model and the results of the prediction were obtained. These results were found very satisfactory as the average absolute error was significantly less. The result of testing data set is given in table-6.

α -amylase production using agro-industrial waste by *Gliomastix indicus* at 100% Moisture content, 30°C incubation temperature, 96 hrs incubation time, 0.1 (w/v%) concentration of ammonium nitrate as supplementary nitrogen source and 4.5 (w/v%) concentration of NaCl as additional salt content have been found to be most optimum. ANN model for process parameters at various levels of moisture content,

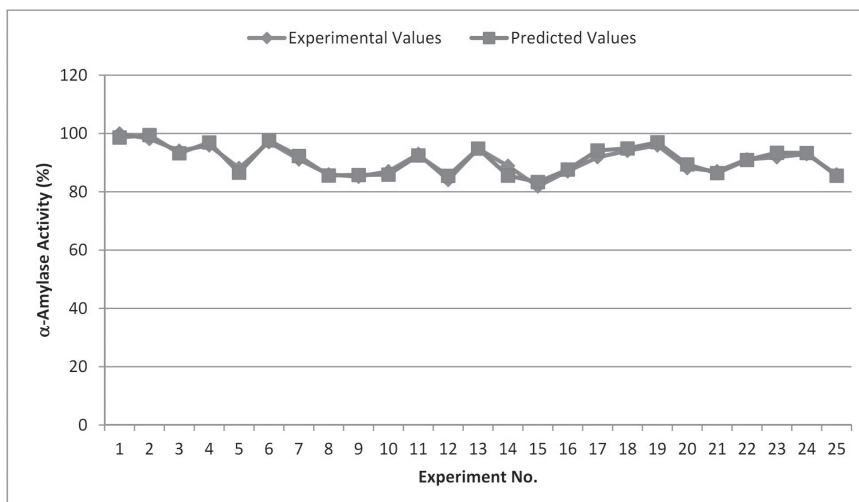


Fig.12: Correlation between experimental and predicted values of α -amylase activity

Table 5: Output of ANN model for the training set

Sl. No.	Moisture Content (%) X_1	Temperature (°C) X_2	NH_4NO_3 (w/v%) X_3	NaCl (w/v%) X_4	α - amylase activity (IU/g)	Actual a-amylase activity (%)	Predicted a- Amylase activity (%)
1	80	30	0.1	4.5	1785.71	100	98.64
2	80	30	0.15	4.5	1752.67	98.15	99.46
3	80	40	0.1	4.5	1679.82	94.07	93.23
4	80	20	0.1	4.5	1713.03	95.93	96.93
5	40	30	0.1	4.5	1574.1	88.15	86.56
6	80	30	0.1	2.5	1732.85	97.04	97.63
7	120	40	0.05	2.5	1626.96	91.11	92.27
8	40	20	0.05	6.5	1534.46	85.93	85.60
9	40	40	0.05	6.5	1521.07	85.18	85.75
10	40	20	0.15	6.5	1554.28	87.04	85.90
11	120	30	0.1	4.5	1660	92.96	92.48
12	40	40	0.15	6.5	1501.25	84.07	85.48
13	80	30	0.1	6.5	1693.03	94.81	94.84
14	40	40	0.1	4.5	1587.32	88.89	85.55
15	40	20	0.05	2.5	1461.6	81.85	83.36
16	120	20	0.15	2.5	1554.28	87.04	87.63
17	120	40	0.15	6.5	1640.17	91.85	94.19
18	120	20	0.1	6.5	1679.82	94.07	94.87
19	80	30	0.05	4.5	1713.03	95.93	96.98
20	120	40	0.15	2.5	1574.1	88.15	89.38
21	40	40	0.15	2.5	1554.28	87.04	86.41
22	120	20	0.05	2.5	1626.96	91.11	90.92
23	120	20	0.15	6.5	1640.17	91.85	93.39
24	120	40	0.05	6.5	1660	92.96	93.30
25	40	20	0.1	2.5	1534.28	85.92	85.51
					RMS error	1.25	
					Average absolute error	1.03	
					Coefficient of correlation	0.97	

Table 6: Output of ANN model for test data set

Sl. No.	Moisture Content (%) X_1	Temperature (°C) X_2	NH_4NO_3 (w/v%) X_3	NaCl (w/v%) X_4	α - amylase activity (IU/g)	Actual α -amylase activity (%)	Predicted α - amylase activity (%)
1	80	40	0.1	6.5	1466.06	82.1	85.99
2	40	30	0.05	4.5	1574.1	88.15	86.78
3	120	40	0.1	2.5	1626.96	90.31	88.47
Average Absolute Error							2.37

temperature, organic nitrogen source and salt, have proved to be good choice for optimization problem because of its higher (approximately one) correlation coefficient and lower RMS and average absolute error. The lower values of errors shows that the network has a good ability to generalize the optimization conditions (14,32).

Conclusion

In this study mustard oil cake has been used for the production of α - amylase and found better and economical solid substrate for production of α -amylase by *Gliomastic indicus* using solid state fermentation. The effect of various physical & chemical parameters that affects the amylase production i.e. moisture content, incubation temperature, incubation time, pH of nutrient, concentration of NaCl, supplementary carbon & nitrogen source have been studied. The study reveals that 80 % of moisture content, 30°C incubation temperature and 0.1% and 4.5% (w/v) of ammonium nitrate and NaCl as additional nitrogen and additional salt content respectively have shown maximum production when incubated for 96 hours. The molecular weight of purified enzyme has been found to be ~56kDa after running it on SDS-PAGE. All the process parameters were further optimized using ANN model with the experimental data collected from various set of experiments. An ANN model has been developed to obviate the necessities of a laboratory experiment for knowing the effect of various process parameters on the final activity of enzyme. A simple ANN

model with four neurons in input and hidden layer respectively and one neuron in output layer was found suitable owing to its lesser RMS error and average absolute error associated with the predicted values. With test case dataset, this model has predicted the α -amylase activity with absolute error of just 2.37. This leads to the recommendation of the ANN model for further investigation of α -amylase production systems with larger number of independent input variables as it has shown very good approximation with small dataset as well.

References

1. Carlsen, M., Sphor, A.B., Nielsen, J. and Villadesn, J. (1996). Morphology and physiology of an α -amylase producing strain of *Aspergillus oryzae* during batch cultivation. *Biotechnol. Bioeng.* 4:266-276.
2. Pandey, A., Selvakumar P., Soccol C.R. and Nigam, P. (1999). Solid state fermentation for the production of industrial enzymes. *Bioresource. Technol.* 77:149-162.
3. Francis, F., Sabu, A., Nampoothiri, K.M., Ramachandran, S., Ghosh, A., Szakacs, G. and Pandey, A.(2003). Use of response surface methodology for optimizing process parameters for the production of α -amylase by *Aspergillus oryzae*. *Biochem. Engg. J.* 15:107-115.
4. Carrizales, V. and Jaffe, W.(1986). Solid state fermentation an appropriate

- biotechnology for developing countries. *Interscience* 11:9-15.
5. Raimbault, M. (1998). General and microbiological aspects of solid substrate fermentation. *Electronic J. Biotechnol.* 1:1-20.
 6. Kunamneni, A., Perumal, K. and Singh, S. (2005). Amylase production in solid state fermentation by the thermophilic fungus. *Thermomyces Lanuginosus*. *J. Biosci. Bioeng.* 100:168-171.
 7. Özdemir, S., Matpan, F., Güven, K. and Baysal, Z. (2011). Production and characterization of partially purified extracellular thermostable α -amylase by *Bacillus subtilis* in submerged fermentation (SmF). *Preparative Biochemistry and Biotechnology*. 41:365-381.
 8. Ma, W.L., Zhao, F.F., Ye, Q., Hu, Z. X., Yan, D. J. and Yang, Y. (2015). Production and partial purification of tannase from *Aspergillus ficuum*. *Preparative Biochemistry and Biotechnology*. 45:754-768.
 9. Sodhi, H. K., Sharma, K., Gupta, J.K. and Soni, S.K. (2005). Production of a thermostable α amylase from *Bacillus* sp PS-7 by solid state fermentation and its synergistic use in the hydrolysis of malt starch for alcohol production. *Process Biochem.* 40:525-534.
 10. Singh, K., Garg, S.K., Kalla, A. and Bhatnagar, A. (2003). Oilcakes as protein sources in supplementary diets for the growth of *Cirrhinus mrigala* (Ham) fingerlings: laboratory and field studies. *Bioresour. Technol.* 86:283-291.
 11. Singh, R.K., Kumar, S. and Kumar S. (2009) Production of α -amylase from agricultural byproducts by *Humicola lanuginosa* in solid state fermentation. *Current Trends in Biotechnology and Pharmacy* 3 :172-180.
 12. Nagalaxmi, S., Vijayalakshmi, M. and Subrahmanyam, A. (2009). *Gliomastix indicus* sp nov. *Current Trends in Biotechnology and Pharmacy*. 3 :111-112.
 13. Nagata, Y. and Chu, K.M. (2003). Optimization of fermentation medium using neural networks and genetic algorithms. *Biotechnology Letters*. 25:1837-1842.
 14. Singh, R.K. and Kumar, P.R. (2014). Development of artificial neural network modeling of p-cresol biodegradation. *International Journal of Advanced Biotechnology and Research* 5: 43-53.
 15. Kammoun. R., Naili, B. and Bejar, S. (2008). Application of a statistical design to the optimization of parameters and culture medium for α -amylase production by *Aspergillus oryzae* CBS 81972 grown on gruel (wheat grinding by-product). *Bioresource. Technology*. 99:5602-5609.
 16. Murado, M.A., Sisi, M.I.G., Gonjalej, M.P., Montemayer, M.I., Pastran, L. and Miron, J. (1993). Amylase production by solid state culture of *Aspergillus oryzae* on polyurethanes foams: some mechanistic approaches from an empirical model. *Process Biochem.* 32:35-42.
 17. Okolo, B.N., Ezeogu, L.I. and Mba, C.N. (2005). Production of raw starch digestive amylase by *Aspergillus niger* grown on native starch sources. *J .Sci. Food & Agriculture*. 69:109-115.
 18. Miller, G.L. (1959). Use of dinitrosalicylic acid reagent for determination of reducing sugar. *Analytical Chemistry*. 31: 426-429.
 19. Laemmli, U.K. (1970). Cleavage of structural proteins during the assembly of the head of bacteriophage T4. *Nature* 227:680-685.
 20. Rumelhart, D.E. and McClelland, J.C. (1986). *Parallel distributed processing Explorations in the microstructure of cognition* M.I.T. Press Cambridge. Mass Vol I.

21. Rumelhart, D.E., Hinton, G.E. and Williams, R.J. (1986). Learning internal representations by error propagation parallel distributed processing: Explorations in the microstructure of cognition M.I.T. Press Cambridge. Vol I.
22. Murty, S.S.N., Ravi, V., Reddy, P. and Reddy, R.C. (1997). Artificial neural networks applied to defluoridation. *Poll. Res.* 16:177-182.
23. Wyman., C..E., Spindler, D.D. and Grohmann, K. (1992). Simultaneous saccharification and fermentation of several lignocellulosic feed stocks to fuel ethanol. *Biomass. Bioenergy.* 28:773-786.
24. Grohmann, K. (1993). Simultaneous saccharification and fermentation of cellulosic substrates to ethanol Bioconversion of forest and agricultural plant residues. Wallingford UK: CAB International. 183-/209.
25. Szczodrak, J. and Targonski, Z. (1989). Simultaneous saccharification and fermentation of cellulose: effect of ethanol and cellulases on particular stages. *Acta Biotechnol.* 9:555-564.
26. Satyanarayana, T. (1991). Production of bacterial extracellular enzymes by solid state fermentation. Wiley Eastern Ltd. 122-129.
27. Feniksova, R.V., Tikhomirova, A.S. and Rakhleeva, E.E. (1960). Conditions for forming amylase and proteinase in surface cultures of *Bacillus subtilis*. *Microbiologia* 29:745-748.
28. Zadrazil, F. and Brunnert, H. (1981). Investigation of physical parameters important for the SSF of straw by white rot fungi. *Eur. J. Appl. Microbiol. Biotechnol.* 11:183-188.
29. Pandey, A., Selvakumar, P., Soccol, C.R. and Nigam, P. (1997). Solid state fermentation for the production of industrial enzymes. *Current Sci.* 77:149-162.
30. Lonsane, B.K., Ghildyal, N.P., Budiatman, S. and Ramakrishna, S.V.(1985). Engineering aspects of solid-state fermentation. *Enzyme and Microb. Technol.* 7:258-265.
31. Pandey. A. (1990). Improvement in solid-state fermentation for glucoamylase production. *Biological. Wastes.* 34:11-19.
32. Uppada, S.R., Balu, A., Gupta, A.K and Dutta, J.R. (2014). Hybrid Neural Network based optimization of process parameters and application of taguchi method for lipase production from co-culture of *Lactobacillus brevis* and *Lactobacillus plantarum* *International Journal of PharmTech Research.* 6:2074-2082.
33. Balkan, B. and Ertan, F. (2005). Production and properties of α amylase from *Penicillium chrysogenum* and its application in starch hydrolysis. *Preparative Biochemistry and Biotechnology.* 35:169-178.
34. Shafique, S., Rukhsana, B. and Shazia S. (2010). Alpha-amylase production by toxigenic fungi. *Natural product research.* 15:1449-1456.
35. Balkan, B. and Ertan, F. (2007). Production of α -Amylase from *Penicillium chrysogenum* under Solid-State Fermentation by Using Some Agricultural By-Products. *Food Technology & Biotechnology.* 45:439-442.
36. Singh, R. K., Mishra, S. K., Kumar, N. (2010). Optimization of α -amylase production on agriculture byproduct by *Bacillus cereus* MTCC 1305 using solid state fermentation. *Research Journal of Pharmaceutical, Biological and Chemical Sciences.* 1 (4): 867-876.
37. Teodor, C.E.D. and Martins M.L.L. (2000). Culture conditions for the production of thermostable amylase by *Bacillus* sp. *Braz. J. Microbiol.* 31:298–302.

Isolation and Characterization of Extracellular Lipase Producing Bacterial Isolates From Effluent Waste of Paint Industry

Shiney Hangloo¹, Anuradha Sourirajan¹, Chand Raina², Asha Chaubey² and Kamal Dev^{*1}

¹ Faculty of Applied Sciences and Biotechnology, Shoolini University, Solan, Himachal Pradesh, India.

² Fermentation Technology Division, Indian Institute of Integrative medicine, canal road, Jammu, India.

*For Correspondence - kamaldevbhardwaj1969@gmail.com

Abstract

The aim of this study was to isolate and select lipase producing bacteria from effluent waste of paint industry. Five lipase producing Gram negative bacterial isolates showed promising extracellular lipase activity. Molecular identification on the basis of 16S rDNA identified bacterial isolates as *Aeromonas* sp. Sh 2 (KT186103.1), *Aeromonas* sp. Sh 8 (KT229540.1), *Aeromonas* sp. Sh 12 (KT427918.1), *Pseudomonas* sp. Sh 13 (KT251204.1), *Pseudomonas* sp. Sh 17 (KT251205.1). Phylogenetic analysis revealed that all the three *Aeromonas* spp. and two *Pseudomonas* spp. are highly divergent within each group. Effect of various physio-chemical parameters showed that pH 7.0 and temperature 37°C were favourable for lipase production in all five isolates. Glucose in combination with peptone enhanced the lipase activity from 1359 to 2347 U_{mg}⁻¹ in *Aeromonas* sp. Sh 2. Combination of glucose with yeast extract improved the lipase activity of *Aeromonas* sp. Sh 8 from 1641 to 2674 U_{mg}⁻¹, whereas glucose with casein hydrolysate increased the lipase activity of *Aeromonas* sp. Sh 12 from 1568 to 1983 U_{mg}⁻¹. *Pseudomonas* sp. Sh 13 and *Pseudomonas* sp. Sh 17 did not show enhanced lipase activity in presence of different carbon or nitrogen sources. These bacterial isolates could be exploited to treat oil and paint based industrial effluents and contribute to reduce environmental hazards.

Key Words: Lipase, p-nitrophenyl palmitate, 16S rDNA, paint industry waste, *Aeromonas*, *Pseudomonas*

Introduction

Today, industrialized world is facing the major problem of environmental pollution due to effluent waste of oil and paint industries. New technologies that emphasize on the detoxification and destruction of the contaminants have been developed to remediate these effluents.

Lipases (triacylglycerol acylhydrolases, E.C. 3.1.1.3) are ubiquitous enzymes having great industrial potential and physiological significance. At oil water interface, lipases catalyze the hydrolysis of triacylglycerols to glycerol and free fatty acids (1). Lipases also catalyze esterification, interesterification and transesterification reactions in organic solvents and supercritical fluids (2, 3). Lipases are secreted by microorganisms (bacteria, yeast, fungi), plants and animals, but bacterial lipases have received more attention, since they have great variety of catalytic activity, easy to manipulate genetically, capable of rapid growth on inexpensive media and are not affected by seasonal fluctuations (4). Some of bacterial lipases belong to genera *Achromobacter*, *Alcaligenes*, *Arthrobacter*, *Bacillus*, *Burkholderia*, *Chromobacterium* and *Pseudomonas* sp. etc (5).

Lipolytic microorganisms have been found in diverse habitats such as industrial wastes,

dairies, oil contaminated soils and vegetable oil processing factories etc (6). Lipase producing *Bacillus* sp. DVL2 was isolated from common city garbage (comprising wastes of kitchens, restaurants, dairies, and sewerage and decaying plant parts) of the Karnal district of Haryana, India (7). *Aeromonas sobria* LP004 secreting lipase was isolated from raw milk (8). Lipases have broad spectrum of biotechnological applications in food, flavour, biopolymers, detergent industries, environmental management, pharmaceuticals, cosmetics and biodiesel production (9-13). Non haemolytic phospholipase C activity was seen on lecithin and p-nitrophenylphosphorylcholine by *Aeromonas hydrophila* lipase (14). Lipase producing *Aeromonas* sp VNT and *Pseudomonas* sp VNT enhanced the reduction of waste activated sludge at low temperature (15).

Bacterial lipases are mostly extracellular and are greatly influenced by nutritional and physio-chemical factors such as pH, temperature, agitation and carbon and nitrogen sources (5). Lipase production requires the study of fermentation conditions, relating carbon and nitrogen sources to temperature and pH conditions (16).

There is no previous report of lipolytic bacteria isolated from paint industrial waste, which mostly contains oil and grease (10%), phenolic compounds (1%) and other traces of metals. These ingredients may act as inducer and substrate for lipase enzymes. Thus, the aim of this study was to isolate and select lipase producing bacteria from paint industrial waste as well as to optimize the growth conditions in order to maximize lipase production.

Materials and Methods

Collection of sample and screening of bacterial isolates for lipase activity: Samples were collected aseptically from effluent waste of paint industry at longitude of 75.1167 and latitude of 32.5667 India. Liquid (1 ml) and solid (1 gm) waste samples were serially diluted from 10^{-1} to 10^{-7} and 100 μ l of each dilution was spread on

NA medium containing 0.5% tributyrin and incubated at 37°C for 48 hours. Colonies showing clear zones were picked and purified by three successive streaking on NA medium containing tributyrin. Selected isolates were further inoculated in nutrient broth at 37°C for 24 hrs and cell free supernatant was obtained by centrifugation at 10,000xg for 10 minutes. The supernatant (100 μ l) was tested against tributyrin (0.5%) and 2-naphthyl acetate (0.25%) for extracellular lipase activity on the basis of zone of hydrolysis. Quantitative lipase assay was also performed to measure intracellular and extracellular lipase activity.

Quantitative lipase assay: The lipase activity was monitored based on hydrolysis of p-nitro phenyl palmitate (p-NPP) as described by Winkler et al (17) with minor modification. Appearance of yellow coloured product was measured at 410 nm. Reaction mixture contained 0.3 ml of 0.01 M phosphate buffer (pH 6.5), 150 μ l of 2.5 mM p-NPP in HPLC grade acetonitrile, 5-10 μ g protein as enzyme source in a total volume of 3 ml. Two controls were simultaneously run, one contained 0.4 ml phosphate buffer and enzyme solution and other contained 0.4 ml phosphate buffer and 150 μ l p-NPP (2.5 mM). After 10 min incubation at 37°C, reaction was terminated by adding 1 ml ethanol and absorbance was measured at 410 nm in a UV-Vis spectrophotometer against the blank. The unknown concentration of p-nitrophenol released was determined from standard curve of p-nitrophenol (10-100 μ m). One Unit (IU) of lipase activity was defined as the amount of enzyme catalyzing the release of 1 μ mol of p-nitrophenol per min from p-NPP under the standard assay conditions. Total protein was estimated by Bradford method using BSA as standard (18).

Microscopic and biochemical characterization: The selected bacterial isolates were examined by Gram's staining and biochemical tests such as catalase, oxidase, urease, amylase, nitrate reductase, IMViC (indole, methyl red, voges proskauer, simmon citrate), triple sugar iron agar as described (19,

20). Carbohydrate fermentation tests were also performed using himedia biochemical test kit (KB001).

Identification and phylogenetic analysis of lipase secreting bacterial isolates:

The bacterial isolates were cultured under optimal growth conditions and cells were harvested at 12,000 xg for 10 min. From each of the bacterial cell pellet, total genomic DNA was isolated (21) and amplification of genomic DNA (100 ng) was done by PCR using 16S rDNA specific primers, 27F and 1492R (22) with programme consisting 35 cycles of initial denaturation at 94°C for 2 min and final denaturation at 94°C for 30 sec, annealing at 40°C for 30 sec, extension at 72°C for 1 min 30 sec and final extension at 72°C for 10 min. The PCR products were resolved on 1% agarose gel, visualised under UV gel documentation system (Alpha Innotech, USA) and then purified with gel extraction kit. Gel purified PCR products of 16S rDNA were sequenced on both the strands using 27 F and 1492 R primers at Eurofins, Bangalore, India. The complete 16S rDNA sequence for each bacterial isolate was generated manually by removing overlapping sequences. The 16S rDNA gene sequence of each bacterial isolate was compared against other known bacterial 16S rDNA sequences available in the Gene bank data base using BLAST (blastn) search (23). The nucleotide sequences were aligned using Clustal W 1.74 (24), phylogenetic tree was constructed by neighbour joining using MEGA4 (25) and bootstrapping was used to estimate the reliability of the phylogenetic reconstructions (1,000 replicates). The nucleotide sequences were submitted in the GenBank data base (<https://www.ncbi.nlm.nih.gov/genbank/>).

Optimization of physical parameters (pH and temperature) for growth and lipase activity:

Bacterial isolates were cultured in nutrient broth adjusted to pH (4-12) with 1N HCl and 1N NaOH as required and incubated at 37°C for 48 hours with shaking at 200 rpm. Effect of temperature was studied by culturing the bacterial isolates in nutrient broth at different incubation temperatures

(25–60°C) for 48 hours. Cell density was measured at 600 nm. Extracellular lipase activity was measured in cell free supernatant at 410 nm as described.

Optimization of chemical parameters (carbon and nitrogen) for bacterial growth and lipase activity:

Bacterial isolates were cultured in minimal salt medium (M9) containing NH₄Cl as nitrogen source supplemented with different carbon sources (1%) such as glucose, starch, sucrose, fructose, trehalose, maltose, lactose, raffinose, galactose and sorbitol. Minimal salt medium (M9) containing glucose as carbon source supplemented with different nitrogen sources (0.25%) such as yeast extract, peptone, casein hydrolysate and NH₄Cl was used to study the role of nitrogen source on growth and lipase activity, the cultures were incubated at 37°C and 200 rpm for 48 h. Effect on growth was studied by measuring cell density at 600 nm and extracellular lipase activity was determined in cell free supernatant at 410 nm as described.

Results

Bacterial isolates secrete lipase: From thirty one bacterial isolates (Sh 1-Sh 31), seven isolates Sh 1, Sh 2, Sh 8, Sh 12, Sh 13, Sh 17 and Sh 18 relatively showed zone of clearance between 15-26 mm on tributyrin and 2-naphthyl acetate (Fig. 1A –D and Table 1). All the seven bacterial isolates were tested for extracellular and intracellular lipase activity. Bacterial isolates Sh 2, Sh 8, Sh 12, Sh 13 and Sh 17 showed proportionally more lipase activity, whereas isolates Sh 8 (1641.33 U_{mg}⁻¹), Sh 12 (1568 U_{mg}⁻¹) and Sh 17 (1490.66 U_{mg}⁻¹) showed highest extracellular lipase activity. Isolates Sh 2 (1232.2 U_{mg}⁻¹) and Sh 12 (1186 U_{mg}⁻¹) showed highest intracellular lipase activity (Fig. 1E). Specific activity was presented in terms of activity mg⁻¹ protein.

Morphological and Biochemical characterization:

The colour of the isolates varied from creamish, whitish to pale yellow. All the bacterial isolates (Sh 2, Sh 8, Sh 12, Sh 13 and Sh 17) were rod shaped, Gram's negative and positive for oxidase, catalase, urease, nitrate test

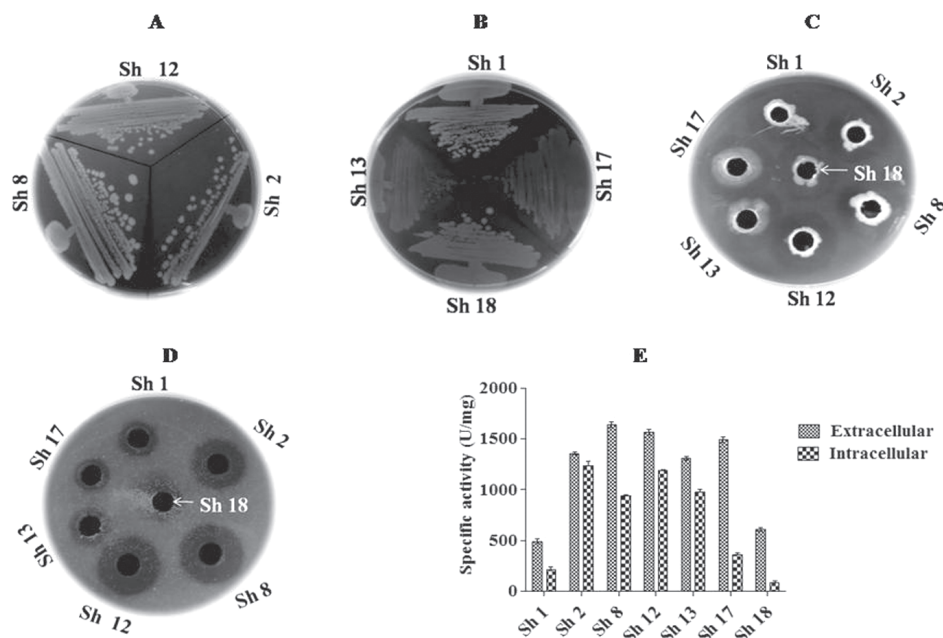


Fig. 1. Qualitative and quantitative assay for screening lipase producing bacterial isolates. Purified bacterial isolates as indicated were streaked on NA medium and incubated at 37°C for 24 hours (A, B). Qualitative lipase assay on tributyrin (C) and 2-naphthyl acetate (D). Comparative extracellular and intracellular lipase assay (E) Mean and standard deviation of three independent experiments was plotted.

whereas negative for methyl red test except Sh 8, which was methyl red positive. Bacterial isolate Sh 2, Sh 8 and Sh 12 were amylase positive, whereas others were negative for amylase test. Protease test was positive for Sh 2, Sh 12 and Sh 17, Simmon citrate test for Sh 2, Sh 8, Sh 13, Sh 17, indole and voges proskauer test for Sh 2 and Sh 12 and triple sugar iron agar test for Sh 2, Sh 8, Sh 12 and negative for others. In the fermentation of various sugars, Sh 2 was positive for mannitol and sucrose, Sh 8 for glucose, arabinose, lactose, mannitol and sucrose, whereas Sh 12 for glucose, arabinose and sucrose (Table 2).

Identification by 16S r DNA sequencing: To identify lipolytic bacterial isolates, 16S rDNA gene was amplified using 16S rDNA specific primers. A PCR product of ~ 1.5 kb was detected in all the five isolates. The amplified 16S rDNA was

sequenced on both the strands and a nucleotide sequence of 1,458, 1,452, 1,411, 1,452 and 1,446 bp was obtained for Sh 2, Sh 8, Sh 12, Sh 13 and Sh 17 respectively. The nucleotide sequence was individually subjected to blast analysis and phylogenetic tree was constructed using Megha 4 (Fig. 2A, 2B). The 16S rDNA nucleotide sequences of all the five lipolytic bacterial isolates have been submitted to the NCBI GenBank database under the accession nos. KT186103.1 (*Aeromonas* sp. Sh 2), KT229540.1 (*Aeromonas* sp. Sh 8), KT427918.1 (*Aeromonas* sp. Sh 12), KT251204.1 (*Pseudomonas* sp. Sh 13), KT251205.1 (*Pseudomonas* sp. Sh 17).

By 16S rDNA sequence analysis, it was found that the lipolytic isolates Sh 2, Sh 8 and Sh 12 showed similarity with *Aeromonas* sp. DS5 (99% similarity with accession no. KJ817212.1),

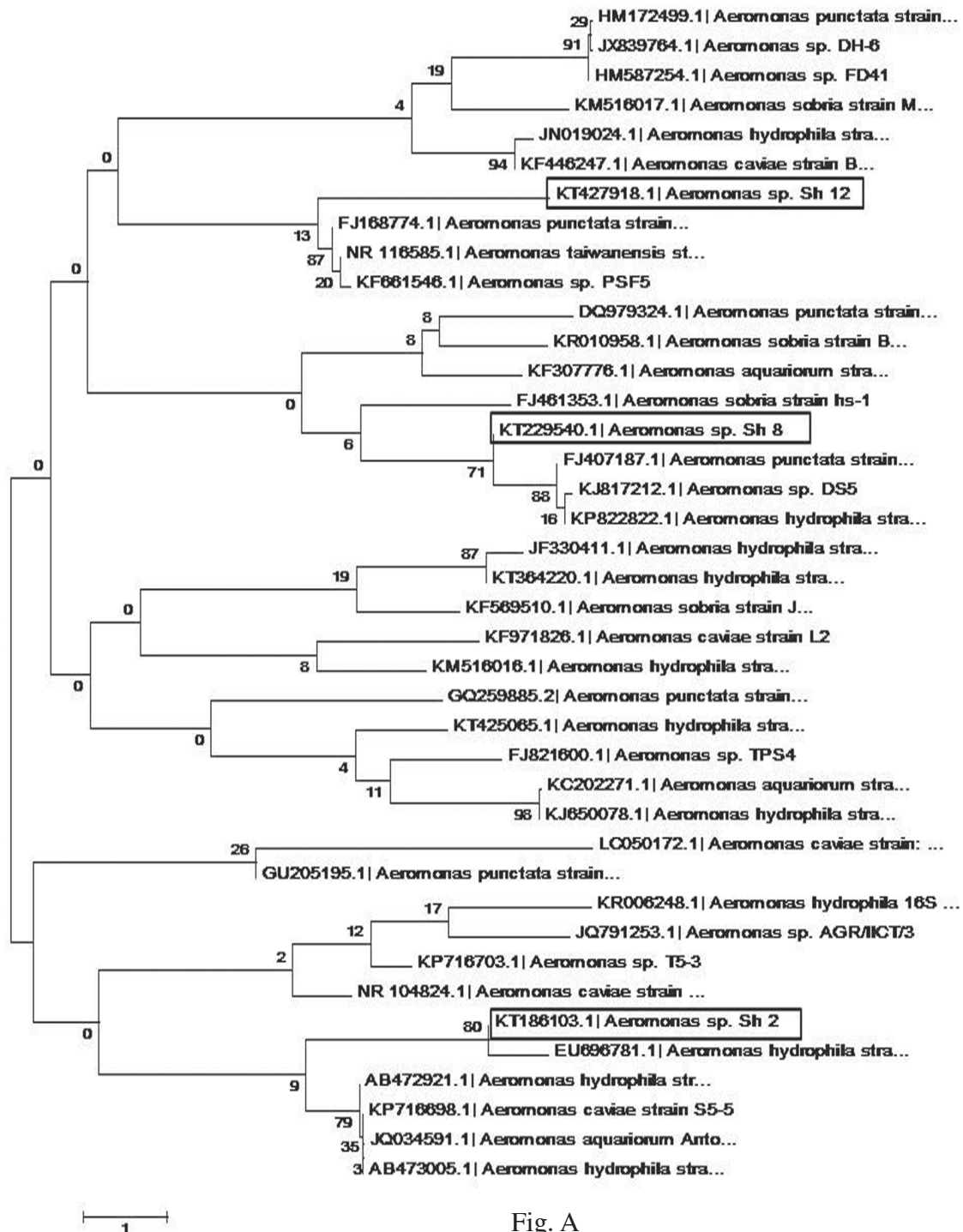


Fig. A

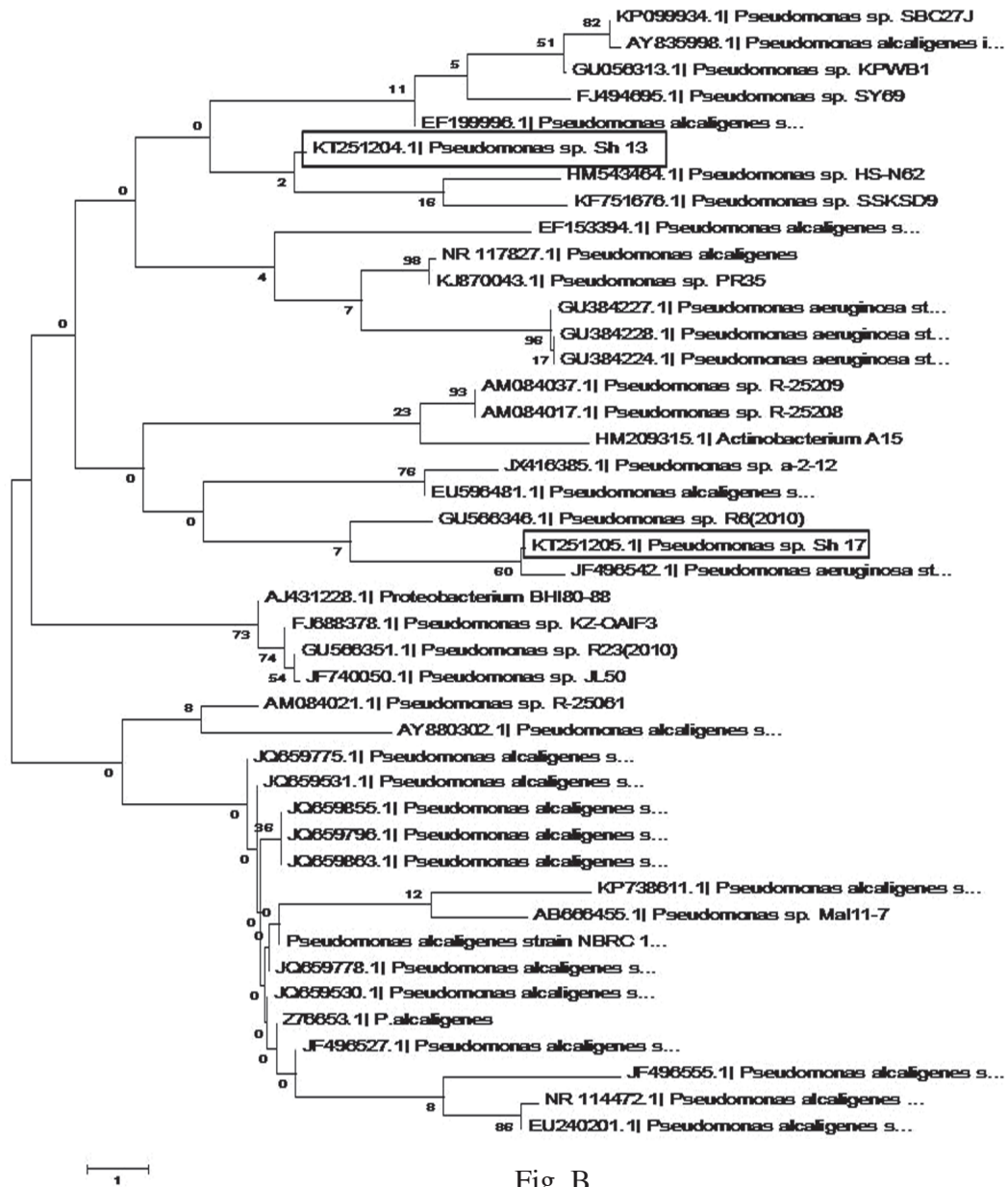


Fig. B

Fig. 2. Identification and phylogenetic analysis 16S rDNA based dendrogram showing phylogenetic relationship of new isolates (Sh 2, Sh 8, Sh 12) with representatives of *Aeromonas* (A) and new isolates (Sh 13 and Sh 17) with representatives of *Pseudomonas* (B) showing $\geq 99\%$ homology

Aeromonas sp. FD41 (99% similarity with accession no. HM587254.1) and *Aeromonas* sp. DH6 (100% similarity with accession no. JX839764.1) respectively. Though the bacterial isolates Sh 13 and Sh 17 showed difference in their 16S rDNA sequence, both showed 99% similarity with *Pseudomonas* sp. R6(2010) (accession no. GU566346.1). Sh 2 isolate was closely related with *Aeromonas hydrophila* strain BJ (EU696781.1) and showed 99% similarity with the strain. Bacterial isolate Sh 8 was closely related with *Aeromonas punctata* strain W20060720 (FJ407187.1), *Aeromonas* sp DS5 (KJ817212.1) and *Aeromonas hydrophila* strain UTMC 2268 (KP822622.1) and showed 99% homology with *Aeromonas punctata*. Isolate Sh 12 was closely related with *Aeromonas punctata* strain 360cc (FJ168774.1), *Aeromonas taiwanesis* A2-50 (NR_116565.1) and *Aeromonas* sp. PSFS (KF661546.1), but did not show homology with any of the three whereas isolate Sh 13 was closely related with *Pseudomonas* sp. HS-N62 (HM543464.1) and *Pseudomonas* sp. SSKSD9 (KF751676.1) and Sh 17 with *Pseudomonas aeruginosa* strain JN-3 (JF496542.1) with 99% homology. Phylogenetic analysis showed that *Aeromonas* sp (Sh 2, Sh 8 and Sh 12) and *Pseudomonas* sp. (Sh 13, Sh 17) are distantly related.

Optimization of physical parameters (pH and temperature) for growth and lipase activity:

Optimum pH and temperature for growth and lipase activity of all isolates was pH 7 and 37°C. Isolates Sh 2, Sh 8, Sh 12, Sh 13 and Sh 17 showed 1494, 1868, 1659.3, 1436.6 and 1616.3 U mg⁻¹ of activity at pH 7 and 37°C (Fig. 3A-D). All the bacterial isolates showed no detectable growth at acidic pH of 4, 5 and alkaline pH of 11 and 12. Optimum growth for isolates Sh 2, Sh 8 and Sh 12 was observed at pH 6-10. All the isolates showed 51-92% decrease in lipase activity at pH 6, 8, 9 and 10 but isolate Sh 8 showed 38% decrease in activity at pH 6.

Though, there was no significant difference in growth at temperature between 25-45°C, lipase activity decreased at 45°C for all the isolates and

at 25°C for Sh 2 and Sh 13 isolates. At 25 and 30°C, all the bacterial isolates retained 75-93% activity, except isolates Sh 13 and Sh 2, which retained 52-59% activity at 25°C. At 45°C, there was 57-70% decrease in activity for all the isolates, except Sh 12, which showed 37% decrease in lipase activity. There was a drastic decrease in growth and activity at 50 and 60°C. Only 2.7-5.5% of activity was retained in all isolates at 50°C and 60°C.

Optimization of chemical parameters (carbon and nitrogen) for growth and lipase activity:

Among different carbon and nitrogen sources tested, glucose was found to be the best carbon source for growth of isolates Sh 12 and Sh 13, while fructose, sucrose and trehalose for isolates Sh 2, Sh 8 and Sh 17. Yeast extract was found to be the best nitrogen source for growth of Sh 2 isolate, casein hydrolysate for Sh 8, Sh 13 and Sh 17 isolate and tryptone for Sh 12 isolate (Fig. 4A, B).

Lipase activity of 1370.66 (Sh 2), 1244.0 (Sh 8) and 1010 U mg⁻¹ (Sh 13) was found to be highest in a medium containing glucose. Isolate Sh 12 (1024.3 U mg⁻¹) and Sh 17 (890.6 U mg⁻¹) showed optimal lipase activity in a growth medium containing fructose and trehalose respectively (Fig 4C). Lipase activity was decreased by 3.3-88% in presence of sugars (sucrose, fructose, maltose, galactose, raffinose, sorbitol, starch, lactose, trehalose) for Sh 2, Sh 8 and Sh 13 isolates and specifically decreased by 6.3-57.1% for Sh 12 isolates in presence of sucrose, maltose, raffinose, sorbitol, lactose, starch and trehalose. The lipase activity of bacterial isolate Sh 17 was also decreased by 5.8-44.4% in medium containing sucrose, maltose, raffinose, sorbitol, lactose, starch as compared to minimal salt medium supplemented with glucose. In contrast lipase activity of Sh 12 was increased by 7.5-25% in a medium containing fructose or galactose and in presence of fructose, galactose and trehalose for Sh 17 isolate, when compared to minimal salt medium supplemented with glucose. Bacterial isolate Sh 2, Sh 13 and Sh 17 showed optimum lipase

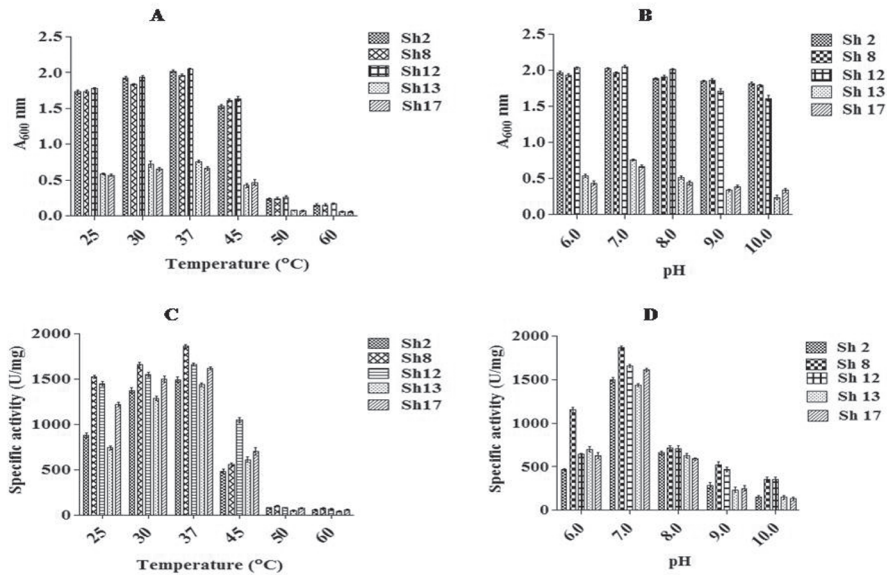


Fig. 3. Effect of physical parameters (temperature, pH) on growth and lipase activity of microbial isolates. Cell density of bacterial cultures was measured at 600 nm and plotted against the indicated temperatures (A) and pH (B). Cell free spent medium was used as a source of lipase and specific activity (U mg^{-1}) of bacterial isolates was plotted against temperature (C) and pH (D). Data of three independent experiments was plotted with standard deviation.

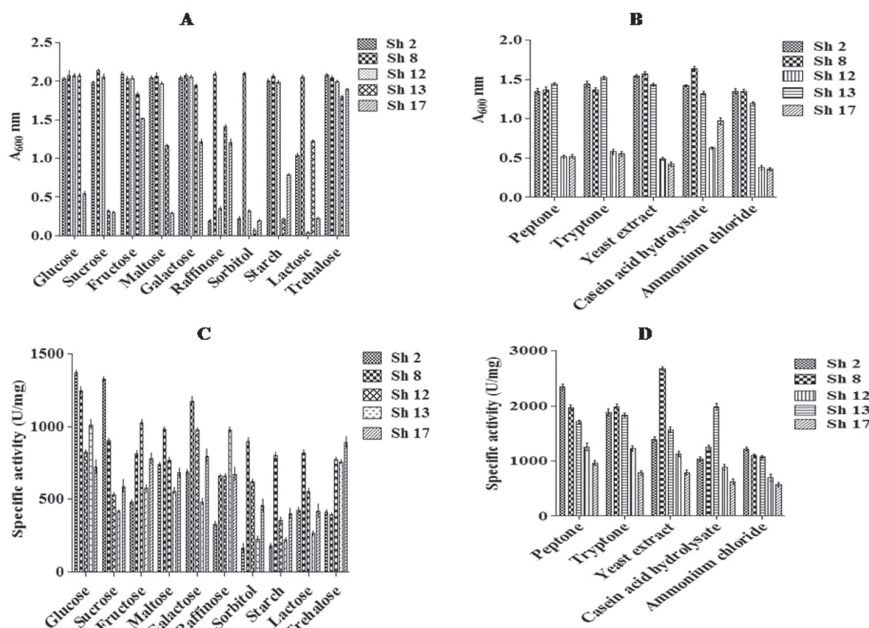


Fig. 4. Effect of Chemical parameters (carbon and nitrogen sources) on growth and lipase activity of microbial isolates. Absorbance of bacterial cultures was measured at 600 nm and plotted against carbon sources (A) and nitrogen sources (B). Cell free spent medium was used as a source of lipase and specific activity (U mg^{-1}) of bacterial isolates was plotted against carbon sources (C) and nitrogen sources (D). Data of three independent experiments was plotted with standard deviation.

activity of 2347, 1256, 968 U_{mg}⁻¹ respectively when grown in a medium supplemented with peptone as nitrogen source. Bacterial isolate Sh 8 and Sh 12 showed optimum activity of 2674 U_{mg}⁻¹ and 1983 U_{mg}⁻¹ in medium supplemented with yeast extract and casein hydrolysate respectively (Fig 4D). Lipase activity was increased by 10-93% in presence of all the nitrogen sources(peptone, tryptone, yeast extract and casein hydrolysate) tested for Sh 8, Sh 12, Sh 13 and Sh 17 isolates. The lipase activity of Sh 2 isolate was also increased by 14.6-92.6% in presence of nitrogen sources such as peptone, tryptone and yeast extract, when compared to minimal salt medium supplemented with ammonium chloride. Lipase activity was decreased by 15% in presence of casein hydrolysate for Sh 2 isolate as compared to minimal salt medium supplemented with ammonium chloride.

Discussion

The effluent waste of oil and paint industries provides environment to enrich lipase degrading bacteria on the basis of type of organic matter present. In the present study, five bacterial isolates (Sh 2, Sh 8, Sh 12, Sh13 and Sh 17) secreting lipase were screened from effluent

waste of paint industry. Molecular identification based on 16S rDNA revealed that, Sh 2, Sh 8 and Sh 12 belongs to *Aeromonas* genera whereas Sh 13 and Sh 17 to *Pseudomonas* genera. Sh 2 isolate showed 99% similarity with an iron reducing bacterial strain *Aeromonas hydrophila* strain BJ isolated from a paddy soil (26). All the bacterial isolates showed extracellular lipase activity in a pH range of 6-8 and temperature 25°C -45°C, but maximum lipase activity was attained at pH 7 and 37°C. In the earlier studies, five lipase producing bacteria such as *Bacillus* sp.1, *Bacillus* sp.2, *Pseudomonas* sp., *Staphylococcus* sp. and *Serratia* sp. were isolated from different industrial effluents (groundnut oil mill, palm oil mill, dairy effluent, slaughter house waste water, soap and detergent effluent and domestic waste water). The maximum lipase activity for *Pseudomonas* sp was found at pH 7 at 35°C for 45 hrs with glycerol and starch as best carbon sources and casein as best nitrogen source (27).

Carbon source has always been the major factor for the expression of lipase activity. Among various carbon sources tested, glucose was found to be best carbon source for lipase activity of Sh 2, Sh 8 and Sh 13 isolates, whereas fructose and trehalose for Sh 12 and Sh 17

Table 1 : Qualitative assay for extracellular lipase production by bacterial isolates using different substrates

	Isolates	Zone of hydrolysis (mm)	
		Tributyryn	2-Napthyl acetate
1	Sh 1	26+2	15+0.5
2.	Sh 2	25+1	20+1
3.	Sh 8	26+2	24+0.5
4.	Sh 12	23+1	22+1
5.	Sh 13	25+1	15+2
6.	Sh 17	26+1	15+1
7.	Sh 18	26+1	15+1

Table -2 : Morphological and biochemical characterization of lipase producing bacterial isolates.

Biochemical Tests	Bacterial isolate				
	Sh 2	Sh 8	Sh 12	Sh 13	Sh 17
Shape	rods	rods	rods	rods	rods
Pigmentation	creamish	creamish	creamish	pale yellow	pale yellow
Gram's Staining	-ve	-ve	-ve	-ve	-ve
Catalase	+ve	+ve	+ve	+ve	+ve
Oxidase	+ve	+ve	+ve	+ve	+ve
Citrate	+ve	+ve	-ve	+ve	+ve
Urease	+ve	+ve	+ve	+ve	+ve
Amylase	+ve	+ve	+ve	+ve	+ve
Nitrate Reductase	+ve	+ve	+ve	+ve	+ve
Methyl red	-ve	+ve	-ve	-ve	-ve
Voges Proskauer	+ve	+ve	+ve	-ve	-ve
Triple sugar iron	+ve	+ve	+ve	-ve	-ve
Indole	+ve	-ve	+ve	-ve	-ve
Protease	+ve	-ve	+ve	-ve	+ve
Carbohydrate Fermentation					
Glucose	-ve	+ve	+ve	ND	ND
Adonitol	-ve	-ve	-ve	ND	ND
Arabinose	-ve	+ve	+ve	ND	ND
Lactose	-ve	+ve	+ve	ND	ND
Sorbital	-ve	-ve	-ve	ND	ND
Mannitol	+ve	+ve	-ve	ND	ND
Rhamnose	-ve	-ve	-ve	ND	ND
Sucrose	+ve	+ve	+ve	ND	ND

-ve - negative result, +ve- positive result, ND-not detected

isolates respectively. In contrast to our study, lactose was reported to be best carbon source for lipase activity of *Bacillus sp.* MPTK 912 (28). The type of nitrogen source in the production medium also influences the lipase activity, besides carbon source. Generally when organic

nitrogen sources such as peptone and yeast extract are used, microorganisms generally provide high yields of lipase. Among various nitrogen sources tested peptone was found to be best nitrogen source for Sh 2 isolate. Similarly, peptone has also been reported as best nitrogen

source for lipase activity of *Staphylococcus* isolated from oil contaminated soils (29) and lipase from *Bacillus subtilis* KPL13 isolated from Kolli hills (30). Yeast extract and casein hydrolysate were found to be best nitrogen sources for lipase activity of Sh 2, Sh 8 and Sh 12 isolates respectively. Combination of olive oil and glucose were seen as best carbon sources and yeast extract as best nitrogen source for lipase activity of *Bacillus licheniformis* (31). Further, it is very interesting that highly diverged *Aeromonas* and *Pseudomonas* spp. were identified, which secrete lipase under different environmental conditions. This study indicates that the toxic substances present in paint industrial waste may contribute to genetic diversity among *Aeromonas* and *Pseudomonas* spp.

Conclusion

Thirty one bacterial colonies were isolated from paint industrial waste. Out of 31 isolates, five bacterial isolates showed highest extracellular activity. In all the five isolates the lipase activity was changed in a medium supplemented with different carbon and nitrogen sources, but optimum activity was observed at temperature 37 °C and pH 7. To the best of our knowledge, this is the first report of co-existence of highly diversified lipase secreting *Aeromonas* and *Pseudomonas* spp. in the effluent waste of paint industry. Further research is required to explore the potential application of lipase secreting bacteria in biotransformation, bio waste management and biodiesel production.

Acknowledgements

The authors are thankful to Shoolini University, Solan and Indian Institute of Integrative Medicine, Jammu for providing financial and infrastructural support for this study. Authors are also thankful to all the members of Yeast Biology Lab at Shoolini University.

References

1. Reis, P., Holmberg, K., Watzk, H., Leser, M. E. and Miller, R. (2009). Lipases at

- interfaces: a review. *Advances in Colloid and Interface Science*, 147-148: 237-250.
2. Romero, C. M., Pera, L. M., Loto, F., Vallejos, C., Castro, G. and Baigori, M. D. (2012). Purification of an organic solvent-tolerant lipase from *Aspergillus niger* MYA 135 and its application in ester synthesis. *Biocatalysis and Agricultural Biotechnology*, 1(1): 25–31.
3. Stergiou, P. Y., Foukis, A., Filippou, M., Koukouritaki, M., Parapouli, M., Theodorou, L. G., Hatziloukas, E., Afendra, A., Pandey, A. and Papamichael, E. M. (2013). Advances in lipase-catalyzed esterification reactions. *Biotechnology Advances*, 31(8): 1846-1859.
4. Hasan, F., Shah, A. A. and Hameed, A. (2006). Industrial applications of microbial lipases. *Enzyme and Microbial Technology*, 39 (2): 235-251.
5. Gupta, R., Gupta, N. and Rathi, P. (2004). Bacterial lipases: an overview of production, purification and biochemical properties. *Applied Microbiology and Biotechnology*, 64: 763–781.
6. Sztajer, H., Maliszewska, I. and Wieczorek, J. (1998). Production of exogenous lipase by bacteria, fungi and actinomycetes. *Enzyme and Microbial Technology*, 10(8): 492-497.
7. Kumar, D., Kumar, L., Nagar, S., Raina, C., Parshad, R. and Gupta, V. K. (2012). Screening, isolation and production of lipase/esterase producing *Bacillus* sp. strain DVL2 and its potential evaluation in esterification and resolution reactions. *Archives of Applied Science Research*, 4(4): 1763-1770.
8. Lotrakul, P. and Dharmsthiti, S. (1997). Purification and characterization of lipase from *Aeromonas sobria* LP004. *Journal of Biotechnology*, 54 (2): 113-120.

9. Horchani, H., Aissa, I., Ouertani, S., Zarai, Z., Gargouri, Y. and Sayari, A. (2012). *Staphylococcal* lipases: Biotechnological applications. *Journal of Molecular Catalysis. B, Enzymatic*, 76: 125–132.
10. Nagar, M., Dwivedi, S. K. and Shrivastava, D. (2013). A Review on Industrial Application in Microbial Lipases. *International Journal of Pharmaceutical and Research Sciences*, 2(4): 631-641.
11. Rahman, N. F., Basri, M., Rahman, M. B., Rahman, R. N. and Salleh, A. B. (2011). High yield lipase-catalyzed synthesis of Engkabang fat esters for the cosmetic industry. *Bioresource Technology*, 102(3): 2168– 2176.
12. Yao, C., Cao, Y., Wu, S., Li, S. and He, B. (2013). An organic solvent and thermally stable lipase from *Burkholderia ambifaria* YCJ01: Purification, characteristics and application for chiral resolution of Mandelic acid. *Journal of Molecular Catalysis. B, Enzymatic*, 85-86: 105-110.
13. Devanesan, M. G., Viruthagiri, T. and Sugumar, N. (2007). Transesterification of *Jatropha* oil using immobilized *Pseudomonas fluorescens*. *African Journal of Biotechnology*, 6 (21): 2497-2501.
14. Ingham, A. B. and Pemberton, J. M. (1995). A lipase of *Aeromonas hydrophila* showing nonhemolytic phospholipase C activity. *Current Microbiology*, 31(1): 28-33.
15. Yasin, N. H, Sanchez-Torres, V. and Maeda, T. (2014). Enhanced reduction of waste activated sludge at a low temperature by locally isolated strains *Pseudomonas sp.* VNT and *Aeromonas sp.* VNT. *Bioresource Technology*, 174: 134-141.
16. Silva, W. O. B., Mitidieri, S., Schrank, A. and Vainstein, M. H. (2005). Production and extraction of an extracellular lipase from the entomopathogenic fungus *Metarhiziumanisopliae*. *Process Biochemistry*, 40 (1): 321-326.
17. Winkler, U. K. and Stuckmann, M. (1979). Glycogen, hyaluronate and some other polysaccharides greatly enhance the formation of exolipase by *Serratia marcescens*. *Journal of Bacteriology*, 138(3): 663–670.
18. Bradford, M. M. (1976). A rapid and sensitive method for the quantitation of microgram quantities of protein utilizing the principle of protein–dye binding. *Analytical Biochemistry*, 72(1): 248–254.
19. Harley, J. P. and Prescott, L. M. (2002). *Laboratory exercises in microbiology* (5th edition), McGraw-Hill, Boston, pp. 125-206.
20. Smibert, R. M., and Krieg, N. R. (1994). Phenotypic characterization. In: Gerhardt, P., Murray, R. G., Wood W. A. and Krieg N. R. (eds). *Methods for general and molecular bacteriology*, American Society of Microbiology, Washington DC, pp. 611–654.
21. Green, M. R. and Sambrook, J. (2012). *Molecular cloning: a laboratory manual* (4th edition), Cold Spring Harbor Laboratory Press, New York, pp. 19-25.
22. Lane, D. J. (1991). 16S/23S rRNA sequencing. In: Stackebrandt E. and Goodfellow M. (eds). *Nucleic acid techniques in bacterial systematic*, Wiley, Chichester, pp. 115–175.
23. Altschul, S. F., Gish, W., Miller, W., Myers, E. W. and Lipman, D. J. (1990). Basic local alignment search tool. *Journal of Molecular Biology*, 215(3): 403–410.
24. Thompson, J. D., Higgins, D. G. and Gibson, T. J. (1994). CLUSTAL W: improving the sensitivity of progressive multiple sequence alignment through sequence weighting, position-specific gap

- penalties and weight matrix choice. *Nucleic Acids Research*, 22(22): 4673–4680.
25. Tamura, K., Dudley, J., Nei, M. and Kumar, S. (2007). MEGA 4: molecular evolutionary genetics analysis (MEGA) software version 4.0. *Molecular Biology and Evolution*, 24(8): 1596–1599.
26. Wang, X. J., Chen, X. P., Kappler, A., Sun, G. X. and Zhu, Y.G. (2009). Arsenic binding to iron (II) minerals produced by an iron (III)-reducing *Aeromonas* strain isolated from paddy soil. *Environmental Toxicology and Chemistry*, 28(11): 2255-2262.
27. Prasad, M. P. and Manjunath, K. (2012). Effect of media and process parameters in the enhancement of extracellular lipase production by bacterial isolates from industrial effluents. *International Journal of Microbiology Research*, 4(8): 308-311.
28. Mukesh Kumar, D. J., Rejitha, R., Devika, S., Balakumaran, M. D., Rebecca, A. I., Kalaichelvan, and P. T. (2012). Production, optimization and purification of lipase from *Bacillus* sp. MPTK912 isolated from oil mill effluent. *Advances in Applied Science Research*, 3(2): 930-938.
29. Sirisha, E., Rajasekar, N. and Narasu, M. L. (2010). Isolation and Optimization of Lipase Producing Bacteria from Oil Contaminated Soils. *Advances in Biological Research*, 4 (5): 249-252.
30. Prasanna, R. M., Mahendran, V. S. and Balakrishnan, V. (2015). Carbon and nitrogen sources enhance lipase production in the bacteria *Bacillus subtilis* kpl13 isolated from soil samples of kolli hills, south india. *International Journal of Science and Nature*, 6(2): 183-187.
31. Daouadji, K. L., Benattouche, Z. and Abbouni, B. (2014). Screening selection identification production and optimization of bacterial lipase isolated from industrial rejection of gas station. *Journal of Chemical and Pharmaceutical Research*, 6(6): 455-559.

Evaluation of Incubation Parameters in a TUNEL assay for Detecting Apoptotic cells in Cumulus Oocyte Complexes and *in vitro* produced early Embryos of Buffalo

Asit Jain^{1#}, Tripti Jain^{2#}, G K Sachdeva, Sachinandan De and Tirtha Kumar Datta*

Animal Genomics Lab, Animal Biotechnology Centre, National Dairy Research Institute, Karnal-132001, Haryana

¹Currently at Department of Animal Genetics and Breeding, College of Veterinary Science and Animal Husbandry, CGKV, Anjora, Durg, Chhattisgarh, India

²Currently at Animal Biotechnology Centre, CGKV, Durg, Chhattisgarh, India

#Contributed equally

*For Correspondence - tirthadatta@gmail.com

Short running title: TUNEL Assay in Buffalo COCs and Embryos

Abstract

Terminal deoxynucleotidyl transferase-mediated dUTP nick end labeling (TUNEL) is used widely for detecting the apoptotic status in biological cells of diverse origin. Reproducing the TUNEL procedure with specialized cells like cumulus oocyte complexes (COCs) poses technical challenge in view of mammalian oocytes which undergo very dynamic transitions in the course of oocyte maturation within a short time. The current work describes a standardized TUNEL protocol where the process of fixation and permeabilization were optimized using different concentrations of paraformaldehyde and Triton X-100 with sodium citrate, respectively. Effectiveness of the procedure was validated at different time intervals of oocyte culture using known oocyte stimulators. The procedure was further validated in the *in vitro* produced early embryos. Consistent and specific signal could be obtained using the procedure depicting the apoptotic status of cumulus cells and early embryos at different cell stages in buffalo.

Key words: Apoptosis, Cumulus Cells, Buffalo, TUNEL, Fixative

Introduction

Apoptosis is a distinct physiological event that triggers characteristic, morphological and

functional changes in the cell and is characterized by cytoplasmic and nuclear fragmentation, chromatin condensation, DNA fragmentation and phagocytosis (1). The inbuilt mechanism of cellular self destruction by apoptosis involves activation of nucleases that degrade the higher order chromatin structure of the DNA into fragments of 50 to 300 kbs and subsequently into smaller DNA pieces of about 200 bps in length (2). Apoptosis is common during embryogenesis (3) and normal tissue and organ involution (4) and occurs naturally at the end of the life span of differentiated cells (5).

The most common method of documenting the apoptotic events in cells includes observation under fluorescence microscope after staining the oocytes with specific fluorphores. By labeling DNA with specific fluochromes such as DAPI (4', 6- diamidino-2-phenylindole), the nuclei with clumped chromatin can be observed using fluorescence microscopy (6).

The terminal deoxynucleotidyl transferase-mediated dUTP nick end labeling assay (TUNEL) has emerged as an effective method for detecting apoptotic programmed cell death (7). This assay relies on the presence of nicks in the DNA which can be identified by terminal deoxynucleotidyl

transferase, an enzyme that catalyzes the addition of dUTPs (secondarily labeled with a marker) which, in turn, detects DNA fragmentation by labeling the terminal end of nucleic acids, resulting from apoptotic signaling cascades (8). However, the TUNEL procedure performed on different cell types suffers from the limitations of varying sensitivity and specificity in a tissue specific manner (9,10). In the apoptotic nucleus, two main obstacles intervening between TUNEL reagents and their targets are DNA hypercondensation and protein environment of DNA (11). Thus the method requires meticulous optimization steps considering typical architecture and morphology of the cells (8). The advanced protocol over conventional one has been tried by incorporating the dUTPs modified by fluorophores or haptens, including biotin or bromine, detected directly in the case of a fluorescently-modified nucleotide (i.e. fluorescein-dUTP), or indirectly with streptavidin or antibodies, if biotin-dUTP or BrdUTP are used, respectively.

The present study was conducted to improve sensitivity and reduce nonspecific labeling by using advanced TUNEL procedure while handling with buffalo COCs. Detailed optimization experiments were conducted by varying concentrations of TX pretreatment and fixatives. The optimized procedure was also validated in *in vitro* produced early embryos of buffalo.

Materials and Methods

All the media and chemicals used in the present study were obtained from Sigma Aldrich Chemical Co. Ltd, St. Louis, MO, USA unless otherwise indicated.

Oocyte collection and grading: Buffalo ovaries were collected from abattoir and transported to the laboratory in phosphate buffer saline (PBS) at 30–32°C, containing 50µg/ml streptomycin and penicillin. Ovaries were washed several times in normal saline and extra tissues attached to ovaries were trimmed off. COCs were aspirated from 3 to 8-mm antral follicles with an 18 gauge

needle attached to a 10 ml syringe in hepes-buffered hamster embryo culture (HH) medium (12). After sedimentation, the bottom layer containing the oocytes and other cells was collected and diluted in HH medium. Under the stereo zoom microscope, the COCs were picked up and washed three times in HH medium. They were evaluated according to morphological criteria and separated according to their quality. Only excellent quality oocytes (those with more than four compact layers of cumulus cells and homogenous cytoplasm) were used for *in vitro* maturation (IVM).

In vitro maturation of oocytes: *In-vitro* maturation of oocytes were carried out as described earlier (13). Briefly, selected COCs were washed three times with serum-free oocyte maturation media (TCM199 HEPES supplemented with 1mg/ml polyvinyl alcohol, 0.33mM sodium pyruvate, 1.0mM Glutamine, 50µg/ml streptomycin and 10.0µg/ml of FSHp). After washing, 20 COCs were placed in 100µl drop of maturation medium and overlaid with mineral oil. Oocytes were allowed to mature for 24 h at 38.5°C in an atmosphere of 5% CO₂.

In vitro fertilization of oocytes: Fertilization of oocytes was carried out in the mSOF (modified synthetic oviductal fluid) based fertilization medium. Briefly, the 24 h matured oocytes were washed three times in modified mSOF medium (mSOF supplemented with 0.19% caïneine sodium benzoate, 10mg/100ml heparin and 0.014% sodium pyruvate and 1% BSA) and transferred to 50µl fertilization drops of the same medium in groups of 20-25. Frozen semen of a Murrah buffalo, known for high rates of *in vitro* fertilization and cleavage, were thawed at 37°C and washed two times in semen wash media (IVF medium without BSA) by centrifugation at 900Xg for 3 min. The semen pellet was resuspended in 1 ml fertilization medium, and 1x10⁶ sperms were transferred to fertilization drops containing matured oocytes and incubated in CO₂ incubator for 14h at 38.5°C and 5% CO₂.

In vitro culture of embryos: Presumptive zygotes were removed from the fertilization

droplets after 14 h of insemination. Cumulus cells and supernumerary spermatozoa attached to the oocytes were mechanically removed by vortex agitation for 3 mins and washed four to five times in mSOF based IVC media. After washing, 15-20 presumptive zygotes were then co-cultured with monolayers of granulosa cells in 100µl of droplets of mSOF media (mSOF supplemented with 0.8% BSA, 5.6mM glucose, 0.33mM pyruvate, 3.3mM lactate, 1 mM glutamine, 1x MEM essential amino acid, 1x non-essential amino acid and 50µg/ml gentamycin) under mineral oil, at 38.5°C and 5% CO₂ in a humidified atmosphere. After 72 h, all presumptive zygotes were transferred to IVC-II medium (mSOF supplemented with 10% FBS, 5.6 mM glucose, 0.33mM pyruvate, 3.3mM lactate, 1mM glutamine, 1x MEM essential amino acid, 1x non-essential amino acid and 50µg/ml gentamycin) and maintained for 8 days post-insemination at 5% CO₂ and 38.5°C with replacement of medium twice after every 48 h. 2-cells, 8-cells and blastocyst stage embryos were collected after two, three and seven days post insemination, respectively.

In situ labeling of fragmented DNA for the detection of apoptotic cells by TUNEL: The TUNEL procedure was performed using the *in situ* cell death detection Kit (Fluorescein; Roche Diagnostics Corporation) as described earlier. The *in vitro*-matured COCs and different stages of early embryos were washed twice in PBS supplemented with 1mg/ml of polyvinylpyrrolidone (PBS-PVP). These cells were fixed in 2 and 4% paraformaldehyde (PFA; Sigma) in PBS (pH 7.4) for 1 h and then washed in PBS-PVP. After fixation, COCs and embryos were pretreated with permeabilization solution (0.5% TX and 0.1% sodium citrate) at room temperature for 1.5 h. As positive-control, *in vitro*-matured COCs and embryos were incubated in 200µl of RNase and proteinase free DNase 1 (Fermentas) at 37°C for 1 h. The COCs were washed in PBS-PVP and incubated in 25µl of TUNEL reaction mixture (supplied in the kit) for 1 h at 37°C in the dark. As negative-control, COCs and embryos were incubated in the absence of TUNEL reaction

mixture. The cells were then incubated in 500µl of DNase free RNase A (50µg/ml) for 1 h, followed by 15-30 min of incubation in 200µl of propidium iodide (6.25µg/ml; Sigma) at room temperature. The COCs and embryos were washed three times in PBS-PVP, then placed on glass slides and mounted with ProLong antifade mounting medium (Invitrogen Life Technologies). Fluorescent images were captured on fluorescence microscope (Olympus, BX-51, Japan). This experiment was repeated three times with 10 COCs or embryos per treatment group.

Experimental design: TUNEL assay was performed using paraformaldehyde (PFA) as a fixative at two different concentrations viz. 2 and 4% (w/v). At first, oocytes/embryos were permeabilized using TX treatment as described above for two different time intervals of 1 and 2 h. A group of COCs fixed with 2% PFA but without any pretreatment was considered as control. The optimized concentration of fixative and permeabilization treatment was further validated on different cell stage embryos.

Results and Discussion

TUNEL is acknowledged as a method of choice for rapid identification and quantification of the apoptotic cell fraction in cultured-cell preparations. In the present study, we attempted to standardize the TUNEL detection of apoptotic cells in COCs and early embryos. Reproducing signal qualities following the TUNEL procedure has also been reported to be sensitive to fixation method and duration (14). In the present study, we observed that 4% PFA in 1xPBS (pH7.4) was optimum in obtaining consistent TUNEL signals (Fig.1E). A lower concentration of PFA (2%) was found inadequate, which often led to morphological distortion of COCs during the staining procedures (Fig.1A-C). This is consistent with earlier studies reporting 2% PFA as insufficient to preserve the nuclear envelope integrity and repositioning of the nuclei. As such 4% PFA was found effective option for cell fixation in immunohistochemistry or TUNEL methods performed on several cell types (12,15).

The sensitivity of TUNEL assay has been increased by incubating cells with detergents, most frequently TX (16). Without pretreatments, the TUNEL sensitivity was found to be low, generating only gross signals entirely masking the tissue detail (Fig.1A). TX treatment for 1 h was also found insufficient in both 2% and 4% PFA groups which was characterized by large background noise signals (Fig.1B&D). But

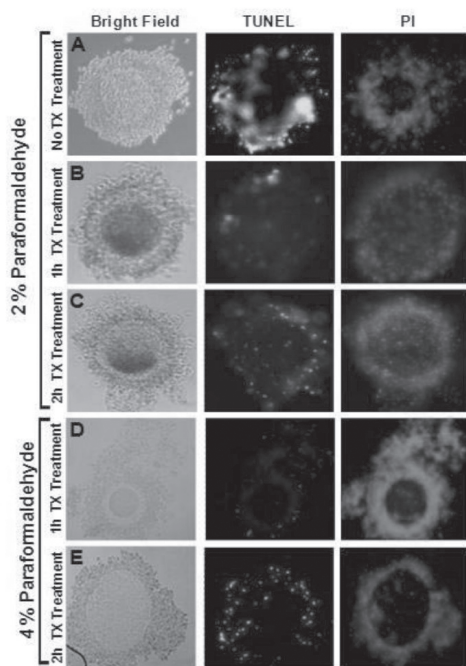


Fig.1: Effect of different concentrations of paraformaldehyde and TX on apoptosis signal specificity in *in vitro* matured buffalo COCs. **A.** TUNEL performed without any pretreatment showed heavy background signals. **B&C.** Fixation by 2% PFA and pretreatment with TX for either 1 or 2 hrs showed gross smudging and unclear tissue morphology in cumulus cells. **D.** 4% PFA fixation and permeabilization treatment for 1 hr lacked clear TUNEL signal and produced heavy background **E.** 4% PFA with 2 hr TritonX-100 pretreatment revealed best TUNEL signal specificity and least background signals. PI: Propidium Iodide stain was used for detection of total cells. TX: TritonX 100 (Sigma). Magnification x200.

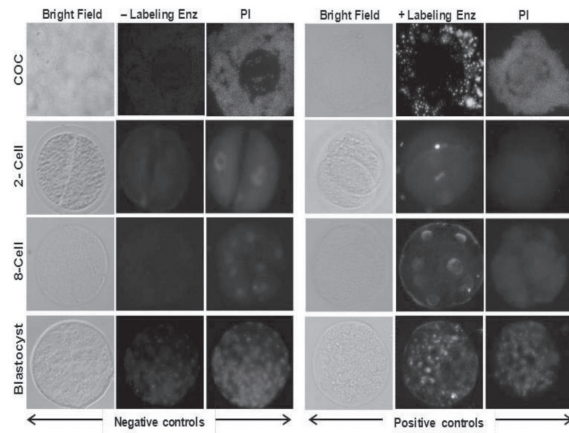


Fig.2: Negative and positive controls used during TUNEL procedure. Negative control samples treated with TUNEL mix lacking TdT resulted in complete absence of TUNEL signals.

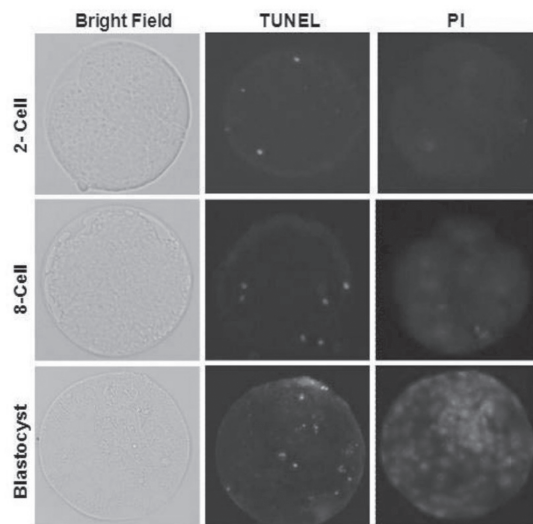


Fig.3: The optimized TUNEL procedure (4% PFA fixation and permeabilization treatment for 2 hrs) was found effective in revealing clear signals in *in vitro* produced embryos at different cell stages.

pretreatments for two hours improved the signal to noise ratio particularly in 4% PFA group (Fig.1E).

Positive and negative controls used in the present study confirmed the specificity of TUNEL results in COCs as wells as in early embryos. For negative control, TUNEL specificity was checked by comparing labeling with cellular morphology (Fig.2). Positive control samples after fixation and permeabilization were incubated with DNase I for 30 min at room temperature to induce DNA strand breaks, prior to labeling procedures. As expected in all cases, the preparations revealed clear-cut TUNEL signals revealing the cumulus cells as well as nuclei at different cell stage embryos (Fig.2). Further, we confirmed the suitability of the optimized TUNEL steps (4% PFA fixation and permeabilization for 2 h) for use in case of early cleaved buffalo embryos which revealed desired signals (Fig.3).

In conclusion, the optimized fixation and permeabilization steps used in the present study for performing the TUNEL procedure allowed repeatable results to monitor apoptosis in cumulus enclosed oocytes and *in vitro* produced early embryos at different cell stages. The protocol optimized will be useful for undertaking studies involving limited number of oocyte or/and embryos samples and experimenting on improving the efficiency of these artificial reproduction technology (ART) procedures.

References

1. Hardy, K. (1999). Apoptosis in the human embryo. *Rev. Reprod.*, 4: 125-134.
2. Arends, M.J., Morris, R.G. and Wyllie, H. (1990). Apoptosis: the role of endonuclease. *American J. Pathol.*, 136:593-608.
3. Van Soom, A.V., Vanroose, G., Laevens, H. and Kruif, A. (2000). Apoptosis in *in vitro* produced bovine embryos. *Theriogenology*, 53: 367-372.
4. Buttyan, R., Zakeri, R., Lockshin, R.A., Wolgemuth, D. (1988). Cascade induction of c-fos, c-myc and heat shock 70k transcripts during regression of the rat ventral prostate gland. *Mol. Endocrinol.* 2: 650-658.
5. Benedett, A., Jezequel, A.M., Orland, I. (1988). Preferential distribution of apoptotic bodies in acinar zone 3 of normal and rat liver. *J. Hepatol.*, 7: 319-324.
6. Li, X., Wang, J., Ye, Z. and Li, J.C. (2012). Oridonin Up-regulates Expression of *P21* and Induces Autophagy and Apoptosis in Human Prostate Cancer Cells. *Int. J. Biol. Sci.*, 8: 901-912.
7. Gavrieli, Y., Sherman, Y. and Ben-Sasson, S.A. (1992). Identification of programmed cell death *in situ* via specific labeling of nuclear DNA fragmentation. *J. Cell Biol.*, 119: 493-501.
8. Negoescu, A., Guillermet, C., Lorimier, P., Brambilla, E. and Labat-Moleur, F. (1998). Importance of DNA fragmentation in apoptosis with regard to TUNEL specificity. *Biomed Pharmacother*, 52: 252-258.
9. Grasl Grasl-Kraup, P.B., Ruttkay-Nedecky, B., Koudelka, H., Bukowska, K., Bursch, W., Schulte-Hermann, R. (1995). *In situ* detection of fragmented DNA (TUNEL assay) fails to discriminate among apoptosis, necrosis, and autolytic cell death: a cautionary note. *Hepatology*, 21: 1465-1468.
10. Cervos-Navarro, J. and Schubert, T.E.O. (1996). Pitfalls in the evaluation of apoptosis using TUNEL. *Brain. Pathol.*, 6: 347-348.
11. Gold, R., Schmied, M., Giegerich, G., Breitschopf, H., Hartung, H.P., Tokyka, K.V., Lassmann, H. (1994). Differentiation between cellular apoptosis and necrosis by combined use of *in situ* tailing and nick translation techniques. *Lab Invest*, 71: 219-225.

12. Bettegowda, A., Osman, V., Patel, K.B.L., Ki-Eun P., Mohamed S., Jianbo, Y., James J.I. and George, W.S. (2008). Identification of Novel Bovine Cumulus Cell Molecular Markers Predictive of Oocyte Competence: Functional and Diagnostic Implications. *Biol. Reprod.*, 79: 301-309.
13. Kumar, P., Verma, A., Roy, B., Rajput, S., Ojha, S., Anand, S., Yadav, P., Arora, J., De, S., Goswami, S.L. and Datta, T.K. (2012). Effect of varying glucose concentrations during *in vitro* maturation & embryo culture on efficiency of in vitro embryo production in buffalo. *Reprod. Dom. Anim.*, 47:269-273.
14. Lucassen, P.J., Chung, W.C.J., Vermeulen, J.P., van Lookeren, Campagne, M., van Dierendonck J.H., Swaab, D.F. (1995). Microwave-enhanced *in situ* end-labeling of fragmented DNA: parametric studies in relation to postmortem delay and fixation of rat and human brain. *J. Histochem. Cytochem.*, 43: 1163.
15. Flemr, M. and Svoboda, P. (2011). Ribonucleoprotein localization in mouse oocytes. *Methods*, 53: 136-141.
16. Desjardins, L. M. and MacManus, J.P. (1995). An adherent cell model to study different stages of apoptosis. *Exper. Cell Res.*, 216: 380-387.

Effect of Growth Regulators on Regeneration Through Leaf and Stem Derived Callus in *Physalis minima* Linn.

Sandhya H. and Srinath Rao*

Plant Tissue Culture and Genetic Engineering Laboratory
Department of Post Graduate Studies and Research in Botany, Gulbarga University
Kalaburagi- 585106 Karnataka, India.

*For Correspondence - srinathraomm@gmail.com

Abstract

Physalis minima L. is a medicinal herb which belongs to the family Solanaceae. A rapid protocol by using leaf and stem derived callus cultures for organogenesis and subsequent plantlet regeneration and survival of regenerated plants was established. Murashige and Skoog's (MS) basal medium supplemented with various concentrations of auxins like 2,4-dichlorophenoxyacetic acid (1 to 3 mg/l), α -naphthaleneacetic acid (1 to 3 mg/l) and cytokinins like 6-benzylaminopurine (BAP) and kinetin (Kn) (0.5 to 1.5 mg/l) were used for morphogenesis. Both the explants responded for callus induction, however, stem explants were found superior than that of leaf. Further increase in callus was observed when 0.5 mg/l Kn was supplemented along with 2,4-D. The frequency of callus induction was 90%. It was noticed that among leaf and stem, leaf explants responded well for regeneration via callus. The highest (95%) percentage of regeneration was recorded on MS medium containing 1 mg/l BAP + 2 mg/l 2,4-D from leaf derived callus after a period of 20 to 25 days. Shoots of about 2 to 3 cm in height were subsequently rooted on MS medium supplemented with 1 mg/l indole-3-butyric acid (IBA), with 85% frequency. Rooted shoots were hardened in liquid half strength MS medium containing 1 mg/l IBA and acclimatized later in the pots containing soil, cocopeat and sand in the ratio 1:2:1 in the Net House.

Key words: *Physalis minima*, leaf, stem, callus, organogenesis.

Introduction

Physalis minima L. belongs to nightshade family (Solanaceae), and is an annual herb and an important medicinal plant in Indian Traditional System of Medicines and yields steroid molecules like physalins which have been shown to possess anti-inflammatory and anti-arthritic activities (1, 2). In India, this plant is widely distributed. It is a quick growing and high fruit-yielding plant (3). *P. minima* is used as a bitter tonic, appetizer, diuretic, laxative and in inflammations and antigonorrhoeic. It is used against the enlargement of spleen and abdominal troubles (4). The leaves are used to relieve headache. A paste of the leaves and stem is used to treat dizziness (5). Decoction of whole plant is consumed in Malaysia as a remedy for cancer (6). Though the plant has immense medicinal value, it is gradually declining in number from the natural habitat due to over exploitation (7). Tissue culture plays a key role for the rapid propagation of medicinal plants, their conservation and in enhancing the production of secondary metabolites (8). Present study was undertaken to examine the potential of different explants with various concentrations of plant growth hormones, alone or in combination with the possibility of developing an efficient protocol for their *in vitro* multiplication of *P. minima*.

Materials and Methods

Healthy plants growing in the Botanical Garden of Gulbarga University, were collected

and brought to the laboratory. Explants were prepared from these garden grown plants. In the present investigations, explants like leaf and stem were used. They were washed under running tap water to remove dust particles and later immersed in a solution containing Bavistin (1.0% w/v, a fungicide) and Tween-20 for 15-20 min and then thoroughly washed under running tap water and rinsed thrice with distilled water. Explants were then sterilized with 70% ethanol for 3-4 min followed by washing with double distilled water for 2-3 times. Furthermore, surface sterilization was carried out using 0.1% mercuric chloride for 3-4 min followed by gentle shaking and subsequently washed thoroughly with sterile distilled water to remove traces of mercuric chloride. Explants were implanted on sterile MS basal medium (9) supplemented with 3% sucrose (w/v), gelled with 0.8% agar (w/v), fortified with vitamins and growth regulators. pH of the medium was adjusted to 5.6 prior to autoclaving at 121°C. All cultures were maintained at 25±1°C with 16/8 h photoperiod at 40 μm m⁻² s⁻¹ provided by cool, white fluorescent tubes. For callus induction, leaf and stem explants were cultured on MS medium with various concentrations of 2,4-D (1 to 3 mg/l) and NAA (1 to 3 mg/l). For organogenesis, leaf and stem explants were cultured on MS medium supplemented with various concentrations of BAP (0.5 to 1.5 mg/l), Kn (0.5 to 1.5 mg/l), 2,4-D (1 to 3 mg/l) and NAA (1 to 3 mg/l). The *in vitro* regenerated shoots were transferred to MS medium containing IBA (1 to 3 mg/l) for rooting. For hardening, 2-3 week old rooted shoots were removed from the culture tubes, thoroughly washed to remove the adhering gel with distilled water and transferred to polycups containing soil, cocopeat and sand in the ratio 1:2:1 and kept in mist house for acclimatization.

Results and Discussion

Callus induction: In the present investigation, leaf and stem explants were cultured on MS medium fortified with various concentrations of 2,4-D and NAA (1 to 3 mg/l) alone or in combination with BAP or Kn for callus induction. Both the explants enlarged in size and thickened

within a week of inoculation. Initiation of callus was observed in both the explants within 10-12 days of incubation. Approximately, 2010±1.10 mg of callus/culture was observed on MS medium supplemented with 2 mg/l 2,4-D in stem explants with 90% frequency followed by leaf (1100±1.2 mg/culture) with 50% frequency (Table-1; Plate-I a and c). Among the different concentrations of auxins used for callus induction, 2 mg/l 2,4-D has been found optimum, while increasing the auxin concentrations above this level reduced callus proliferation. However, NAA showed poor response with respect to induction and further growth of callus at all the concentrations used. Further enhancement of callus growth was observed in stem and leaf explants when 0.5 mg/l Kn was added to 2 mg/l 2,4-D-containing medium with a frequency of 90% in stem (3580±0.00 mg/culture) and 70% in leaf (2850±1.1 mg) explants (Table-2; Plate-I b and d). It is apparent that hormones work better when supplied in combination than alone. It is concluded from the data that stem has been found as a better explant for callus induction as compared to leaf. Also, 2 mg/l 2,4-D and 0.5 mg/l Kn seemed optimum for callus induction. Our results supported the results of other workers (10,11) who found that same combinations of growth regulators and explants proved efficient for callogenesis.

Regeneration from callus cultures: *In vitro* plant regeneration depends on the type of explants and is influenced by different concentrations and combinations of growth regulators in the medium. Different explants were cultured on MS medium supplemented with various auxins and cytokinins in varied combinations. The results indicated that plant growth regulators significantly affected regeneration response of the explants. Callus obtained from both the explants was transferred onto MS medium supplemented with 2 mg/l 2,4-D + BAP or Kn (0.5 to 1.5 mg/l respectively). Multiple shoots were initiated from leaf derived callus cultures on medium supplemented with 1 mg/l BAP and 2 mg/l 2,4-D. Another

experiment was conducted to investigate the interaction of BAP or Kn by keeping the concentration of 2,4-D constant (2 mg/l). BAP at a concentration of 1mg/l elicited the best response (9.52 ± 1.20) with 95% frequency (Table-3; Plate I a, b) than Kn (data not shown). Afroz et al. (7) observed that presence of BAP in the medium was necessary for proliferation of *P. minima*. BAP was reported to be the most effective cytokinin for shoot bud regeneration in most of the Solanaceous plants such as *Solanum trilobatum* (12,13), *Capsicum annum* (14) and *Solanum laciniatum* (15).

Root induction: Well-developed shoots were excised and transferred to the medium containing different concentrations of IBA (1 to 3 mg/l) for root induction. The frequency of rooting (85%) and the number of roots (13.20 ± 1.20) was high on medium supplemented with 1 mg/l IBA (Table-4; Plate IIc). Roots were thick and elongated. Similar results were also reported by Ramar and Ayyadurai (16) in *P. minima*. Plantlets were transferred to disposable plastic cups containing soil, cocopeat and sand in the ratio of 1:2:1 and covered with polybags and hardened for 4-weeks and successfully transferred into the greenhouse with a survival rate 50% (Plate 2).

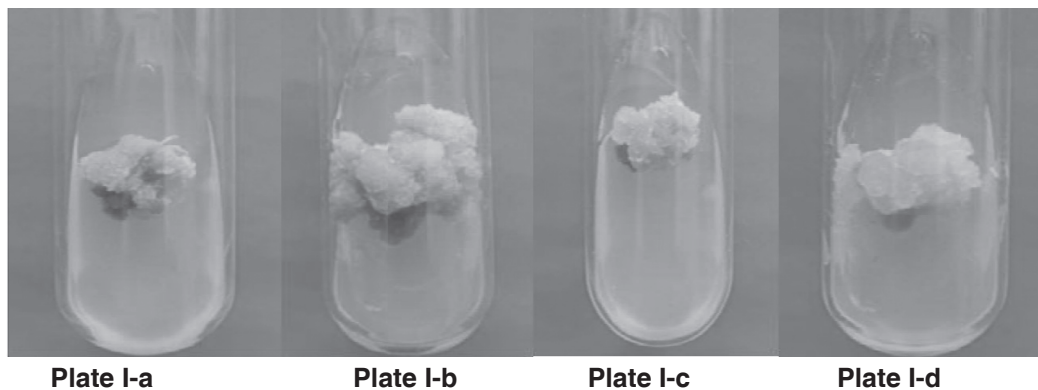


Plate – I. *In vitro* callus induction of *Physalis minima* L. a) Induction of callus from stem explant on MS + 2 mg/l 2,4-D. b) Induction of callus from stem explant on MS + 2 mg/l 2,4-D + 0.5mg/l Kn. c) Induction of callus from leaf explant on MS + 2 mg/l 2,4-D. d) Induction of callus from leaf explant on MS + 2 mg/l 2,4-D + 0.5mg/l Kn

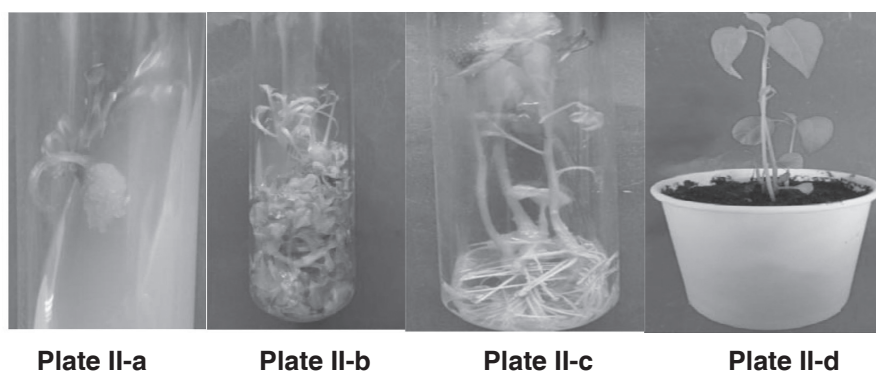


Plate II. *In vitro* shoot induction, proliferation and acclimatization of plants from leaf explants of *P. minima* L. a) Initiation of shoot through leaf-derived callus culture on MS + 2 mg/l 2,4-D + 1mg/l BAP. b) Multiple shoot formation from leaf derived callus on MS + 2 mg/l 2,4-D + 1mg/l BAP after 20 days. c) Root induction on MS + 1 mg/l IBA. d) Acclimatized potted plant.

Table-1: Effect of 2,4-D and NAA on growth of callus derived from leaf and stem explants of *P. minima* L.

Growth regulators (%)	Conc. mg/l	Stem			Leaf		
		Fresh Wt. (mg)	Dry Wt. (mg)	Frequency (%)	Fresh Wt. (mg)	Dry Wt. (mg)	Frequency
2,4-D	1.0	1125±1.15 ^c	138±0.11 ^c	40	1002±0.00 ^a	115±0.00 ^a	40
	2.0	2010±1.10 ^a	428±0.11 ^a	90	1100±1.20 ^b	199±1.00 ^a	50
	3.0	1850±1.00 ^b	231±1.10 ^b	60	985±1.00 ^a	96±1.17 ^c	45
NAA	1.0	1021±0.05 ^b	130±0.20 ^b	45	1095±1.20 ^b	187±0.01 ^c	60
	2.0	1195±1.23 ^a	228±0.01 ^a	70	1011±0.20 ^b	119±1.37 ^c	50
	3.0	1101±1.10 ^a	201±0.00 ^a	50	986±1.25 ^c	96±0.10 ^b	45

Data represent average of three replicates; each replicate consists of 25 cultures. Mean ± Standard error. Mean followed by the different superscripts in column are not significantly different from each other. a=P<0.05, b=P<0.01 and c=P<0.001 levels according to ANOVA.

Table-2 : Effect of 2,4-D (2 mg/l) in combination with Kn on induction and growth of callus in *P. minima* L.

Growth regulators (%)	Conc. mg/l	Stem			Leaf		
		Fresh Wt. (mg)	Dry Wt. (mg)	Frequency (%)	Fresh Wt. (mg)	Dry Wt. (mg)	Frequency
2,4-D +Kn	2.0+0.5	3580±0.00 ^a	595±1.12 ^b	90	2850±1.10 ^b	250±1.00 ^c	70
	2.0+1.0	2310±1.00 ^c	445±0.00 ^c	80	2010±1.00 ^a	195±1.20 ^a	65
	2.0+1.5	2110±1.20 ^c	430±0.10 ^c	70	1810±1.15 ^a	120±0.10 ^b	50

Data represent average of three replicates; each replicate consists of 25 cultures. Mean ± Standard error. Mean followed by different superscript in columns are not significantly different from each other. a=P<0.05, b=P<0.01 and c=P<0.001 levels according to ANOVA.

Table 3: Effect of 2,4-D in combination with BAP on organogenesis of leaf and stem-derived callus in *Physalis minima* L.

Growth Hormone	Conc. (mg/l)	No. of multiple shoots	
		Leaf	Frequency (%)
2,4-D+BAP	2.0+0.5	6.12±1.01 ^a	70
	2.0+1.0	9.52±1.20 ^b	95
	2.0+1.5	4.20±0.20 ^c	60

Data represent average of three replicates; each replicate consists of 25 cultures. Mean ± Standard error. Mean followed by the different superscript in column are not significantly different from each other. a=P<0.05, b=P<0.01 and c=P<0.001 levels according to ANOVA.

Table 4 : Effect of IBA alone in MS medium on *in vitro* rooting of *Physalis minima* L. after 4-weeks of culture.

Growth Hormone	Conc. (mg/l)	No. of roots/shoot	Frequency (%)
IBA	1.0	13.20±1.20 ^a	85
	2.0	7.35±1.00 ^b	75
	3.0	4.30±0.10 ^a	60

Data represent average of three replicates; each replicate consists of 25 cultures. Mean ±Standard error. Mean followed by the different superscripts in column are not significantly different from each other. a=P<0.05, b=P<0.01 and c=P<0.001 levels according to ANOVA.

Conclusion

The present paper describes an improved and successful tissue culture method for propagation of *Physalis minima*, an important medicinal plant. This study also provides a rapid technique of mass propagation of *P. minima*.

References

- Patel G.K, Bapat V.A. and Rao P.S. (1987). Protoplast culture and genetic transformation in *Physalis minima* L. Proceedings: Plant Sciences 97: 333-335.
- Patel T, Shah K, Jiwan K and Neeta Shrivastava (2011). Study on the antibacterial potential of *Physalis minima* Linn. Indian Journal of Pharmaceutical Science 73: 111-115.
- Patel P.R, Gol N.B, Tadapaneni V, and Rao R. (2009). Physicochemical changes in sunberry (*Physalis minima* L.) fruit during growth and ripening. Fruits 66: 37-46.
- Chothani D.L and Vaghasiya H.U. (2012). A phytopharmacological overview on *Physalis minima* Linn. Indian Journal of Natural Products and Resources. 3: 477-482.
- Sheeba E., Palanivel S. and Parvathi S. (2015). *In vitro* flowering and rapid propagation of *Physalis minima* Linn. - A medicinal plant. International Journal of Innovative Research in Science, Engineering and Technology. 4 : 18763-18768.
- Zakaria M. and Mohamad AM (2010). Traditional Malay medicinal plants. ITNM. pp 175-185.
- Afroz F., Hassan A. K. M. S., Bari L. S., Sultana R., Begum N., Jahan M. A. A. and Khatun R. (2009). *In vitro* shoot proliferation and plant regeneration of *Physalis minima* L. a perennial medicinal herb. Bangladesh J. Sci. Ind. Res. 44: 453-456.
- Agbor A. G. and Ngogang J. Y. (2005). Toxicity of herbal preparations. Cam. J. Ethanbot. 1: 23-28.
- Murashige T. and Skoog F. (1962). A revised medium for rapid growth and bioassays with tobacco cultures. Physiol. Plant. 15: 473-497.
- Mungole A. J., Doifode V. D., Kamble R. B., Chaturvedi A. and Zanwar P. (2011). *In vitro* callus induction and shoot regeneration in *Physalis minima* L. Annals of Biological Research 2: 79-85.
- Sheeba E., Palanivel S. and Parvathi S. (2013). Effect of plant growth regulators on callus induction in *Physalis minima* Linn. International Journal of Innovative Research in Science, Engineering and Technology 2: 4847- 4851.

12. Alagumunian S, SaravanaPerumal V, Balachandar R, Ramesh Kannan K and Rao M.V. (2004). Plant regeneration from leaf and stem explants of *Solanum trilobatum* L. Current Science 86: 1478-1480.
13. Jawahar M., Amalan Robert G. and Jeyaseelan M. (2004). Rapid proliferation of multipleshoots in *Solanum trilobatum* L. Plant Tissue Culture 14: 107-112.
14. Sanatombi and Sharma G. J. (2007). Micro propagation of *Capsicum annum*. L. Notulae Botanicae Horti Agrobotanici Cluj-Napoca. 35: 57-64.
15. Pooja Bhatnagar, Madhurima Bhatnagar, Amarjit Nath K. and Sharma D.R. (2004). Production of solasodine by *Solanum laciniatum* using plant tissue culture technique. Indian Journal of Experimental Biology, 42: 1020-1023.
16. Ramar K. and Ayyadurai V. (2015). Journal of international academic research for multidisciplinary. 3: 119-124.

National Seminar on
**RECENT TRENDS IN NANO TECHNOLOGY
AND AQUACULTURE TECHNOLOGIES**
(RTNAT - 2016)



18-19 August, 2016

Sponsored by
UGC, New Delhi



ज्ञान - विज्ञान विमुक्तये

Organized by
Department of Fishery Science and Aquaculture
SRI VENKATESWARA UNIVERSITY
Tirupati - 517 502, Andhra Pradesh, India

Organizing Secretary
Dr. S. Janardana Reddy
Mobile : +91 9949786291, +91 8500959334
E-mail : sjanardanareddy@gmail.com
rtnat2016@gmail.com

Synthesis of Silver Nanoparticles from Different Plant Leaf Extracts and Its Analysis using UV-Spectroscopy

Lavanya Kakarla¹ and Chakravarthy Rama² *

^{1,2}Department of Biotechnology, K L University, Green Fields, Vaddeswaram – 522502, Guntur, Andhra Pradesh, India

*For Correspondence - drrchakravarthy@gmail.com

Abstract

The synthesis of silver nanoparticles has attracted much attention because their unique shape-dependent optical, electrical, and chemical properties have potential applications in nanotechnology. Silver nanoparticles are used in photographic reactions, catalysis, and chemical analysis. An attempt has been made to study the formation of the metal nanoparticles by reduction of the aqueous metal ions during exposure to the broth of boiled sunflower leaves may be easily followed by UV–vis spectroscopy. After adding the leaf broth to silver nitrate solution, immediately a yellowish brown color forms indicating that silver nanoparticles have been formed.

Key words: UV visible spectroscopy, *Helianthus annuus*, *Coriander sativum*, Nanoparticles, Nanotechnology.

Introduction

Silver (Ag) is a transition metal element having atomic number 47 and atomic mass 107.87. The medicinal uses of silver have been documented since 1000 B.C. Silver is a health additive in traditional Chinese and Indian Ayurvedic medicine. Its action as an antibiotic comes from the fact that it is a non-selective toxic “biocide.” In the late 1970s, Robert O. Becker discovered that silver ions promote bone growth and kill surrounding bacteria. Silver kills some 650 different disease causative organisms (1). Silver based topical dressing has been widely used as a treatment (2) for infections in burns, open wounds and chronic ulcer (3). The Silver

nanoparticles and Ag+ carriers can be beneficial in delayed diabetic wound healing as diabetic wounds are affected by many secondary infections (4). These nanoparticles can help the diabetic patients in early wound healing with minimal scars. Silver nitrate is still a common antimicrobial used in the treatment of chronic wounds. In its modern form, silver nanoparticles have become the promising (5) antimicrobial material in a variety of applications because they can damage bacterial cells by destroying the enzymes that transport cell nutrient and weakening the cell membrane or cell wall and cytoplasm (6). For instance, an increasingly popular application is to use pure silver, or silver-coated, nanoparticles in food packaging materials such as plastic bags, containers, films or pallet. The synthesis of silver nanoparticles has attracted much attention because their unique shape dependent optical, electrical, and chemical properties have potential applications in nanotechnology (7). Silver nanoparticles are used in photographic reactions, catalysis, and chemical analysis (8,9).

Materials and Methods

Preparation of Leaf extract: The Leaf broth, used for reduction of Ag+ and synthesis of silver nanoparticles was prepared by taking thoroughly washed and finely cut leaves (Coriander and Sunflower leaves) in a separate 500 ml conical flask.

Use extract from: Coriander leaves: 20 g and sunflower leaves: 20 g to the biomass, 100 ml of

sterile distilled water was added and then boiled for 2 min in microwave (12). After boiling, the solution was decanted and filtered, and stored at 4° C for further experiments.

Biosynthesis of Nanoparticles using Leaf extract: 5 ml of the each broth was added to 100 ml of 1mM aq. AgNO₃ solution and kept at 30°C. (Different plant extracts require different times to complete the reaction). After 3-5 minutes, the solution develops distinct characteristic color (yellowish brown). The bio reduction of ions in solution was monitored by periodic sampling of aliquots (0.1 mL) of aqueous component and measuring UV-Vis spectra of the solution. The nanoparticle solution was diluted to 20 times with distilled water to avoid errors due to high optical density of the solution. A UV-Vis spectrum of the solution is measured in 10-mm-optical-path-length quartz cuvettes with UV-Vis spectrophotometer at a resolution of 1 nm between 300 and 600 nm (Exciton band near 430 nm for silver).

Results and Discussion

Synthesis of Silver Nanoparticles from Sunflower (*Helianthus Annuus*): Silver exhibits yellowish-brown color in water, these colors arise due to excitation of surface plasmon vibrations in the metal nanoparticles. Metal nanoparticle is formed due to the reduction of the metal ions by the *Helianthus annuus* leaf broth (10) and this

can be identified by UV-vis spectroscopy. The UV-vis spectra of silver nanoparticles taken at different hours of intervals are analyzed (shown in graphs 1, 2). Sunflower also serves as good source of synthesis of silver nanoparticles. Formation of the metal nanoparticles by reduction of the aqueous metal ions during exposure to the broth of boiled sunflower leaves may be easily followed by UV-vis spectroscopy. After adding the leaf broth to silver nitrate solution, immediately a yellowish brown color forms (Table. 1 & 2) indicating that silver nanoparticles are been formed (Fig.1). It is observed that the silver surface plasma on resonance band occurs at 430 nm.

Synthesis of Silver Nanoparticles Using Coriander (*Coriandrum Sativum*): Coriander serves as good source of synthesis of silver nanoparticles (11, 12). Formation of the metal nanoparticles by reduction of the aqueous metal ions during exposure to the broth of boiled coriander leaves may be easily followed by UV-vis spectroscopy. After adding the leaf broth to silver nitrate solution, immediately a yellowish brown color forms (see Tables 3 & 4) indicating that silver nanoparticles are been formed (Fig. 2). It is observed that the silver surface plasma on resonance band occurs at 460 nm. The UV-vis spectra of silver nanoparticles taken at different hours of intervals are analyzed (Fig. 3, 4, 5, 6 & 7).

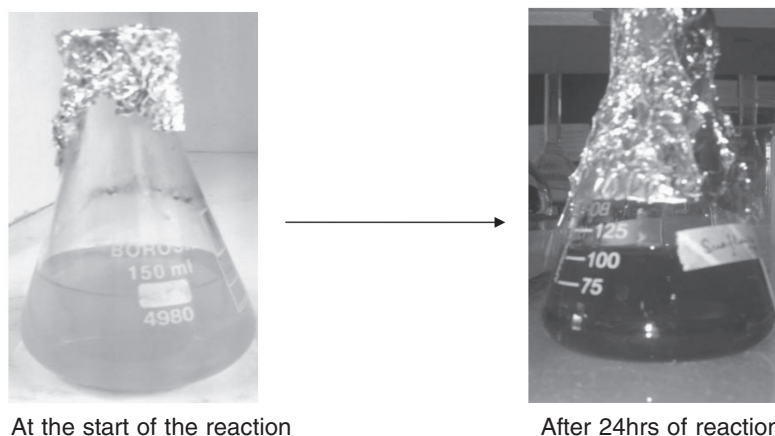


Fig. 1. Nanoparticles solution (Sun flower)

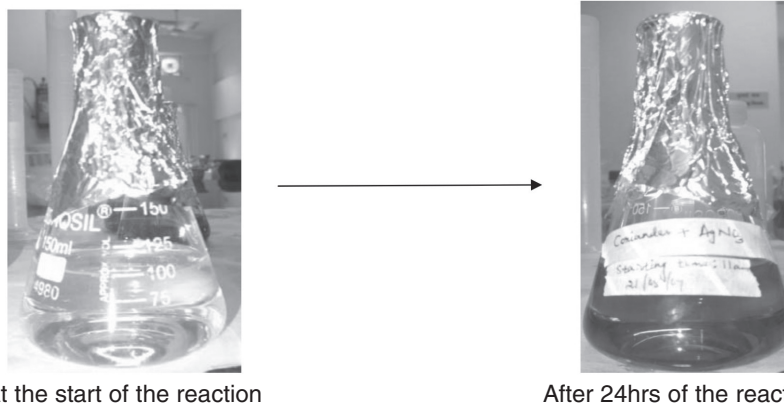


Fig. 2. Nanoparticles solution (Coriander)

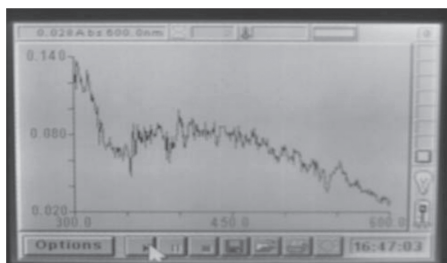


Fig. 3. UV-vis absorption spectrum of silver nanoparticles after 3hrs of the reaction sunflower

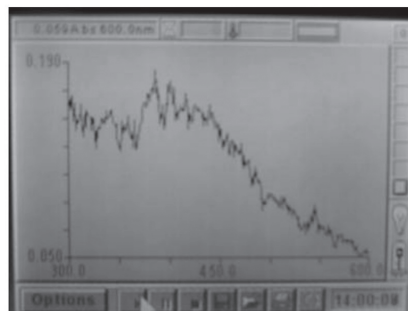


Fig. 6. UV-vis absorption spectrum of silver nanoparticles after 2hrs of the reaction

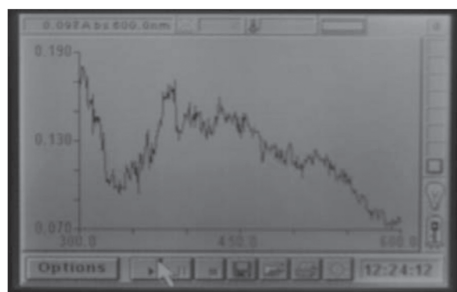


Fig. 4. UV-vis absorption spectrum of silver nanoparticles after 22hrs of the reaction

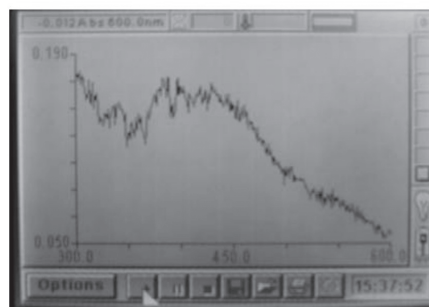


Fig. 7. UV-vis absorption spectrum of silver nanoparticles after 3hrs of the reaction

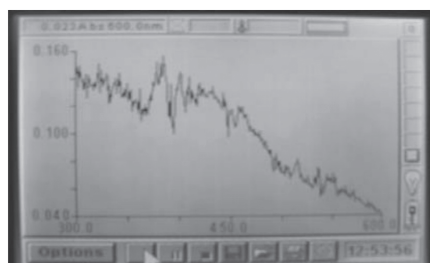


Fig. 5. UV-vis absorption spectrum of silver nanoparticles after 1hr of the reaction coriander

Conclusion

The silver nanoparticles having their applications in various fields, its synthesis from the plant systems is economically viable. An attempt has been made to study Sunflower and coriander leaf extracts which serves as a good source for synthesis of silver nanoparticles, which

Table 1. OD values taken at each interval for sunflower after 3 hrs

	300nm	400nm	500nm	600nm
Blank	0.003	-0.000	0.001	-0.000
Sample	0.023	0.017	0.010	0.002

Table 2. After 22hrs OD values taken at each interval for sunflower

	300nm	400nm	500nm	600nm
Blank	0.006	-0.014	-0.003	-0.002
Sample	0.024	0.020	0.019	0.004

Table 3. After 1hr OD values taken at each interval for Coriander

	300nm	400nm	500nm	600nm
Blank	0.011	0.002	0.012	0.003
Sample	0.124	0.088	0.064	0.025

Table 4. OD values taken at each interval for coriander after 2hrs

	300nm	400nm	500nm	600nm
Blank	0.006	-0.013	-0.006	-0.002

can be separated from the solution and used commercially.

Acknowledgments

We would like to express our thanks to HOD & Management, K L University for their support and encouragement and Ruska laboratories, Hyderabad for sample analysis.

References

1. Becker, R.O. (1999). Silver ions in the treatment of local infections. *Met Based Drugs*. 6: 297–300.
2. Senapati, S., Mandal, D., Ahmad, A., Khan, M.I, Sastry M and Kumar R. (2004). Fungus mediated synthesis of silver nanoparticles: a novel biological approach. *Indian J Phys*. 78: 101–105.
3. Leela, A and Vivekanandan M. (2008). Tapping the unexploited plant resources for the synthesis of silver nanoparticles. *African Journal of Biotechnology*, 7: 3162-3165.
4. Kumar, V and Yadav SK. (2008). Plant-mediated synthesis of silver and gold nanoparticles and their applications. *Journal of Chemical Technology & Biotechnology*, 84:151-157.
5. Armendariz,V., Herrera, I., Peralta Videa, JR., Jose-Yacaman, M., Troiani, H., Santiago, P and Gardea Torresdey, JL. (2004). Size controlled gold nanoparticle formation by *Avena sativa* biomass: use of plants in nanobiotechnology. *J Nanoparticle Res*. 6: 377–382.
6. Kuzma J. (2007). Moving forward responsibly: Oversight for the nanotechnology-biology interface. *Journal of Nanoparticle Research*. 9, 165–182.
7. Mohanpuria, P., Rana, NK and Yadav SK. (2008). Biosynthesis of nanoparticles: technological concepts and future applications. *J Nanopart Res*. 10: 507-517.
8. Ankamwar, B., Damle, C., Ahmad, A and Sastry, M. (2005). Biosynthesis of gold and silver nanoparticles using *Embllica officinalis* fruit extract, their phase transfer and transmetallation in an organic solution. *J. Nanosci Nanotechnol*, 5: 1665–1671.
9. Tokeshi, M and Baba Y. (2008). Nanotechnologies in the biosciences. *Anal Bioanal Chem*. 391, 2693–2694.
10. Chaudhary, M., Pasricha, R., Ahmad, A and Sastry M. (2006). Synthesis of gold nanotriangles and silver nanoparticles using *Aloe vera* plant extract. *Biotechnol Prog*. 22: 577–583
11. Gardea Torresdey, JL., Gomez, E., Peralta Videa, JR., Parson, JG., Troiani, H and Jose-Yacaman M. (2003). *Alfalfa* sprouts: a natural source for the synthesis of silver nanoparticles. *Langmuir*,19:1357–1361.
12. Narayanan, KB and Sakthivel N. (2008). Coriander leaf mediated biosynthesis of gold nanoparticles. *Materials Letters*. 62: 4588–4590.

Pyrosequencing- A Pioneer Technique of New Epoch

Rekha Khandia and Ashok Munjal*

Department of Genetics, Barkatullah University, Bhopal, 462026, India

*For Correspondence - ashokmunjal70@yahoo.co.in

Abstract

Sanger's dideoxy chain termination method was the widely used technology for DNA sequencing since its inception. However, the technique has its own limitations like it is costly, time consuming, labor intensive and faces the problem of clone biasness. Pyrosequencing has emerged as a novel sequencing technique, which offers potential advantages in terms of accuracy, cost effectiveness, flexibility, parallel processing, high throughput and further it can be easily automated. It can be widely accepted for the detailed characterization of nucleic acids. The technique is advantageous in DNA sequencing, genotyping, single nucleotide polymorphism analysis, allelic discrimination, allelic quantification and whole-genome sequencing. The technique may be broadly used in area of biotechnology, clinical genetics and pharmacogenetics. Due to efficacy and reliability, the technique may be used in the high-throughput analysis of bacterial and viral samples as well as metagenomic studies. Currently, the technique is the basis of next generation sequencing platform, offered by 454 Life Sciences as an array-based pyrosequencing technology.

Keywords : Pyrosequencing, real time PCR, diagnosis, luciferase, apyrase, emulsion PCR

Introduction

The sequencing of DNA molecules started with the development of chemical cleavage method of Maxam-Gilbert during 1970s (1) followed by di-deoxy chain termination method (2). However, the whole genome sequencing of the any organism was difficult and time

consuming task, hence leads to search for other alternatives. This has resulted in emergence of numerous sequencing methodologies, which can sequence about 2.8×10^6 base pairs/ day. Most of the modern technologies used for sequencing are modifications of Sanger's method. Ronaghi et al. (3) developed pyrosequencing, a simple technique analysing short to medium length DNA sequences. It can be used to analyse genetic variations like single-nucleotide polymorphisms (SNPs), determination of short sequence repeats (SSRs) and allelic imbalance in RNA, DNA methylation status and assessment of gene copy number (4). It is based on the principle "Sequencing by synthesis" (5). It is able to characterize diverse sequence populations with detection of low frequency variations efficiently. Highly sensitive mutational analysis like discovery of unknown mutations, quantification of alleles in mixed populations, characterization of contiguous and multivariable mutations can be performed. Its precision and accuracy provided with increased discriminatory power and sensitivity is pre-requisite of forensic analysis. This technique involves a cascade of enzymatic reactions; into which new strand is synthesized by addition of nucleotides and after each addition one pyrophosphate (PPi) is released. Because of the release of PPi (6), the reaction is called pyrosequencing. After each addition of nucleotide to the growing end, one PPi is released and visible light is generated, which is proportional to the number of incorporated nucleotides during synthesis of its complementary strand enzymatically (7).

The pyrosequencing completes in four stages: (i) amplification of target DNA by

emulsion PCR. In order to prepare DNA for sequencing, first genomic DNA is sheared mechanically or enzymatically and short oligonucleotide adapters are linked to the template DNA. To increase the copy number of target DNA, it is amplified in emulsion PCR, instead of cloning it in bacteriophage vector. In emulsion PCR, on the surface of agarose beads, short oligonucleotide primers, which have sequence complimentary to adapter sequence, is attached. Water in oil emulsion is prepared and concentration of template DNA is kept so that each micelle contains only one template strand. This micelle also contains the *Bst* polymerase and dNTPs. Thermal cycling of this water and oil micelle is called emulsion PCR. Breaking of this micelle releases millions of copy of template DNA, ready to be sequenced. (ii) Bead containing template on its surface is deposited in the picotiter microwell (iii) Immobilized enzymes (ATP sulphurylase, luciferase, apyrase and DNA polymerase) are also deposited and subjected to thermal cycling (iv) the pyrosequencing reaction takes place, in which, complementary strand is synthesized using enzymes and other substrates present in reaction mixture, It result in pyrogram, a collection of signal peaks, corresponding to the nucleotide incorporated (8). For detection of pathogen from clinical samples, the technique is rapid and reliable. It is having important role during diagnosis, treatment and prophylactic measurements. Considering the various uses of pyrosequencing, in present article the technique is discussed in detail with elaborating its uses.

Pyrosequencing technique is based on sequencing-by-synthesis principle (9, 10). The method is based on the sequencing of single stranded DNA and now-a-days sequencing of double stranded DNA is also possible (11). The detection system is based on finding of released PPI during the strand synthesis. The primer is hybridized with single-stranded DNA template and mixed with adenosine -5'- phosphosulphate (APS), luciferin and the enzymes; DNA polymerase, ATP sulphurylase, luciferase and

apyrase (12). Sequentially the solutions of A, C, G and T nucleotides are added and removed by apyrase. During the polymerization step, one nucleotide is added by DNA polymerase and simultaneously PPI is released in a ratio proportional to the incorporated nucleotide. The PPI released is now converted to ATP by ATP sulphurylase enzyme in the presence of APS. The resulting ATP provides the energy and drives the luciferase enzyme mediated luciferin to oxyluciferin conversion, and visible light is detected. This light signal may be recorded using a photomultiplier or charge coupled device (CCD) camera. The detected signal is observed as a peak of signal in the pyrogram and the peak is analogous to electropherogram in dideoxy sequencing. Apyrase enzyme cleaves remaining ATP and non-incorporated dNTPs from the reaction mixture. Usually a time lapse of 65 seconds is kept between a nucleotide dispensation (5). Apyrase enzyme is added to remove unused dNTP without in between washing step. The enzyme is strong catalyst and even in low quantities, it efficiently degrades the unincorporated nucleosides triphosphates to diphosphates and further diphosphates to nucleoside monophosphate. Apyrase is resistant to accumulation of end products in comparison to other nucleotide-degrading enzymes (7). During pyrosequencing, detection of false signals also occurs, when dATP was added into the pyrosequencing solution since dATP is a substrate for luciferase. The problem was resolved by addition of dATP α S instead of dATP in the polymerization reaction (13). dATP α S, being inert for luciferase, can be incorporated efficiently by all DNA polymerases tested leading to successful use of the strategy for sequencing of PCR-generated DNA material.

Pyrosequencing modus operandi

1. Preparation of DNA template

Solid phase template preparation and enzymatic template preparation are the methodologies used for generating primed DNA template for pyrosequencing. Streptavidin-coated magnetic beads are

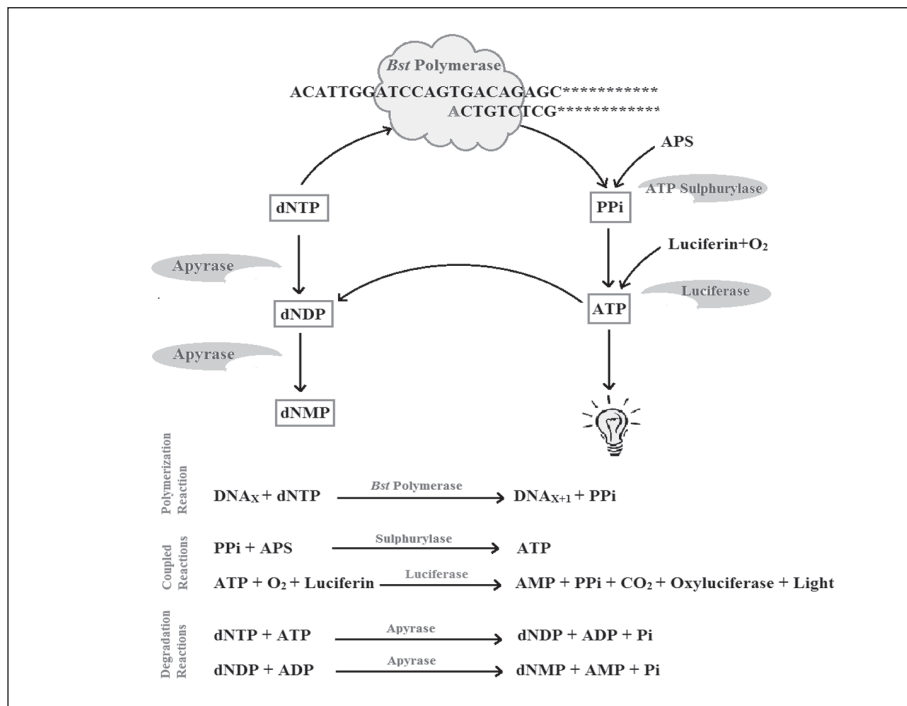


Fig. 1: Pyrosequencing; schematic illustration with concerned enzymatic reactions.

used to prepare primed DNA template in solid-phase template preparation. Template preparation by such system provides superior quality sequence data with less background signals. The template may be further purified by ethanol precipitation followed by alkali denaturation to yield ssDNA. Exonuclease I and a nucleotide-degrading enzyme are used in enzymatic template preparation method. Post-amplification exonuclease I degrades the unused PCR primers and nucleotide-degrading enzyme removes the nucleotides. Enzymatic template preparation method is used to sequence double-stranded DNA template (11).

2. Polymerization step

The synthesis of new strand includes the hybridization of DNA template with primer, which is further extended by polymerase enzyme. The nucleotides dATP, dTTP,

dCTP, dGTP are added sequentially, if the added nucleotide is complimentary to the base in template strand, it is incorporated in the growing strand and PPI is released (14).

3. Enzymology of pyrosequencing

The activity of following enzymes is crucial for the precision of this DNA sequencing technology:

- (i) DNA polymerase- In pyrosequencing, generally *Bst* DNA Polymerase, obtained from *Bacillus stearothermophilus* containing the 5' → 3' polymerase activity but lacking 5' → 3' exonuclease activity is used for incorporating the nucleotides in complimentary strand.
- (ii) ATP sulfurylase: The enzyme is member of transferase family. ATP Sulfurylase catalyses formation of ATP from adenosine 5'-phosphosulphate (APS) and pyrophosphate (PPI).

- (iii) Luciferase: Firefly luciferase is a euglobulin protein and it induces oxygenation of luciferin to yield oxyluciferin using molecular oxygen and ATP. It is a two step process; in first step luciferin is adenylated and luciferase acts as an oxygenase on adenyl-luciferin complex producing oxyluciferin and carbon dioxide. The resultant, oxyluciferin is a unstable, excited compound producing photon of light upon reaching to its ground state. The amount of generated light is equal to the proportion of ATP generated.
- (iv) Apyrase enzyme continuously degrade unincorporated nucleotides and ATP

The light generated through enzyme coupled reaction, is captured and recorded and converted to electrical signal by a charge coupled device (CCD) camera and each signal is depicted as a peak in electric pyrogram. A computer generated software couple the signal and the nucleotide addition at particular moment and thus the signals are converted to a nucleotide sequence. The height of each light signal is proportional to the number of nucleotides incorporated. During recent years, deoxyadenosine alfa-thio triphosphate (d α ATPS) is substituted for the natural deoxyadenosine triphosphate (dATP). d α ATPS, instead of dATP is used as it does not serve as energy for luciferase enzyme and also used by polymerase efficiently. As the sequencing process proceeds, signal peaks are generated in program. The ascending slope of curve shows the activities of DNA polymerase and ATP sulfurylase, the height indicates the activity of luciferase and descending slope exhibits the nucleotide degradation.

Applications of pyrosequencing

For detailed study and characterization of any organism, it is essential to elucidate the nucleotide sequence of its genome. Pyrosequencing has opened up new avenues for performing sequence-based DNA analysis. Since it has proven its efficacy in surveillance of emerging drug-resistant pathogens of human and

animal origin (15). Currently this method is widely used in many fields such as classifying single nucleotide polymorphism (16), identification of bacteria and viruses (17), fungal and viral typing (18-19), difficult secondary DNA structure sequence determination (13), mutation detection (20), clone scrutiny (21) and DNA/RNA methylation analysis (22-24).

a) DNA methylation analysis: DNA methylation is considered as an important epigenetic modification. A methyl group is added to cytosine and adenine nucleotides, where it repress the gene transcription and also associated with several important cellular processes like genomic imprinting, X-chromosome inactivation, aging and carcinogenesis. Anomalous methylation of specific genes has been directly linked with the activation of proto-oncogene, tumor response to chemotherapy and patient survival (25). Thus, a quantitative measurement of DNA methylation can give estimate about the magnitude of developmental and pathological disorders. Among eukaryotes, methylation generally takes place at CpG island, where cytosine is immediately followed by guanine residue. Quantification of methylation can be done in this CpG island area (26). DNA methylation pattern may be linked to the tumor type and abnormal gene expression pattern and cellular response to demethylating agents. Assessment of methylation pattern changes, with regards to tumorigenesis, genetic imprinting, and exposure to environmental toxins may provide an insight for developing therapeutics against methylation associated disorders. DNA methylation is also found to be associated with alteration in organism behavior. A DNA methylation level at the Dopamine Receptor D4 (DRD4) gene is statistically associated with personality and behavioral traits in both humans and non-human animals. Such epigenetic traits are considered to control the behavior. Variation in methylation level is detected to bring behavioral changes in Great tit (*Parus major*) birds by pyrosequencing technique (27).

b) Study of microbial community: At present thousands of organisms have been sequenced. The sequence elucidate about their virulence, metabolism, mode of infection and potential targets for antimicrobial agents as well. Pyrosequencing technique has emerged out as an excellent diagnostic tool for detection and identification of microbial community. Generally for detection purpose, DNA markers present in both the conserved as well as variable regions are targeted. The bacterial strains are usually identified by sequencing the 16S rRNA gene. The 16S rRNA gene (16S rDNA) is having highly conserved regions flanked by variable and species specific sequences, signature to one specific organism (28). 16S rRNA sequencing is also used to distinguish pathogenic bacteria from commensals to saprophytic bacteria, present in the same habitat and identification of contaminating bacteria in industrial waste water systems (29). The technique is also used for typing fungal isolates, obtained from clinical cases of immune-compromised patients. On the basis of observation of sequencing data, it was found that 18 to 32 bases are sufficient for discriminate between *Candida tropicalis*, *C. albicans*, *C. krusei*, *C. parapsilosis*, *C. glabrata*, and *Aspergillus spp* (23). A combination of multiplex real-time PCR and pyrosequencing detected the presence of *Bacillus anthracis* in milk, apple juice, and bottled water by targeting pXO1 and pXO2 plasmids and genomic DNA (30). Barcoded pyrosequencing for 16S rDNA has helped in providing the insight into the presence of bacterial communities in faecal microbiota of diarrhea affected population (31).

c) Detection of viral pathogens: Molecular biology is largely dependent on sequencing techniques for a variety of application like determination of genetic variance within and among populations, pathogen testing and typing and determination of resistance. Since pyrosequencing is a robust, accurate, quantitative, and cost effective technique, providing real time data, increasingly it is becoming a standard laboratory technique. Several diagnostics tests have been developed

for detection of important animal/bird's diseases like rabies, new castle diseases, avian influenza etc. Rabies is a fatal zoonotic disease caused by rabies virus, a member of Rhabdoviridae family and Lyssavirus genus. Sometimes rabies related lyssavirus also cause endemic in human population; therefore, it is pre-requisite to develop a reliable molecular detection module for differential diagnosis of rabies from the rabies related lyssaviruses. The target may be achieved by targeting the 3' terminus of the nucleoprotein (N) gene developed for rapid characterization of lyssaviruses in pyrosequencing protocol (32). For detecting molecular markers responsible for resistance to M2 ion-channel blockers and for NA inhibitors in influenza A H5N1, H7N9 viruses Pyrosequencing may be used (33, 34). Its combination with RT-PCR techniques, provides rapid, reliable, high-throughput and cost-effective screening of NA inhibitor-resistant influenza A viruses of subtype H1N1, H3N2 and H5N1 (35). Due to the increasing diversity among H5N1 viruses due to antigenic shift and drift, pyrosequencing RT-PCR is a powerful tool to distinguish viruses belonging to the different HA clades. The same may be achieved by amplifying the specifically variable region of the HA gene (36). New castle disease causes respiratory and neurological ailment in birds and lead to substantial economic losses. NDV viruses are different in pathogenicity, and hence only detection in any specimen is not sufficient to provide exact information regarding the pathogen, hence assessment of virus pathotype is required. Pyrosequencing based Real time PCR has been developed for rapid and reliable detection and pathotyping of NDV virus. The results obtained from pyrosequencing are high quality, rapid and cost-efficient and generate ample sequencing data in comparison to the classical procedures based on chain termination method. These qualities make pyrosequencing a dependable choice as diagnostic tool for NDV virus (37).

d) Resequencing: Those genes, which are associated with mutations, can be resequenced and resequencing for scanning of mutations can

be important application of pyrosequencing. Resequencing gives longer read length than *de novo* sequencing because here the supply of nucleotide may be specified as per previously generated program and mutation at specific site may be reconfirmed (5). The same strategy has been used for resequencing of the p53 tumor suppressor gene, where mutations in the gene were effectively determined and quantified (38). In resequencing, for sequencing a homopolymeric region, a single nucleotide may be added several times as per the signal of previous pyrogram.

e) Genetic testing of polymorphism: Flexibility in primer placement in the pyrosequencing offers an opportunity to assess virtually all genetic markers. All sequence information like short tandem repeats, insertion and deletions, SNPs, and variable gene copy number can be deduced in a single run.

Advantages of pyrosequencing over Sanger's method

Pyrosequencing is an alternative to the conventional Sanger method. It was first developed at the KTH Royal Institute of Technology, Sweden. Its several advantages like rapidity, reliability, flexibility, ease-of-use and real time data visualization makes it a favoured research tool. In pyrosequencing, the fluorescence signals are converted into nucleotide sequence and there is no requirement of manual reading as in case of Sanger's method of sequencing there is requirement of reading electropherogram. It is faster and cheaper technique where DNA is sequenced by method generally called as "sequencing by synthesis". It avoids the use of expensive and hazardous incorporation of labeled primers or labeled nucleotides. Unlike Sanger sequencing, where a gap of at least 20-30 bases from the sequencing primer occurs, pyrosequencing generates the data immediately downstream the sequencing primer (5). Sample preparation process is relatively fast and consumes only 15 minutes opposing to Sanger sequencing, where it may take upto 4 h including lengthy time periods

for PCR cleanup, cyclic amplification and dye cleanup. The greatest advantage is that pyrosequencing generate hundreds of thousands of sequence reads in a single run generating larger magnitude of data.

454 GS FLX Titanium pyrosequencing based system was developed having capacity to read up to 700 bp with 99.9% accuracy. Nowadays it is possible to obtain up to 14 gigabase data per run (39), with the advantage of completion of run within 10 hours (40). Pyrosequencing technique avoids the bias inherent to the cloning procedure and directly the DNA can be sequenced without further steps of genomic shearing followed by cloning and subsequent procedures. In the pyrosequencing method, using the barcoding multiplex approach, in which unique sequences are incorporated into the primers and barcoded amplicons are generated, sequences from different samples can be identified in the same run (41). Multiplexing increase the throughput and efficiency, and cost per data obtained is reduced (42). The technique has shown its efficacy in analysis of polymorphic DNA. This is used in determining the allelic frequency of any gene in any given population. Though the technology has formed the basis of one of the Next Generation Sequencing platform and there are possibilities of improvement in technique to make it more useful (7).

Disadvantages of pyrosequencing

Although pyrosequencing is a popular sequencing technique, however the method has some limitations too. It may encounter the problem, when a long stretch of homopolymer is available. Such error may misinterpret as rare operational taxonomic unit (OTU) (43). Several new strategies are employing now to combat these noises (44). In homopolymeric regions, nonlinear light response is generated followed by incorporation of 5-6 similar dNTPS. This leads to difficulty in determining the actual number of nucleotide incorporated. Excessive research has indicated incorporation of 10 identical adjacent nucleotide due to apyrase. However specific

software algorithms should be utilized to prevent such errors (45). Short read length is also a limitation of this techniques as some bacteria need full 1.6 kb sequencing of 16S rRNA gene to be reliably identified, however generally near about 500 bp sequencing is considered to be sufficient for distinguishing large number of bacteria (46).

Conclusion

Pyrosequencing is a newly emerging technique used in Next Generation Sequencing platforms. It can generate about 400 Mb data in a 10 hr run in a single machine. It is a useful technique, currently being used for generating high throughput sequencing data, allelic discrimination; SNP detection and pathogen detection, metagenome study and in future several enhancements in the technique may be useful in increasing its applicability in emerging areas of science.

Acknowledgments

Financial assistance from DBT Builder Programme is gratefully acknowledged.

References

1. Maxam, A.M. and Gilbert, W. (1977). A new method for sequencing DNA. *Proceedings of the National Academy of Sciences*, 74:560–4.
2. Sanger, F., Nicklen, S., Coulson, A.R. (1977). DNA sequencing with chain-terminating inhibitors. *Proceedings of the National Academy of Sciences*, 74: 5463-5467.
3. Ronaghi, M., Karamohamed, S., Pettersson, B., Uhlen, M., Nyren, P. (1996). Real-time DNA sequencing using detection of pyrophosphate release. *Analytical Biochemistry*, 242: 84-89.
4. Sharon, M. (2007). *Pyrosequencing Protocols (Methods in Molecular Biology)*; 373 Humana Press.
5. Fakruddin, M.D. and Chowdhury, A. (2012). *Pyrosequencing- An Alternative to Traditional Sanger Sequencing*. *American Journal of Biochemistry and Biotechnology*, 8 (1): 14-20.
6. Ahmadian, A., Ehn, M., Hober, S. (2006). *Pyrosequencing: History, biochemistry and future*. *Clinica Chimica Acta*, 363:83-94.
7. Ronaghi, M. (2001). *Pyrosequencing sheds light on DNA sequencing*. *Genome Research*, 11: 3-11
8. Clarke, S.C. and Diggie, M.A. (2004). *Pyrosequencing: Sequence typing at the speed of light*. *Molecular Biotechnology*, 28: 129-138.
9. Melamede, R.J. (1985). *Automatable process for sequencing nucleotide*. United States Patent 4863849.
10. Hyman, E.D. (1988). *A new method of sequencing DNA*. *Analytical Biochemistry*, 174: 423-436.
11. Nordstrom, T., Ronaghi, M., Forsberg, L., de Faire, U., Morgenstern, R., Nyren, P. (2000). *Direct analysis of single-nucleotide polymorphism on double-stranded DNA by pyrosequencing*. *Biotechnology and Applied Biochemistry*, 31: 107–112.
12. Gharizadeh, B., Ghaderi, M., Nyren, P. (2007). *Pyrosequencing technology for short DNA sequencing and whole genome sequencing*. *Technology*, 47:129-132.
13. Ronaghi, M., Nygren, M., Lundeberg, J., Nyren, P. (1999). *Analyses of secondary structures in DNA by pyrosequencing*. *Analytical Biochemistry*, 267: 65-71.
14. Agah, A., Aghajan, M., Mashayekhi, F., Amini, S., Davis, R.W., Plummer, J.D., Ronaghi, M., Griffin, P.B. (2004). *A multi-enzyme model for pyrosequencing*. *Nucleic Acids Research*, 32(21): e166.
15. Bright, R.A., Medina, M.J., Xu, X.Y., et al. (2005). *Incidence of adamantane resistance among influenza A (H3N2) viruses isolated worldwide from 1994: a cause for concern*. *Lancet*, 366: 1175–1181.

16. Hossein, F.R., Nader, P., Ronaghi, M. (2002). Pyrosequencing: An accurate detection platform for single nucleotide polymorphisms. *Human Mutation*, 19(5): 479-485.
17. Jonasson, J., Olofsson, M., Monstein, H.J. (2002). Classification, identification and subtyping of bacteria based on pyrosequencing and signature matching of 16S rDNA fragments. *acta pathologica, microbiologica, et immunologica Scandinavica*, 110: 263–272.
18. Gharizadeh, B., Kalantari, M., Garcia, C.A., Johansson, B., Nyren, P. (2001). Typing of human papillomavirus by pyrosequencing. *Lab Investigation*, 81: 673-679.
19. Gharizadeh, B., Oggionni, M., Zheng, B., Akom, E., Pourmand, N., et al. (2005). Type-specific multiple sequencing primers: A novel strategy for reliable and rapid genotyping of human papillomaviruses by pyrosequencing technology. *Journal of Molecular Diagnostics*, 7: 198-205.
20. Ahmadian, A., Lundeberg, J., Nyren, P., Uhlen, M., Ronaghi, M. (2000). Analysis of the p53 tumor suppressor gene by pyrosequencing. *Biotechniques*, 28:140-147.
21. Nourizad, N., Ehn, M., Gharizadeh, B., Hober, S., Nyren, P. (2003). Methylotrophic yeast *Pichia pastoris* as a host for production of ATPdiphosphohydrolase (apyrase) from potato tubers (*Solanum tuberosum*). *Protein Expression and Purification*, 27: 229-237.
22. Neve, B., Froguel, P., Corset, L., Vaillant, E., Vatin, V., Boutin, P. (2002). Rapid SNP allele frequency determination in genomic DNA pools by pyrosequencing. *Biotechniques*, 32: 1138-1142.
23. Gharizadeh, B., Ohlin, A., Molling, P., Backman, A., Amini, B., Olcen, P., Nyren, P. (2003a). Multiple group-specific sequencing primers for reliable and rapid DNA sequencing. *Molecular and Cellular Probes*, 17: 203-210. PMID:12944124.
24. Gharizadeh, B., Zheng, B., Akhras, M., Ghaderi, M., Jejelowo, O., et al. (2006). Sentinel-base DNA genotyping using multiple sequencing primers for high-risk human papillomaviruses. *Molecular and Cellular Probes*, 20: 230-238.
25. Costello, J. and Plass, C. (2001). Methylation matters. *Journal of Medical Genetics*, 38(5): 285–303.
26. Colyer, H.A.A., Armstrong, R.N., Sharpe, D.J., Mills, K.I. (2012). Detection and Analysis of DNA Methylation by Pyrosequencing. *Methods in Molecular Biology*, 863: 281-292.
27. Oers, K.V., Verhulst, E.C., Mateman, C.A., Zwier, M.V., Caro, S.P., Verhoeven, K.J.F. (2015). Evidence from Pyrosequencing indicates that natural variation in animal personality is associated with DRD4 DNA methylation. *Molecular Ecology- special issue on Epigenetic Studies in Ecology and Evolution*.
28. McCabe, K.M. (1995). Amplification of bacterial DNA using highly conserved sequences: automated analysis and potential for molecular triage of sepsis. *Pediatrics*, 95:165–9.
29. Tewari, D., Cieply, S., Livengood, J. (2011). Identification of bacteria recovered from animals using the 16S ribosomal RNA gene with pyrosequencing and Sanger sequencing. *Journal of Veterinary Diagnostic Investigation*, 23(6):1104-1108
30. Janzen, T.W., Thomas, M.C., Goji, N., Shields, M.J., Hahn, K.R., Amoako, K.K. (2015). Rapid detection method for *Bacillus anthracis* using a combination of multiplexed real-time PCR and pyrosequencing and its application for food biodefense. *Journal of Food Protection*. 78(2):355-61.
31. Rodriguez, C., Taminau, B., Brévers, B., Avesani, V., Broeck, J.V., Leroux, A., Gallot, M., Bruwier, A., Amory, H., Delmée, M., Daube, G. (2015). Faecal microbiota

- characterisation of horses using 16 rdna bar-coded pyrosequencing, and carriage rate of *Clostridium difficile* at hospital admission. *BMC Microbiology*, 15:181,1-14
32. Bnedictis, P.D., Battisti, C.D., Dacheux, L., Marciano, S., Ormelli, S., Salomoni, A., Caenazzo, S.T., Lepelletier, A., Bourhy, H., Capua, I., Cattoli, G. (2011). Lyssavirus Detection and Typing Using Pyrosequencing. *Journal of Clinical Microbiology*, 49(5): 1932-1938
33. Deyde, V.M., Tung, N., Bright, R.A., et al. (2009). Detection of molecular markers of antiviral resistance in influenza A (H5N1) viruses using a pyrosequencing method. *Antimicrobial Agents and Chemotherapy*, 53(3):1039–1047.
34. Lackenby, A., Democratis, J., Siqueira, M.M., Zambon, M.C. (2008). Rapid quantitation of neuraminidase inhibitor drug resistance in influenza virus quasispecies. *Antiviral therapy*, 13(6):809–820.
35. Duwe, S. and Schweiger, B. (2008). A new and rapid genotypic assay for the detection of neuraminidase inhibitor resistant influenza A viruses of subtype H1N1, H3N2, and H5N1. *Journal of Virological Methods*, 153(2):134-41.
36. Ellis, J.S., Smith, J.D., Braham, S., Lock, M., Barlow, K., Zambon, M.C. (2007). Design and validation of an H5 TaqMan real-time one-step RT-PCR and confirmatory assays for detection and verification of influenza A H5 infections in humans. *Journal of Clinical Microbiology*, 45(5):1535–1543.
37. De Battisti, C., Salomoni, A., Ormelli, S., Monne, I., Capua, I., Cattoli, G. (2013). Rapid pathotyping of Newcastle Disease Virus by pyrosequencing. *Journal of Virological Methods*, 188(1-2):13-20.
38. Garracia, C.A., Ahmadian, A., Gharizadeh, B., Lundeberg, J., Ronaghi, M., Nyren, P. (2000). Mutation detection by pyrosequencing: Sequencing of exons 5-8 of the p53 tumour suppressor gene. *Gene*, 253: 249-257.
39. Huse, S. M., Huber, J.A., Morrison, H.G., Sogin, M.L., Welch, D.M. (2007). Accuracy and quality of massively parallel DNA pyrosequencing. *Genome Biology*, 8: 7 article R143
40. Engelbrektson, A., Kunin, V., Wrighton, K.C., Zvenigorodsky, N., Chen, F., Ochman, H., Hugenholtz, P. (2010). Experimental factors affecting PCR-based estimates of microbial species richness and evenness. *The ISME Journal*, 4:642–647.
41. Tringe, S.G. and Hugenholtz, P. (2008). A renaissance for the pioneering 16S rRNA gene. *Current Opinion in Microbiology*, 5:442-6.
42. Parameswaran, P., Jalili, R., Tao, L., Shokralla, S., Gharizadeh, B., Ronaghi, M., Fire, A.Z. (2007). A pyrosequencing-tailored nucleotide barcode design unveils opportunities for large-scale sample multiplexing. *Nucleic Acids Research*, 35(19):e130.
43. Siqueira, J.F., Fouad, A.F., Rôças, I.N. (2012). Pyrosequencing as a tool for better understanding of human microbiomes. *Journal of oral microbiology*, 4: 10.3402/jom.v4i0.10743.
44. Reeder, J. and Knight, R. (2010). Rapidly denoising pyrosequencing amplicon reads by exploiting rank-abundance distributions. *Nature Methods*, 7(9):668-9.
45. Fakruddin, R.M.M., Mazumdar, R.M., Chowdhury, A., Hossain, N., Mahajan, S., Islam, S. (2013). Pyrosequencing-A Next Generation Sequencing Technology. *World Applied Sciences Journal*, 24 (12):1558-1571.
46. Clarridge, J.E. (2004). Impact of 16S rRNA gene sequence analysis for identification of bacteria on clinical microbiology and infectious diseases. *Clinical Microbiology Review*, 17(4):840-62.

NEWS ITEM

SCIENTIFIC NEWS

India was part of Antarctica billions years ago:

Geologists have found evidence supporting the hypothesis that Indian subcontinent was part of Antarctica a billion years ago but were separated and re-united several times due to tectonic movement of plates before the evolution of mankind. A group of geologists from India and Switzerland researching on evolution of the Earth's crust studied ancient rocks of the continental crust in the Eastern Ghats area and found important clues to the formation of the continents. "It is for the first time that we have been able to prove the hypothesis that the continent of Antarctica and subcontinent India were once a single large continent that broke apart about 1.5 billion years ago," the group of geologists from IIT Kharagpur, who led the research. India and Antarctica then got separated by an ocean. "This ocean closed again with the movement of the landmasses and the two continents approached each other until they collided again around one billion years ago to form the Eastern Ghats mountain belt," they said.

Indian American's start-up 'Moon Express': In a first, the Federal Aviation Administration has given license to a private US company, co-founded by an Indian American, to launch a spacecraft and land on moon in 2017. This breakthrough US policy decision provides authorisation to Moon Express for a maiden flight of its robotic spacecraft onto the Moon's surface, the company said in a media release.

There have been no private space missions so far beyond Earth's orbit and only state agencies have performed outer space missions. "The sky is not the limit for Moon Express, it is the launchpad. Space travel is our only path forward to ensure our survival and create a limitless future for our children," The researchers said "In the immediate future, we envision bringing precious resources, metals, and moon rocks back to earth,"

The federal interagency's approval of the Moon Express 2017 lunar mission establishes an important precedent for the private sector to engage in peaceful space exploration, bringing with it monumental implications for the advancement of technology, science, research, and development, as well as commercial ventures that expand Earth's economic sphere, the company said.

Zebra fish gives a new hope to fight the rare human disease: Scientists from the Delhi-based

CSIR-Institute of Genomics and Integrative Biology are a step closer to bringing hope to children born with a rare disorder — CHARGE syndrome — if the results seen in zebrafish are reproducible in humans. The results of a study were published on July 13 in the Journal Human Molecular Genetics. About 1 in 20,000 people in the world, and an estimated 50,000 in India alone, are born with CHARGE syndrome — multiple life-threatening problems such as deafness and blindness, heart defects, genital problems and growth retardation and facial bone and nerve defects that cause breathing and swallowing difficulties. There is a high death rate in the very first year in children born with CHARGE. A mutation in the CHD7 gene is responsible for 60-70 per cent of all CHARGE defects. The expression of the gene peaks in the early stages of embryo development, starting from 2-4 cells. The team from IGIB studied the fertilised egg of a zebrafish to better understand the CHARGE syndrome. Following fertilization, zebrafish embryos are transparent. This allows scientists to observe the inside of the embryo and watch in real time how various organs develop. Since most organs begin forming in the first 24-36 hours and are fully formed within five days, it allows researchers to study the development of an organism from egg to maturity. An RNA injected into a one-cell embryo interferes with the making of the CHD7 protein, thus producing a zebra fish embryo with very similar problems as the human babies with CHARGE syndrome. The researchers found that the CHD7 protein causes CHARGE syndrome by modifying a second gene — sox10. "They mentioned that they found more sox10 protein. So if the CHD7 mutation was producing more sox10 protein, we wanted to know if we can reduce the defects by reducing the amount of sox10 protein" they said.

Nanoparticles bundles a giant medicinal punch in green tea: It is well known that green tea has many superior medical benefits — antibacterial activity, offers protection against many types of cancer, has anti-diabetic, and anti-inflammatory properties, to name a few. But all these benefits have been based on studying the infusion that is got when the tea bags are dipped into hot water for about 3-4 minutes to allow the active components seep into the water. But a study published in January 2016 in the journal Scientific Reports has gone beyond studying the infusion and found the answers to what renders the green tea its medicinal properties. The researchers looked at the tiny particles suspended in the tea

infusion to understand if these particles played a positive or negative role in the well established bioactivity of green tea. "After seeping a bag of green tea we can always find fine particles suspended in the tea infusion. These fine particles are of three different sizes — macro, micro and nano. This raised the curiosity to probe the role of those particles in the green tea effect, and they studied the suspended particles by assessing its antibacterial activity against oral microflora. The reason for picking oral microflora to test the effectiveness of the suspended particles is because the oral microflora are the first to come in contact with green tea in the mouth. Also, green tea is known to prevent dental caries. The antibacterial activity seen in green tea comes from catechins, phenolics, flavonoids, with catechins playing a predominant role compared with the other two. The researchers studied the effect of all three sizes of suspended particles for their antibacterial properties and found that the higher the epigallocatechin gallate or EGCG (the major bioactive ingredient in green tea) content the better the antibacterial effect against the oral microflora.

A kind of Culex mosquito can also spread Zika:

The public Brazilian laboratory Fundacion Oswaldo Cruz (Fiocruz) announced that researchers found the presence of the Culex quinquefasciatus mosquito infected by the Zika virus in three out of 80 groups of mosquitoes analysed up until now. The 80 groups were from the metropolitan area of Recife, regional capital of Pernambuco in the northeast. In two samples it was detected that the mosquitoes were not fed which showed the virus was spread in the insect's organism without being transmitted in a feed recently infected by Zika. Up until now, transmission of the virus was only known through the Aedes aegypti mosquito, the same insect that spreads dengue and chikungunya. The Culex quinquefasciatus is known in Brazil as the domestic mosquito and in Recife, where the majority of Zika cases in the country have been registered, the population of this mosquito is estimated to be 20 times larger than that of the Aedes aegypti. "The current study is very relevant since the control measures of the vectors are different," according to researchers of Fiocruz laboratory while ensuring that the risk of contagion during the upcoming Olympic Games in Rio de Janeiro is very low.

Novel cereal varieties to check green house gases developed by scientists:

A team of researchers from India and the United Kingdom have come together to develop new cereal crop varieties that use nitrogen efficiently, thereby reducing greenhouse emissions and making agriculture more profitable and sustainable. The partnership will explore natural

variations of cereals and basic research in model plants to deliver new varieties of cereals with enhanced nitrogen use efficiency. With funding of £10 million (GBP) through the Newton Bhabha Fund, UK; Biotechnology and Biological Research Council (BBSRC), UK; and the Department of Biotechnology (DBT) of the Government of India, four new Virtual Joint Centers in Agricultural Nitrogen will be created. These are delivered in partnership with BBSRC, the Natural Environment Research Council (NERC) and the DBT. The Centers comprise of multiple research organizations in India and the UK, with each center receiving a co-investment of approximately £2.5M, said an official statement from International Crops Research Institute for the Semi-Arid Tropics (ICRISAT). The Cambridge-India Network for Translational Research in Nitrogen (CINTRIN), one of the four centres, is led by the National Institute of Agricultural Botany (NIAB) in the UK and the ICRISAT in India. It also brings together the Department of Plant Sciences and Sainsbury laboratory, University of Cambridge, the Punjab Agricultural University (PAU), the National Institute of Plant Genome Research (NIPGR), India, ADAS UK Ltd. and agri-IT specialist KisanHub.

'Guided chemotherapy missiles' as a novel way to fight cancer cells:

Scientists have engineered novel proteins that work like 'guided missiles' which seek out cancer cells and deliver chemotherapy drugs to treat hard-to-reach tumours without harming healthy cells. Although chemotherapy drugs do often effectively kill cancer cells, they also damage other quickly dividing cells in the body, causing side effects ranging from cosmetic, like hair loss, to disabling. Sometimes, the drug dose needed to kill a tumour may be more than what a person's body can handle. This might happen if the tumour does not have much of a blood supply and very little of the drug, which is delivered through the bloodstream, can get in. A dose high enough to infiltrate the tumour could be deadly to other cells in the body. Some recently approved therapies get around this problem using antibodies to deliver a drug directly to tumours, bypassing healthy cells and possibly overcoming some of the uglier aspects of cancer chemotherapy.

Researchers at Stanford University has built on this antibody approach using an engineered protein rather than an antibody to direct the drug to the tumour. Although the two techniques are conceptually similar, the specialized protein has the potential advantage of being able to pass through the barrier that protects the brain, thereby being able to treat brain tumours. It is also smaller than the antibody and might be able to reach dense tumours with little blood supply.

SCIENTIFIC INVENTIONS

Digital information can be stored in DNA scientists

worked out: The Scientists aim to help companies and institutions archive huge amounts of data for decades or centuries, at a time when the world is generating digital data faster than it can store it. Technology moves on, and data can't be retrieved if the means to read it is no longer available. So for that and other reasons, long-term archiving requires repeatedly copying the data to new technologies. The difference between DNA and digital devices into this world comes the notion of DNA storage. DNA is by its essence an information-storing molecule in the form of four-letter DNA code. That really refers to sequences of four building blocks abbreviated as A, C, T and G found in the DNA molecule. Specific sequences give the body directions for creating particular proteins. Digital devices, on the other hand, store information in a two-letter code that produces strings of ones and zeroes. A capital 'A', for example, is 01000001. How to convert from digital to DNA? Converting digital information to DNA involves translating between the two codes. In one lab, for example, a capital A can become ATATG. The idea is once that transformation is made, strings of DNA can be custom-made to carry the new code, and hence the information that code contains. Major advantage embodies is its durability. Scientists can recover and read DNA sequences from fossils of Neanderthals and even older life forms. So as a storage medium, "it could last thousands and thousands of years," the researchers from University of Washington, who works with Microsoft on DNA data storage, says accordingly.

OPPORTUNITIES

CSIR-Nehru Science Postdoctoral research Fellowship Scheme: CSIR-Nehru Science Postdoctoral research Fellowship Scheme, has been instituted to identify promising young researchers with innovative ideas and provide them with training and research opportunities in niche areas of basic science, engineering, medicine and agriculture. Mode of selection: Eligible candidates can apply in the prescribed format, available on the website: www.csirhrdg.res.in, any time of the year. However, the selections will be made twice a year, in the months of June and December

International Centre for Theoretical Science, Tata Institute of Fundamental Research (ICTS-TIFR) post doctoral fellowships: Invites applications from

highly motivated candidates for postdoctoral positions. ICTS also has an active in-house research program. Current research spans the areas of astrophysical relativity, biophysics, statistical physics and turbulence, interdisciplinary and applied mathematics, condensed matter physics and string theory. Other areas under consideration are cosmology, multiscale and complex systems including interfaces with theoretical biology, mathematics, computer science and computational sciences with strong interface to other research areas at ICTS. Interested candidates apply online-https://www.icts.res.in/postdoctoral_fellowships. Applications will be normally reviewed twice every year, once in December (deadline for application: 15 December) and once in July (deadline for application: 15 June). Applications received after the deadline may also be considered

ICMR CENTENARY -Post Doctoral Research Fellow (Scheme):

ICMR Postdoctoral Research Fellowship Scheme is being instituted to foster high quality research opportunities to promising fresh PhD/MD/MS holders in the cutting edge areas of basic science, communicable and non communicable diseases, and reproductive health including nutrition at ICMR Institutes /Centers. Selection of the "ICMR Centenary Postdoctoral Research Fellows" will be made through interview of short listed candidates by specially constituted Committees by Director General based on their publications, citation and its impact factor. Selection will be made twice in a year and this will be 31st December and 30th June every year. All correspondence pertaining to "ICMR CENTENARY - Postdoctoral Research Fellowship" should be sent to Email: drencejain@gmail.com

SERB-National Post Doctoral Fellowship: The SERB-National Post Doctoral Fellowship (N-PDF) is aimed to identify motivated young researchers and provide them support for doing research in frontier areas of science and engineering. The call for applications for SERB-N PDF will be notified twice a year through the websites www.serbonline.in and www.serb.gov.in. The application form along with a research proposal highlighting the objectives of the research work to be undertaken should be submitted online through the website www.serbonline.in. Call for proposal will be made open for NPFD during April and October months of every year. Candidates lapsing their eligibility by September 2016 are given with an extension of one-month period, applicable only for this year.



MS in Pharmacy from USA

1st semester at Alliance - JNTUH in India and remaining courses & research in USA at the University of the Pacific, California, USA.



University of the Pacific, USA has entered into collaboration with JNTUH & Alliance Institute, India, for offering Masters (MS) program in Industrial Pharmaceutics. In this program students take courses in the first semester at Alliance-JNTUH and after successful completion of first semester at Alliance and fulfilling admission, TOEFL and visa requirements, students can go to USA to complete remaining courses and research at Thomas J Long School of Pharmacy and Health Sciences, University of the Pacific. Upon successful completion of the requirements, University of the Pacific will award Master's degree.

If students fail to meet University of the Pacific admission/visa requirements, they have an option to continue their course and research work at Alliance -JNTUH or do research work at the Pacific to fulfill requirements for MS degree in India.

Admissions are based on
GPAT / PGECET / JNTUH Entrance

MS DEGREE AWARDED BY
University of the Pacific,
Stockton, CA- USA

10th Annual Convention of ABAP

International Conference on

Environmental Conservation and Human Health - Challenges & Strategies

Special Sattellite Meetings on

“Biodiversity, Conservation and Development Strategies”

“Advances in Pharmacology and Toxicology”

Biotechnology for the Welfare of the Society”

21-23 December 2016

Organised by

DEPARTMENT OF ZOOLOGY

Sri Venkateswara University

Tirupati - 517 502, Andhra Pradesh, India



In Association with

ASSOCIATION OF BIOTECHNOLOGY AND PHARMACY

Mobile : +91 9866206362

E-mail : icechsvu2016@gmail.com - Website : www.svuniversity.ac.in

Registered with Registrar of News Papers for India
Regn. No. APENG/2008/28877

Association of Biotechnology and Pharmacy

(Regn. No. 28OF 2007)

Executive Council

Hon. President

Prof. B. Suresh

Hon. Secretary

Prof. K. Chinnaswamy

President Elect

Prof. T. V. Narayana

Bangalore

General Secretary

Prof. K.R.S. Sambasiva Rao

Guntur

Vice-Presidents

Prof. M. Vijayalakshmi

Guntur

Prof. T. K. Ravi

Coimbatore

Treasurer

Prof. P. Sudhakar

Advisory Board

Prof. C. K. Kokate, Belgaum

Prof. B. K. Gupta, Kolkata

Prof. Y. Madhusudhana Rao, Warangal

Prof. M. D. Karwekar, Bangalore

Prof. K. P. R. Chowdary, Vizag

Dr. V. S.V. Rao Vadlamudi, Hyderabad

Executive Members

Prof. V. Ravichandran, Chennai

Prof. Gabhe, Mumbai

Prof. Unnikrishna Phanicker, Trivandrum

Prof. R. Nagaraju, Tirupathi

Prof. S. Jaipal Reddy, Hyderabad

Prof. C. S. V. Ramachandra Rao, Vijayawada

Dr. C. Gopala Krishna, Guntur

Dr. K. Ammani, Guntur

Dr. J. Ramesh Babu, Guntur

Prof. G. Vidyasagar, Kutch

Prof. T. Somasekhar, Bangalore

Prof. S. Vidyadhara, Guntur

Prof. K. S. R. G. Prasad, Tirupathi

Prof. G. Devala Rao, Vijayawada

Prof. B. Jayakar, Salem

Prof. S. C. Marihal, Goa

M. B. R. Prasad, Vijayawada

Dr. M. Subba Rao, Nuzividu

Prof. Y. Rajendra Prasad, Vizag

Prof. P. M. Gaikwad, Ahmednagar

Printed, Published and owned by Association of Bio-Technology and Pharmacy # 6-69-64 : 6/19, Brodipet, Guntur - 522 002, Andhra Pradesh, India. Printed at : Don Bosco Tech. School Press, Ring Road, Guntur - 522 007. A.P., India Published at : Association of Bio-Technology and Pharmacy # 6-69-64 : 6/19, Brodipet, Guntur - 522 002, Andhra Pradesh, India. Editors : Prof. K.R.S. Sambasiva Rao, Prof. Karnam S. Murthy